Human Tectorial Membrane Waves

by

Shirin Farrahi

Submitted to the Department of Electrical Engineering and Computer Science
in partial fulfillment of the requirements for the degree of

Doctor of Philosophy

at the

MASSACHUSETTS INSTITUTE OF TECHNOLOGY

September 2013

Author .....
Department of Electrical Engineering and Computer Science
August 30, 2013

Certified by .....
Dennis M. Freeman
Professor of Electrical Engineering and Computer Science
Thesis Supervisor

Accepted by .....
Leslie A. Kolodziejski
Professor of Electrical Engineering and Computer Science
Chair, Department Committee on Graduate Students

Human Tectorial Membrane Waves

by

Shirin Farrahi

Submitted to the Department of Electrical Engineering and Computer Science
on August 30, 2013, in partial fulfillment of the
requirements for the degree of
Doctor of Philosophy

Abstract

It is widely believed that humans are better than other mammals at discriminating different frequency sounds. However, mechanisms that could account for such differences are unknown. Recently the TM has been shown to support longitudinally propagating waves, and these waves have been implicated in tuning properties in a mutant mouse model of hearing. In this study we investigate the possibility that sharper tuning in humans could result from differences in human TM waves relative to those of tow other mammals: guinea pigs and mice.

The TM is a fragile tissue made up mostly of water and thus may be drastically changed when cochlear samples are fixed. We looked at the morphology of unfixed human TM samples for the first time and found some systematic differences compared to guinea pig and mouse TMs. Namely, human TM samples have a sharper angle of collagen fibers and a thicker Hensen's stripe. Otherwise, TM samples from humans are comparable to those from the other mammals in this study.

Human TM wave measurements were performed 48 hours post-mortem. To determine what effect this amount of time could have on TM properties, we aged mouse cochleae and compared the resulting properties to those from freshly dissected TM samples. We found that TM fixed charge density decreased when samples were aged. We studied the effect of charge on TM waves using pH to modulate fixed charge and KCl to modulate charge shielding. Although we found a significant effect on TM wave properties due to pH, charge shielding had little to no effect on wave properties. These results suggest that the changes in wave properties due to pH do not arise because of changes in charge but from another mechanism such as conformational changes of proteins in the TM. We also found that TM wave properties in aged samples were not significantly different from those in fresh preparations. These experiments led us to conclude that charge does not play a role in TM wave properties. Although surprising, this result is consistent with the fact that TM waves involve shearing displacements, as opposed to bulk compression, of the TM.

We performed measurements of TM wave decay constants and wave speeds in humans, guinea pigs and mice and found that in all three species, wave properties were consistent with those previously seen in mice. Namely, apical TM wave speeds

(1 - 3 m/s) were significantly smaller than basal wave speeds (3 - 10 m/s), and basal TM decay constants (100 - 150 μm) were smaller than apical decay constants (150 - 250 μm). We also saw that wave speeds increased with frequency and decay constants decreased with frequency. Overall, TM wave properties were not significantly different between humans, guinea pigs and mice as expected from the fact that we did not see significant differences in TM morphology. However, if we use each animal's cochlear map to convert distance measurements into frequency measurements, a different picture emerges. By scaling TM wave properties by the cochlear map, human TM wave decay constants (0.03 - 0.05 octaves) are significantly smaller than those in mice (0.1 - 0.2 octaves) and guinea pigs (0.05 - 0.09). We conclude that this smaller spread of excitation in TM waves contributes to the sharper frequency selectivity in humans. Although radial cross-sections of the organs of Corti are indistinguishable in these three species, there are significant differences in spread of excitation when measured in octaves of frequency rather than meters. Our findings show that the wave properties of the TM in combination with the cochlear map can be used to predict frequency selectivity in the cochlea, suggesting that the remarkable sharpness of tuning in humans can be explained by the presence of waves coupled with the cochlear map. Our results demonstrate the importance of measuring spread of excitation on a physiologically relevant scale.

Thesis Supervisor: Dennis M. Freeman
Title: Professor of Electrical Engineering and Computer Science

Acknowledgments

I would like to thank my supervisor, Denny Freeman, who was always able to help with any question or problem I had and who is a great scientific mentor. Despite his busy schedule, he spent countless hours giving me feedback, and I know his influence will leave a lasting impression on my future work. Next I'd like to thank my committee members: Chris Shera, John Guinan, and Martha Gray. They were very encouraging and gave insightful comments that helped greatly with my thesis progress. I'd especially like to thank Chris Shera for generously providing his data and code and helping us with data interpretation. This made a significant difference in my final thesis outcome. I'd also like to thank Elizabeth Olson for being very generous with her time and providing some helpful insights into this work.

Before starting at MIT, I was worried about the pressure and the types of people I might encounter, but it turns out I was very fortunate to work with such a friendly helpful group. For their suggestions, help, and friendness, I'd like to thank the members of the micromechanics group: Roozbeh Ghaffari, Scott Page, and Jonathan Sellon. A.J. Aranyosi was extremely helpful during my first few years in the group and continued to provide technical assistance to me after he left the group. Janice Balzer has also been very helpful over the years as our group's administrative assistant.

It has been a pleasure working with Heidi Nakajima over the last two years. She has been extremely helpful, supportive, and encouraging. She not only provided us with the human temporal bones that allowed us to perform the work outlined here, she also spent a lot of time with me to teach me how to drill the bones open and extract tissues. She is a great mentor and an inspiration. It's no exaggeration to say that this work would not have been done without Diane Jones who extracted all of the bones from the donors. I'd also like to thank John Rosowski from the Massachusetts Eye and Ear Infirmary for his insights and encouragement over the years. Jen O'Malley from the MEEI Otopathology lab was also very kind in collecting images for me from their collection.

I have made so many friends at MIT that I apologize if I forget some names here,

but I'd first especially like to thank Anna Fendyur who I met only a year ago but who has been very supportive over that time. Whenever I returned from a coffee break with her, I would suddenly find a solution to the problem I was struggling with before. I'd also like to the following who made my time at MIT memorable: Katarina Blagovic, Salil Desai, Ann Hickox, Pavitra Krishnaswamy, Leon Li, Daniel Prashanth, and Oshani Seneviratne. I hope we can stay in touch for many years to come.

My family has played such a big role in my studies over the years that I don't know where I would be without them. My sister, Katayoun, finished her PhD a few years ago and has been a role model for my whole life. My brother-in-law, Farzad, has not only been a good friend but has also been available for advice on surgical techniques. My parents, Bijan and Hengameh, have been an inspiration and have been more supportive than I can explain. It has been difficult being so far away from them during my time at MIT. Although not a substitute, it has been wonderful having my husband's family nearby. Thank you to Parvin, Freidoun, Zartosht, Joni, Arta, Kristyn, Rosemary, Meredith, and Ida for welcoming me to the family.

Finally, I've saved this special last mention for my husband, Arya, whose love and support has been amazing during my time at MIT. Whenever I had a problem, he would always listen to it carefully and put it in perspective, making it seem manageable. I can't believe that we've already been married for six years. Time flies when you're having fun.

Contents

List of Figures

List of Tables

Chapter 1

Introduction

Hearing plays a critical role in the development of human speech and intelligence. It is widely known that without hearing, normal speech will not develop. Around the world, newborn babies are now routinely screened at birth for hearing loss because of the significant impact this disability can have on a person's development and early education [94].

In addition to its critical role in our development and daily lives, hearing is a remarkable sense for study in its own right. The human cochlea can detect motions of the eardrum smaller than the diameter of a hydrogen atom and can perform high quality spectral analysis to discriminate as many as 30 frequencies in the interval of a single semi-tone [49, 13]. Historically, these remarkable properties were associated very high sensitivity and selectivity of neural components of hearing. More recently it has been shown in animals that the mechanical responses of the cochlear structures are equally sensitive and selective [64].

Among mammals, human hearing has widely been assumed to be unique. We are the only animals to create complex speed and music. Detailed measurements have suggested much better discriminating capabilities in human neural responses and speech discrimination tasks compared to other mammals [7, 85]. These high level differences are not surprising given that our brains are more sophisticated than those of other mammals. However, measurements by Shera et al. have suggested that the difference in humans also lies in peripheral hearing mechanics [81]. This is

far more surprising given that the structure of the organ of Corti is remarkably well conserved across all mammals.

The goal of this thesis is to understand how the tectorial membrane, an acellular gel overlying hair bundles in the cochlea, contributes to the unusually sharp cochlear tuning exhibited in human hearing. To accomplish this goal, I will present dynamic properties of the TM for the first time from unfixed human bones and relate these properties to those predicted for human hearing. This chapter will review basic cochlear function and will outline the known properties of the TM.

1.1 The Cochlea

The mammalian cochlea is made up of the external ear, the middle ear, and the inner ear. When sound is directed into the ear canal, it hits the tympanic membrane and enters the middle ear. The three middle ear bones – the malleus, incus, and stapes – are set in motion and act as an impedance matching system between the air outside the eardrum to the fluid inside the inner ear. The last of these bones, the stapes, transmits vibrations to the cochlea through the oval window. As the oval window vibrates, differential pressure is set up across the organ of Corti, setting the basilar membrane into motion 1-1. The basal region of the basilar membrane, close to the stapes, is most sensitive to high frequencies while the apical region, further down the spiral, is sensitive to low frequencies [91].

As the organ of Corti vibrates, mechanical stimuli are converted to neural signals via the inner hair cells. The outer hair cells are believed to play an electromotile role in the cochlea whereby their cell bodies expand and contract to produce mechanical amplification [8]. The tectorial membrane (TM) is an acellular tissue overlying the hair bundles. Its motions are directly responsible for stimulating the hair bundles in order to allow mechanical stimuli to be transduced by the hair cells.

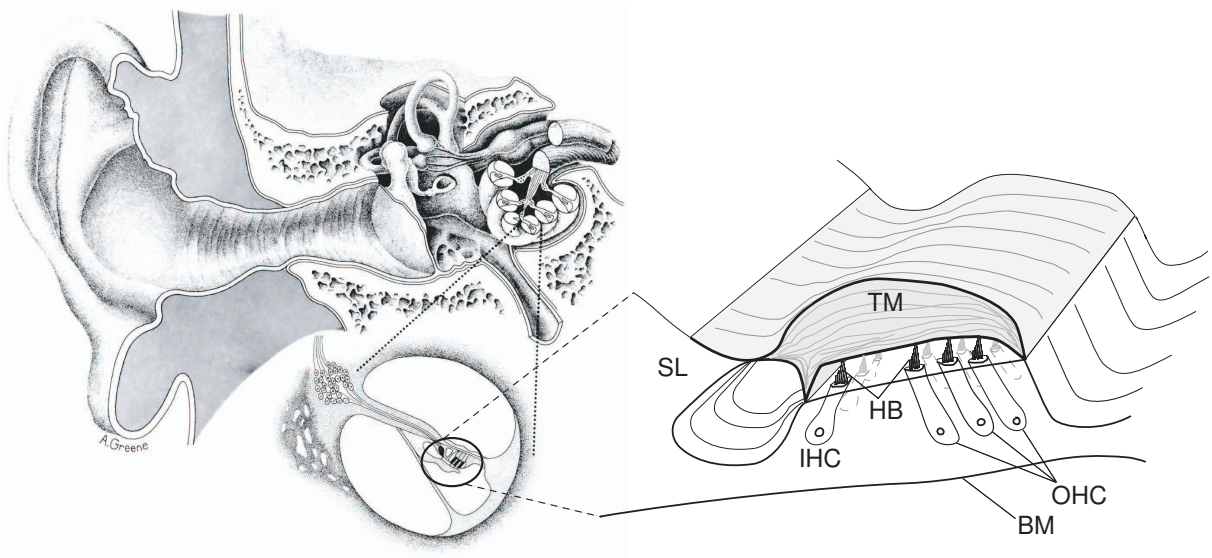

Figure 1-1: Anatomy of the human ear
Anatomy of the human ear showing the ear canal through which sound enters, the middle ear bones, and a cross-section of the spiraling inner ear or cochlea. To the right is a detailed view of the organ of Corti containing the sensory structures of the cochlea. Labeled structures in the organ of Corti: SL = spiral limbus, TM = tectorial membrane, IHC = inner hair cell, HB = hair bundles, BM = basilar membrane, OHC = outer hair cells. Picture drawn by Anne Greene

1.2 Cochlear coordinate system

The following coordinate system for the cochlea will be used throughout this thesis:

Radial: Extends from the spiral limbus to the marginal band of the TM. The positive direction is towards the marginal band.

Longitudinal: Extends from the base to the apex of the cochlea. Positive direction is towards the apex.

Transverse: Direction normal to the surface of the BM and the TM. The positive direction is towards scala media.

These coordinates will be labeled on images.

1.3 The tectorial membrane

The tectorial membrane (TM) is a highly hydrated extracellular matrix that resides above the hair bundles. Because of its strategic position above the mechanosensory hair bundles of both inner and outer hair cells, the TM is believed to play a critical role in the deflection of hair bundles. Recently, genetic studies have confirmed the importance of the TM in hearing, where manipulations of genes targeting TM proteins have resulted in significant hearing deficits – TectA, which encodes α-tectorin [51, 50, 93, 71], TectB, which encodes β-tectorin [77], Col9A1, which encodes a polypeptide in collagen IX [88] and Col11A2, which encodes a polypeptide in collagen type XI [60]. These mutations cause severe hearing deficits, even when the TM is nearly unchanged in its microscopic physical orientation and structural attachments to the sensory receptors as viewed under a light microscope.

The TM is an acellular gel whose two main constituents are water (97% by weight) and collagen. The collagen fibrils are largely oriented radially along the organ of corti, more or less perpendicular to the cochlear spiral (figure 1-2). Other than the collagen fibrils, the main structural feature of the TM is Hensen's stripe, which overlies the inner hair cells in the cochlea. This is a slight protuberance from the undersurface of the TM very close to the inner hair cell bundles. Scanning electron micrograph images of the undersurface of the TM have shown that outer hair cell bundles are stuck inside the TM [54]. However, it is unclear how close contact is between the inner hair cell bundles and the TM.

Due to the largely radial orientation of collagen fibers in the TM, it is highly anisotropic. The radial stiffness of the TM is roughly twice its longitudinal stiffness [2, 36].

1.3.1 Biocomposition

Other than water, the TM contains a variety of collagen types including the most abundant, type II, as well as types V, IX and XI. A variety of other constituents can also be found inside the TM which are critical to its properties and which give

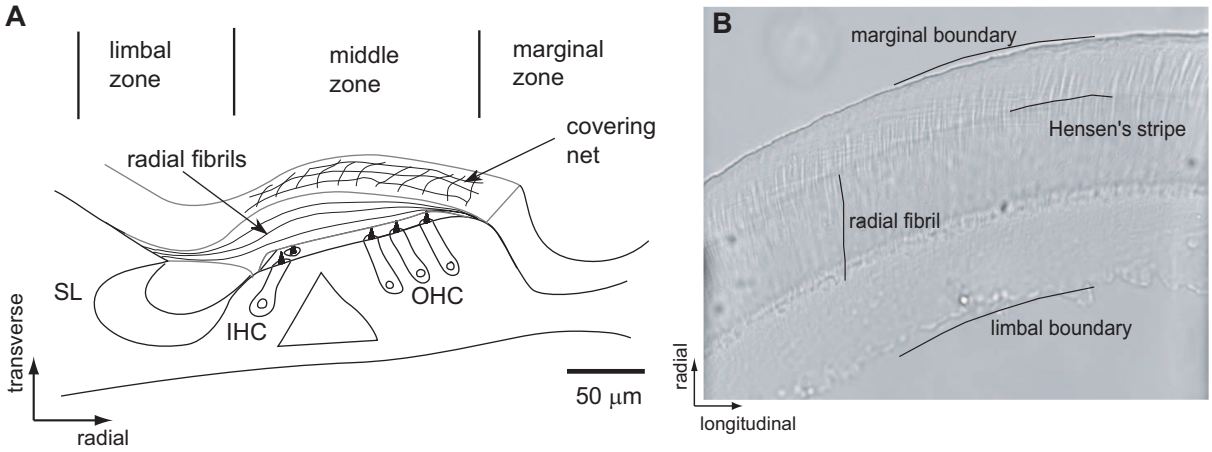

Figure 1-2: Regions of the tectorial membrane
A: Cartoon of the organ of Corti showing the regions of the TM. The limbal zone is very thin and is the strongest attachment of the TM to the cochlea. The middle zone covers the organ of Corti. The marginal zone is the region between the outer hair cells and the marginal band. B: Image of mouse TM sample from the basal region of the cochlea. A radial collagen fibril is highlighted along with the marginal band; Hensen's stripe, where the inner hair cells lie; and the limbal boundary, where the TM was once attached to the cochlea. Adapted from [28]

it negative fixed charge [92, 24, 31]. Glycosaminoglycans (GAGs) are polysaccharide chains sulfated and carboxylated sugars create the TM's negative fixed charge.

The TM also contains two non-collagenous proteins that comprise the striated sheet matrix, α and β-tectorin [32]. The striated sheet matrix is the mesh within which the collagen fibrils are contained. Interestingly, these two proteins are not found anywhere outside of the inner ear, although their structure is similar to many other proteins containing zona pellucida (ZP) domains [52].

Recently, it has been shown that mutations in the genes encoding α and β-tectorin, TectA and TectB, respectively, cause significant changes to hearing phenotypes [51, 50, 77]. In particular, TectB$^{-/-}$ mutant mice were missing the striated sheet matrix and Hensen's stripe [77].

Finally, otogelin is another protein involved in organizing the fibrillar structure of the mammalian TM [84] and is also found in the vestibular portion of the inner ear.

1.3.2 Classical TM models

Historically, the TM has been modeled as a stiff lever with a pivot at the spiral limbus [17, 46, 6, 66] as illustrated in 1-3. In this conception, the TM is assumed to have an infinite radial stiffness. In addition to the stiff lever model, the TM has been modeled as a resonant mass–spring system [97, 3, 67] or as a mass [56]. In these models, the longitudinal coupling in the TM is assumed to be negligible so that the TM's action is constricted to a single cross-section in the organ of Corti.

These models exclude important global phenomena, such as longitudinal coupling (spread of excitation) [96, 2, 61]. It is now clear that the TM's physical properties vary with longitudinal position [30, 29, 27, 26, 36, 73, 59, 38, 37], and that longitudinal coupling manifested in the form of traveling waves contributes to hearing mechanisms [29, 30, 80, 72, 39, 61, 5, 55, 47].

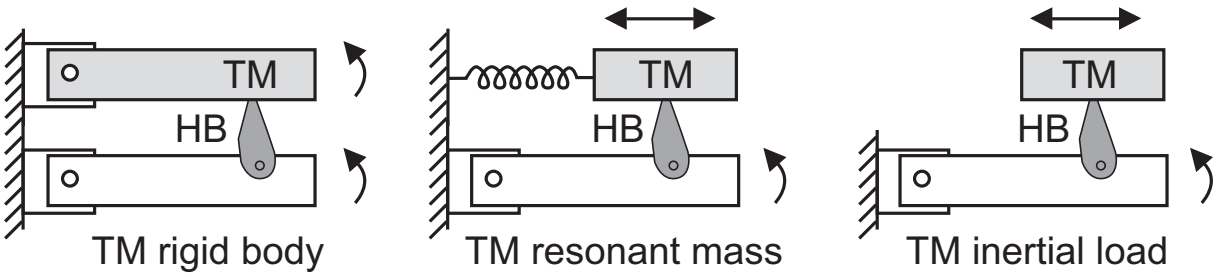

Figure 1-3: Classical cochlear models incorporating the TM
The TM has been modeled as a stiff lever [17, 46, 6, 66], a resonant system [97, 3, 67], and as a pure inertial load [56] on top of the hair bundles in previous two-dimensional cross-sectional models of the cochlea. (Adapted from [1]).

1.3.3 Measurement of TM material properties

In order to measure TM material properties, a probe whose stiffness is close to the stiffness of the TM must be used. By applying a known force to the TM and measuring the resulting displacement of the probe, the material properties of the TM can be measured. This basic method has been used to determine TM material properties using a variety of probes, including strands of hair [91], glass pipettes [98], magnetic beads [2], AFM tips [83, 73, 27], osmotic pressure [59], and microfabricated probes

[36]. The earlier measurements were performed *in situ* [91, 98]; however, in order to visualize the TM which is almost perfectly transparent, these studies dyed the TM which may change its material properties and had to apply forces that were much larger than the forces typically seen by the TM. Therefore, all later measurements of TM properties extracted the tissue from the organ of Corti in order to perform measurements.

Most of the methods described above have problems in that their application is limited to frequencies less than 10 Hz, well below the relevant range of hearing for most mammals. Of the methods listed above, magnetic beads allow measurements to 1 kHz [2] and microfabricated probes allow measurements in the 10's of kHz [36]. However, these methods have problems with repeatability given that fine control of contact between the probe and the TM are difficult to repet. A fundamentally different method that allows measurement of TM material properties to 30 kHz without requiring any probes is to stimulate the TM using longitudinal shear waves [29].

1.4 TM Waves

Recently Ghaffari et al. showed that the TM has longitudinal coupling manifested in the form of traveling waves [29]. The speed of these waves is closely matched to basilar membrane wave speeds, suggesting that these waves could couple in the cochlea to help create some of the remarkable properties of mammalian hearing. These TM waves extend over large cochlear distances and stimulate multiple rows of hair cells (Figure 1-4) [29].

Treating the TM as a viscoelastic solid and fitting a model of TM waves to measurements from TM samples, Ghaffari et al. showed that waves can be used to find the shear material properties of the TM [29]. This method of measuring material properties allows for easy comparison across multiple samples. In chapter 4, we use this method to compare TM material properties across multiple species.

Including longitudinal coupling in the TM is a fundamentally different way of looking at its role in the cochlea. Meaud and Grosh included longitudinal coupling

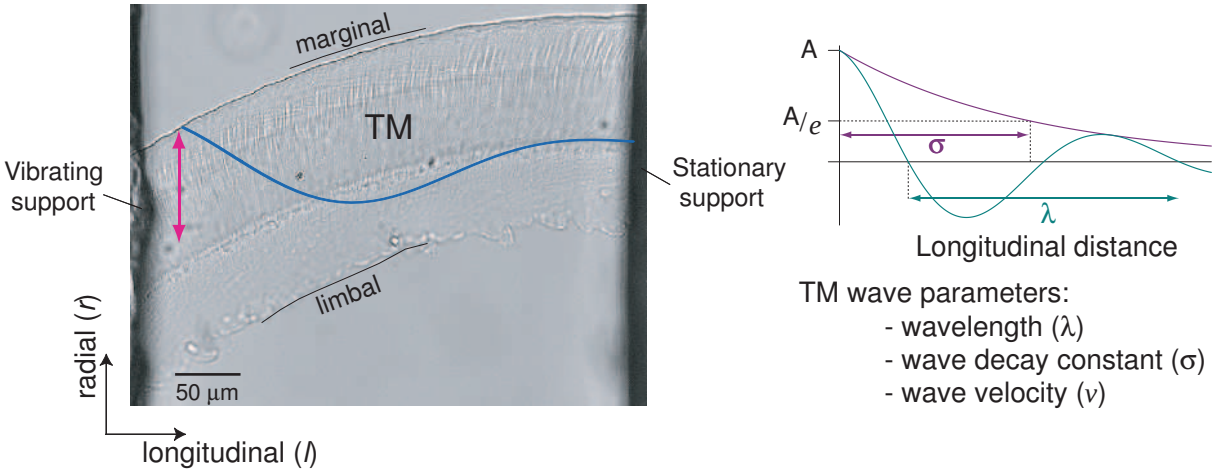

Figure 1-4: TM wave measurement system
Left panel: an excised mouse TM from the basal region of the cochlea is suspended over two platforms. The left side is stimulated at acoustic frequencies to launch a longitudinal wave along the surface of the TM. Right panel: from the resulting motion, a wavelength, λ, speed, v, and decay constant, σ, can be obtained. The decay constant is the distance over which the wave envelope decays by a factor of e. Figure adapted from Ghaffari et al. [29].

in a cochlear model and found that it resulted in cochlear responses that are closer to those from micromechanical measurements of the basilar membrane [61].

1.4.1 TM Waves in the TectB Mutant Model of Hearing

TectB$^{-/-}$ mutant mice have a very interesting phenotype. Compared to normal mice, their sharpness of tuning in the base is actually higher. This roughly factor of two increase in sharpness of tuning in the base in mutants is accompanied with a small decrease in the sensitivity of hearing [77]. In the apex, these mice have greatly increased thresholds of hearing. As far as can be seen from scanning electron micrograph images of the cochlea in these mutant mice, there are no changes to the organ of Corti other than those found in the TM.

Ghaffari et al. showed that the hearing phenotypes seen in these mutant mice relate strongly with TM wave properties. Specifically, TM wave spread of excitation in samples taken from the basal regions of TectB$^{-/-}$ mutant mice is significantly reduced [30]. This decrease in spread of excitation of TM waves correlates strongly

with the sharper cochlear tuning seen in these mice. Looking at the cochlear place-frequency map, we see that a smaller spread of excitation in space should translate to fewer hair cells being coupled and a tuning curve with a smaller Q value (Figure 1-5). Conversely, the TM wave speed in apical samples from TectB$^{-/-}$ mutant mice is significantly decreased, suggesting that the coupling between the TM wave and basilar membrane wave has broken down, causing greatly reduced sensitivity of hearing.

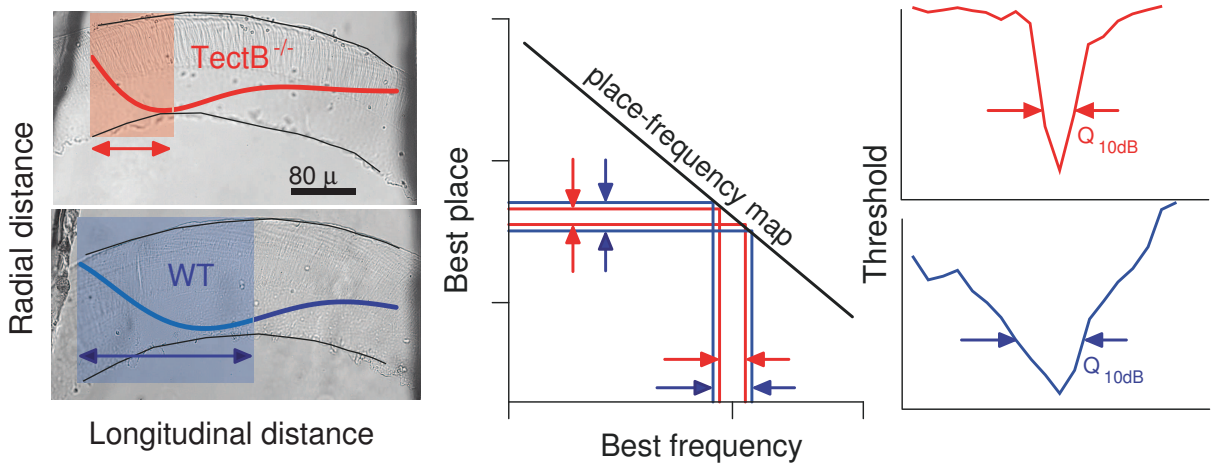

Figure 1-5: TM wave spread of excitation in TectB mutant mice correlates with sharper tuning
TM samples from wild type (WT) and TectB$^{-/-}$ mutant mouse models are shown on the left with their approximate spread of excitation highlighted. These differences in spread of excitation when seen relative to the cochlear map, shown in the middle, translate to the tuning curves measured by Russell et al. in the WT versus mutant mice shown on the right. Figure adapted from Ghaffari et al. [30].

1.5 Thesis organization

This thesis is organized into three chapters looking at the extent to which TM wave properties could be important to human hearing. Since TM samples from human bones could only be measured two days after death, in the first chapter, we study the potential effects of waiting this amount of time on TM waves. In the second chapter (chapter 3), we determine if our findings in chapter 2 agree with predictions from models of TM wave propagation. We conclude the thesis by comparing TM waves in different mammalian species to see if their properties underlie the cochlear tuning

differences predicted to exist in these species.

Each chapter is organized as a separate paper for publication and can be read independently of the others. Methods and introductory material may be repeated across chapters.

Chapter 2

The role of charge in tectorial membrane waves

The freshest TM samples that we could hope to obtain from human donors were such that we could take the measurements within 48 hours after death. In order to determine the potential effects of this amount of time on TM properties, we performed a series of experiments on mice to mimic the conditions in which human bones were treated. In this chapter, we outline our findings on the effect of aging on TM fixed charge density. To clarify the link between TM fixed charge and waves, we performed a careful study of the effect of charge on TM waves. We modulated TM charge using pH and charge shielding.

In this study, we show that pH modulates TM stiffness and the spread of excitation of TM waves. Previously, we found that TM fixed charge density drops by roughly a factor of two in magnitude in acidic conditions [31]. To explore the possibility that charge is the mechanism behind the stiffness and spread of excitation changes we observe with decreased pH, we also decreased TM fixed charge using another method: increasing KCl in the bath surrounding the TM. By increasing the concentration of mobile ions around the TM, we get increased shielding of the TM's fixed negative charges by these mobile ions, resulting in an effective decrease in the TM's fixed charge magnitude (i.e. charge shielding). We show that this causes no significant effect on TM wave properties, suggesting that charge is not the mechanism controlling TM

shear modulus and wave properties.

Sharpness of tuning in the cochlea has been associated with viscous parameters related to the tectorial membrane such as subtectorial damping [3]. However, in the TectB mutant mouse, the only mutant model to date where sharpness of tuning increased due to the mutation [77], TM stiffness decreased with little change in shear viscosity [30]. In this study, we also show that TMs from TectB$^{-/-}$ mutant mice do not show significant changes in fixed charge density compared to wild types, further suggesting that charge is not the important mechanism controlling TM stiffness and cochlear spread of excitation.

2.1 Materials and Methods

2.1.1 Preparation of the isolated TM

TM segments were isolated from the cochleae of adult mice (strain B6129F1, 4-12 weeks old; Jackson Lab, Bar Harbor, ME) as described previously [79]. Briefly, the cochlea was excised and placed in an artificial endolymph (AE) bath containing 174 mM KCl, 5 mM Hepes, 3 mM dextrose, 2 mM NaCl, and 0.02 mM $CaCl_2$. The bath was titrated to either pH 7.3 or 4 using small quantities of 1M KOH and HCl, respectively. The bone surrounding the cochlea was chipped away using a 26 gauge needle until the cochlear turns and organ of Corti were exposed. Segments of the tectorial membrane were then removed using a sterilized eyelash. The care and use of animals in this study were approved by the Massachusetts Institute of Technology Committee on Animal Care.

2.1.2 Aging of mouse TM samples

In cases where mouse TM samples were aged for 48 hours, the animals were euthanized by carbon dioxide asphyxiation followed by decapitation. The mouse TMs were extracted as much as possible in a manner similar to the way human TM samples were extracted. To this end, heads were refrigerated overnight after which temporal

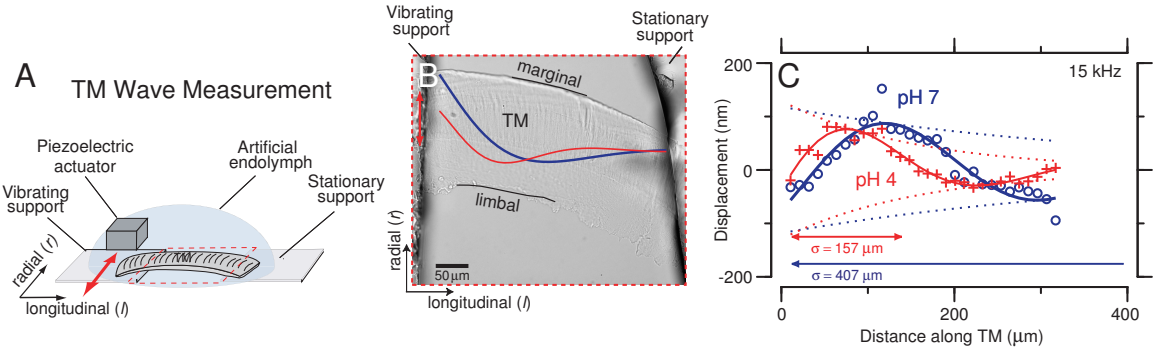

Figure 2-1: Wave chamber experimental setup
A: Longitudinally propagating waves were launched on suspended segments of mouse TM taken from the basal region of the cochlea using a piezo-electric actuator. Adapted from Ghaffari et al. [29]. **B:** Image of a mouse TM sample suspended in the wave chamber. **C:** Wave decay constant (σ) and speed (v) were measured by fitting the decaying wave measured along the TM. A sample snapshot shown at pH 7 (o) and 4 (+) at 15 kHz.

bones were extracted and bullae were opened and placed in 0.9% saline. After several hours in the saline solution, cochleae were dissected and placed in an artificial endolymph bath. The cochleae were refrigerated in AE until approximately 36 hours after the animal's time of death, at which point the cochleae were dissected using a scalpel blade (no. 11) and TM samples were extracted using a sterilized eyelash. TM wave measurements were performed approximately 48 hours post mortem.

2.1.3 Measuring TM wave properties

TM waves were generated and measured using an optical measurement system and wave chamber as described by Ghaffari et al. [29]. Briefly, isolated TM segments from the basal turn of mouse cochleae were suspended between two supports (figure 2-1) using Cell Tak bioadhesive (Collaborative Research, Bedford, MA). One of the supports was glued down and thus remained stationary while the other was attached to a piezo-electric actuator (Thorlabs Inc., Newton, NJ). The TM was stimulated in the radial cochlear direction, and motions along its surface were measured at audio frequencies (1-40 kHz). Measurements were taken first under physiological conditions, then the medium was replaced with an AE bath equilibrated at pH 4 or containing

1M KCl, depending on the experiment. The preparation was left to equilibrate for 10 minutes before we performed measurements. After the measurements were complete, the bath was returned to normal AE and measurements were repeated. Each time the AE bath was varied, the exchange was performed manually by extracting and replacing 0.5 mL of AE at a time from a total bath volume of approximately 1 mL. In the pH experiments, this process was repeated until the last 1 mL sample of the extracted fluid measured within 0.1 units of the desired pH using a commercial pH meter (Corning). In the KCl experiments, the exchange was repeated until the total volume surrounding the TM was replaced at least three times.

Motion amplitude and phase were measured using a stroboscopic computer vision technique that allows images to be captured at several phases of motion [15]. Radial TM displacement and phase were determined from a one-dimensional FFT taken at evenly spaced points along the TM. Spatial decay constant, σ, was defined as the distance in μm along the TM over which the wave magnitude decays by a factor of e. The σ values for each TM were determined by fitting an exponential to the overall magnitude of the response along the TM. Speed, v, was determined by fitting a straight line to the phase as a function of distance along the TM and multiplying the inverse slope by angular frequency.

2.1.4 Measuring TM radial shear impedance

Radial TM shear impedance was measured using microfabricated probes as described previously [36]. Briefly, basal TM samples were immersed in AE and adhered to a glass slide using Cell Tak. The square tip of a microfabricated probe (Figure 2-2) was then lowered onto the surface of the TM using a micromanipulator (Rucker and Kolls Inc., Milpitas, CA). To reduce variability caused by radial gradients in stiffness, the probe tip was centered on Hensen's stripe. The base of the probe was stimulated in the radial direction using a piezo-electric actuator from 1-40 kHz. Displacements of the base and tip of the probe were measured which were predominantly in the radial direction. Probe resonances were observed at some frequencies where motions were both radial and longitudinal, but those frequencies were excluded from the analysis

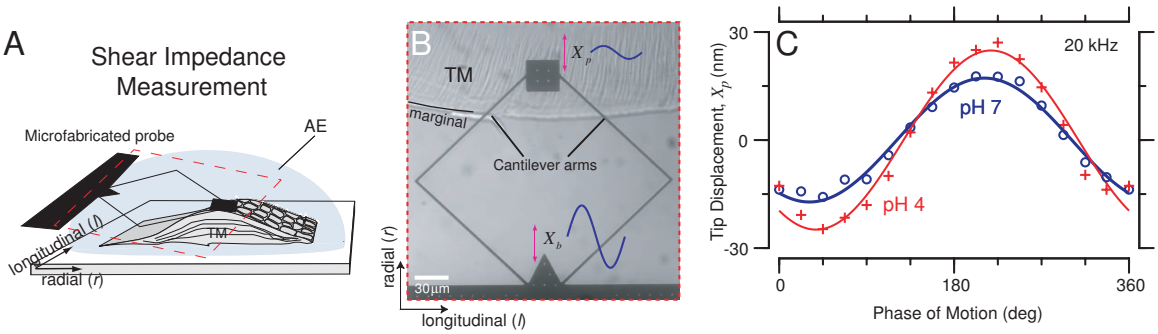

Figure 2-2: Shear impedance experimental setup
A: Microfabricated probes were lowered onto the surface of mouse TM samples tacked to a glass slide. The bases of the probes were stimulated in the radial cochlear direction using a piezo-electric actuator as described in Gu et al. [36]. **B:** Image of TM sample with a probe on its surface in the imaging configuration used to measure shear impedances. **C:** Impedances were determined by fitting the resulting motions at pH 7 (o) and 4 (+) with sinusoids. A sample measurement is shown of the probe tip at pH 7 and 4 at 20 kHz.

presented here. The impedance of the TM was determined by the following equation:

$$Z_{TM}(\omega) = k_{mp}\frac{X_b(\omega) - X_p(\omega)}{j\omega X_p(\omega)} \tag{2.1}$$

where X_b is the displacement of the probe base, X_p is the displacement of the probe tip, and k_{mp} is the stiffness of the probe in the radial direction (57 mN/m). The bath surrounding the TM was exchanged using the same procedure described for wave measurements.

2.1.5 Measuring TM fixed charge density

TM fixed charge density was measured as described previously [31]. Briefly, TM samples from the apical half of the cochlea were placed over a $25\mu m$ hole in a glass slide separating two fluid-filled compartments (figure 2-3). An artificial endolymph bath surrounded the TM in the top chamber while AEs of different potassium chloride concentrations were flowed through the bottom chamber. This created a potential difference which could be measured between the two fluid compartments. Measuring this potential at varying salt concentrations, we calculated the fixed charge density

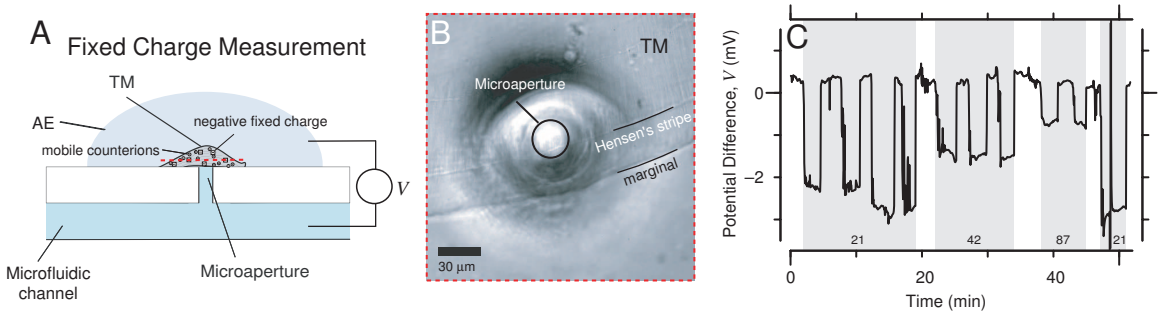

Figure 2-3: TM fixed charge measurement setup
A: TM fixed charge was measured by placing the TM over a microaperture and measuring the potential difference, V, between two baths as the concentration of KCl in the microfluidic channel below the TM was varied as described in Ghaffari et al. [31]. **B:** Image of TM placed over a microaperture. **C:** Sample measurements of the potential difference, V in mV, measured across the microaperture as varying concentrations of KCl were flowed through the channel. The concentration of KCl in the AE below the TM is given in mM along the bottom of the graph. The TM was periodically lifted off of the hole to electrically connect the two baths as seen on the plot where the potential difference periodically jumps to zero.

of the TM using a Donnan relationship:

$$V = \frac{RT}{F}\left(\sqrt{\left(\frac{c_f}{2C_\Sigma}\right)^2 + 1} + \frac{c_f}{2C_\Sigma}\right). \tag{2.2}$$

2.2 Results

2.2.1 TM fixed charge density changes when tissue is aged for 48 hours

We purposely aged mouse bones in a similar manner to the human temporal bones used for experiments in chapter 4. We measured the fixed charge density of these samples and found it to be lower than what we previously measured in fresh samples [31]. In order to quantify this difference, we performed measurements in fresh TM samples taken from the apical half of mouse cochleae and compared these to our measurements in those that were purposely aged for 48 hours. These results are

shown in figure 2-4, where we can see a measurable drop in fixed charge density when samples were purposely aged for 48 hours.

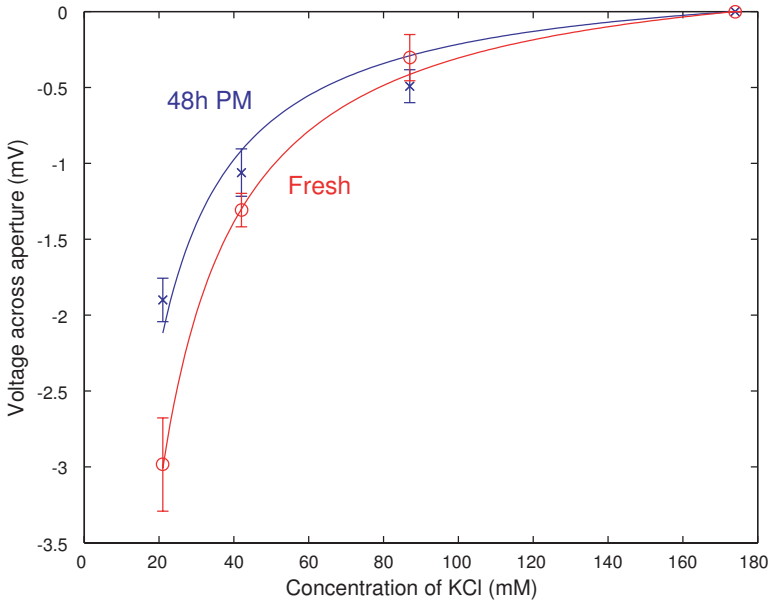

Figure 2-4: Measuring the effect of time after death on mouse TM fixed charge density The voltage measured across the microaperture covered by the TM is plotted as a function of the concentration of KCl in the chamber below the TM in samples from fresh and purposely aged mouse TM samples. The lines represent fits of the data with a Donnan relationship as described in equation 2.2. The median and interquartile range of the fit parameters are as follows: fresh $c_f = -5.6 \pm 0.4$ mmol/L (n = 2), 48h post-mortem $c_f = -3.9 \pm 0.3$ mmol/L (n = 3).

2.2.2 TM fixed charge density shows no difference between aged human and mouse

We measured the fixed charge density of TM samples taken from human and mouse cochleae approximately 48 hours post-mortem. As shown in figure 2-5, we did not see a measurable difference in the fixed charge density between these two species. As will be described in chapter 4, since TM wave properties and material properties are comparable across human, guinea pig and mouse TM samples, it is not surprising that TM fixed charge density is similar across human and mouse TM samples.

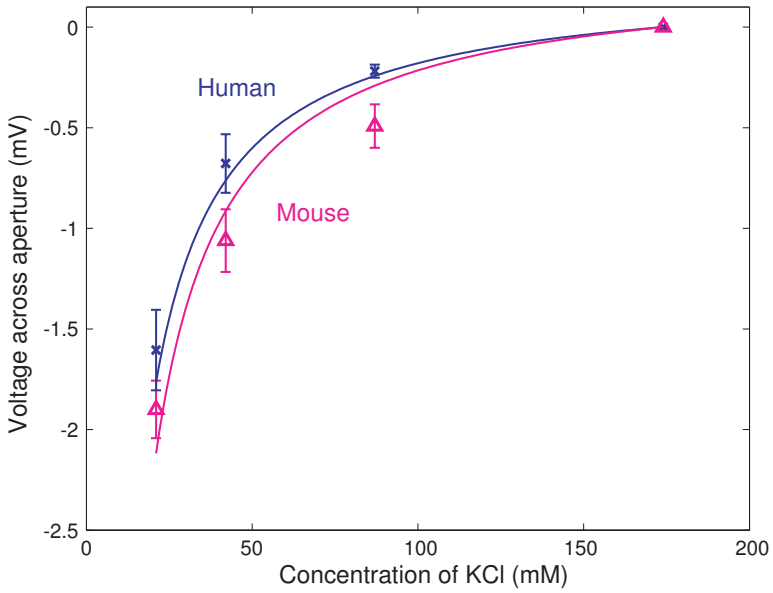

Figure 2-5: Human versus mouse TM fixed charge density
The voltage measured across the microaperture covered by the TM is plotted as a function of the concentration of KCl in the chamber below the TM in samples from humans (x) and mice (Δ). The lines represent fits of the data with a Donnan relationship as described in equation 2.2. The median and interquartile range of the fit parameters are as follows: human $c_f = -3.3 \pm 0.3$ mmol/L (n = 2), mouse $c_f = -3.9 \pm 0.3$ mmol/L (n = 3).

2.2.3 Effects of altering pH on TM waves

We previously measured the effect of lowering pH from 7 to 4 on TM fixed charge density and found that it changed TM fixed charge from -7.1 ± 2.0 mmol/L to +3.0 mmol/L [31]. Therefore, we used this as a way of controllably varying the TM's fixed charge to see how this might affect TM waves.

To characterize the effect of pH on TM waves, we measured TM wave decay constant, σ, and speed, v, at physiologic and reduced pH in basal mouse TM segments. Figure 2-1 C shows representative wave snapshots at pH 7 and 4 showing the spatial extent of waves at different pHs. Previous studies showed that upon changing bath pH from 7 to 4, a slight swelling of the TM should occur ($< 10\%$) [24]. Slight changes in focus were observed over the course of our measurements when pH was varied; however, they were not significant enough to require us to change the focal plane of the measurement system. Figures 2-6 A and B show wave parameters plotted against

frequency. Generally, wave decay constants, σ, decrease with frequency, and wave speeds, v, increase with frequency, as observed previously by Ghaffari et al. [29, 30]. Decay constants at pH 7 are significantly higher than those at pH 4. Computing the median and interquartile ranges for the data from the five samples shown in figure 2-6 from 10 - 20 kHz for each pH, we get the following parameters: $\sigma_{pH7} = 322 \pm 52\mu$m and $\sigma_{pH4} = 142 \pm 28\mu$m ($MED \pm \frac{IQR}{2}$. For wave speeds, the differences between measurements at pH 7 and pH 4 are less significant: $v_{pH7} = 6.7 \pm 1.4$ m/s $v_{pH4} = 6.3 \pm 1.3$ m/s.

To clarify the changes in wave parameters due to lowered pH, we paired the measurements from five TM segments and collapsed across frequency. In this way, the only difference presented is the change in wave parameters due to pH. In the bottom row of figure 2-6, each point represents two measurements on a single TM segment where the x-value is the wave parameter measured at pH 7, and the y-value is the same measurement at pH 4. Looking at the data this way, we see that a significant majority of decay constant points fall below the unity line, meaning their values were lower at pH 4 (Median $\pm\frac{IQR}{2}$: $\frac{\sigma_{pH4}}{\sigma_{pH7}} = 0.58 \pm 0.15$). In the case of speed, we see a slight decrease when going from pH 7 to pH 4; however, the observed decrease is less than the interquartile range of the data (Median $\pm\frac{IQR}{2}$: $\frac{v_{pH4}}{v_{pH7}} = 0.85 \pm 0.19$).

This significant decrease in decay constant with a less significant change in speed was seen in all five preparations measured. The decrease in decay constant was found to be largely reversible when the bath surrounding the TM was returned to physiological pH. Specifically, upon returning to pH 7, decay constants on average returned to 98% of their original values, and speeds returned to 90% of their original values.

2.2.4 Effect of varying pH on TM shear impedance and material properties

To measure the effect of pH on TM material properties, we performed shear impedance measurements on basal mouse TM segments at physiologic and acidic pH. Figure 2-

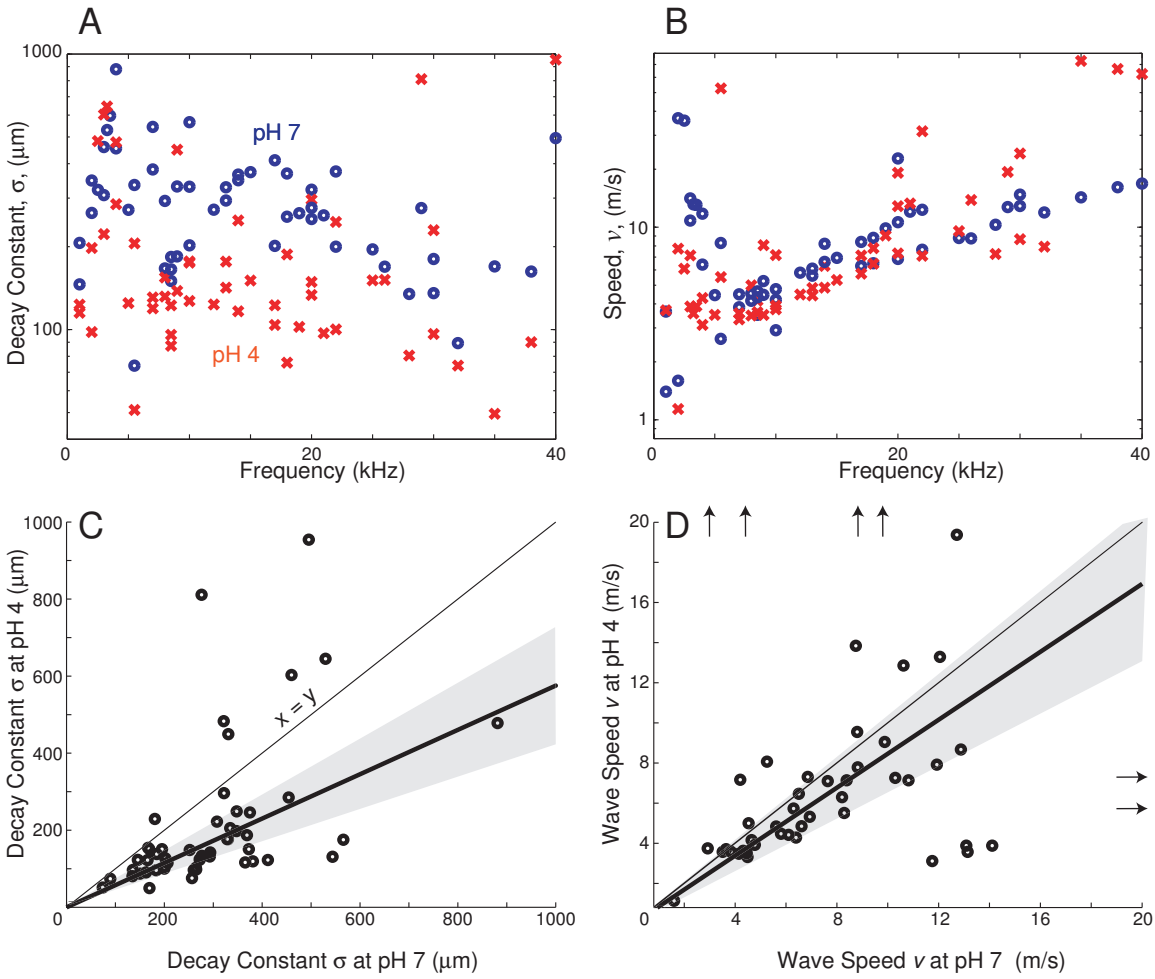

Figure 2-6: TM wave parameters measured at physiologic and acidic pH. A, B: Wave parameters as a function of frequency (n = 5 TM samples). Wave decay constants, σ, and wave speeds, v, are shown at pH 7 (o) and 4 (x). C, D: Wave parameters from the top row collapsed across frequency. Each point represents one frequency for a single piece of TM at physiologic (x-axis) and acidic (y-axis) pH values. Median and inter-quartile ranges indicated by thick lines and shaded regions, respectively, and should be compared to the thin, unity line ($\frac{\sigma_{pH4}}{\sigma_{pH7}} = 0.58 \pm 0.15$; $\frac{v_{pH4}}{v_{pH7}} = 0.85 \pm 0.19$ ($MED \pm \frac{IQR}{2}$)). Any data point that falls outside the axis ranges is indicated by an arrow.

2 C shows representative displacements of the tip of the probe, X_p, during shear impedance measurements at pH 7 and 4. The displacements of the base of the probe, X_b, are significantly larger and do not vary with pH. From these tip and base displacements, we computed shear impedance values, Z_{TM}, from equation 2.1. All of the shear impedance measurements at pH 7 and pH 4 are plotted as a function of frequency in figures 2-7 A and B. The real part of shear impedance (figure 2-7 A) is the viscosity-related term, while the imaginary part multiplied by frequency (figure 2-7 B) is the tissue's stiffness. As expected from previous TM shear impedance measurements, we see that the TM is stiffness-dominated at low frequencies [36]. Here, we show this to be true for the majority of the mouse's frequency range of hearing. We also show a significant decrease in stiffness as pH is lowered but a less significant decrease in the viscosity-related term.

We calculated TM material parameters from shear impedance measurements, Z_{TM}, using the following relationship:

$$\begin{aligned} G^* &= j\omega Z_{TM} \tfrac{T}{\pi r^2} \\ &= G' + j\omega\eta \end{aligned} \tag{2.3}$$

where T is the TM thickness (taken as 100 μm for basal TM samples) and r is the radius of the force probe (roughly 25μm including surrounding tissue that moves) [10]. The resulting parameters are G', the shear storage modulus, which relates to the tissue's stiffness, and η, the shear viscosity. These material parameters are plotted in figures 2-8 A and B as a function of frequency. Median and interquartile ranges from 10 - 20 kHz for the four samples shown in figure 2-8 are as follows: $G'_{pH7} = 23.4 \pm 3$ kPa, $G'_{pH4} = 13 \pm 3$ kPa, $\eta_{pH7} = 0.11 \pm 0.04$ Pa·s, $\eta_{pH4} = 0.11 \pm 0.02$ Pa·s ($MED \pm \frac{IQR}{2}$). In figures 2-8 C and D, these parameters are plotted as matched pairs, where each point represents two measurements at a single frequency on a single sample (Median and IQR slopes: $\frac{G'_{pH4}}{G'_{pH7}} = 0.60 \pm 0.19$, $\frac{\eta_{pH4}}{\eta_{pH7}} = 0.82 \pm 0.23$).

We see that lowering pH decreases G' while keeping η roughly unchanged. By shearing the TM using the probe as shown in figure 2-2, we are measuring shear

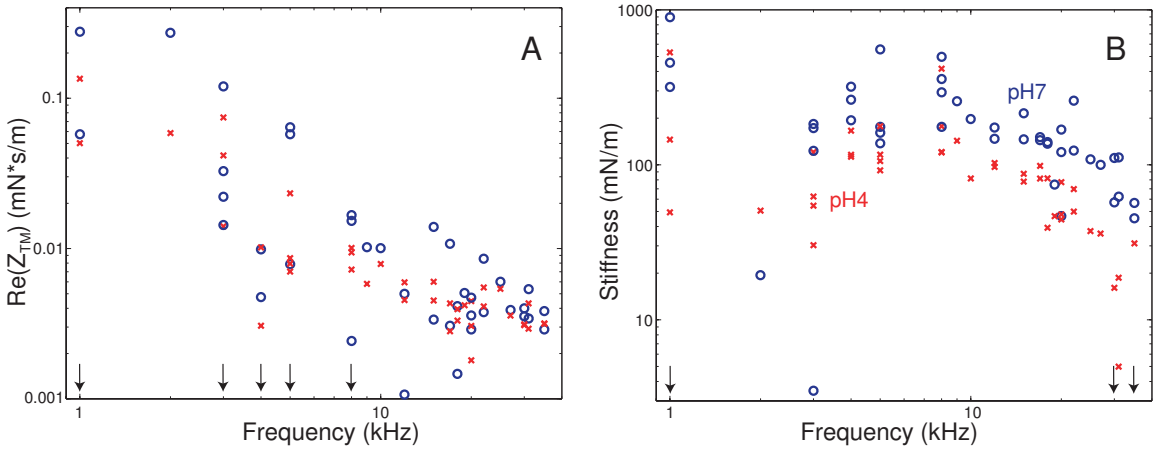

Figure 2-7: Shear impedance measurements at physiologic and acidic pH.
A, B: Shear impedance measurements as a function of frequency (n = 4 TM samples). The real component of shear impedance, $Re(Z_{TM})$ (A), plotted against frequency at pH 7 (o) and pH 4 (x). Stiffness is computed from the imaginary component of TM impedance multiplied by frequency, $\omega Im(Z_{TM})$ (B).

parameters through the body of the TM. Although we are stimulating radially, the shear direction is in the transverse cochlear direction. These parameters are relevant to TM waves since the TM's transverse properties are believed to be similar to its longitudinal properties given the structure of the TM's striated sheet matrix [41].

2.2.5 Effect of altering KCl concentration on TM wave properties

To clarify the mechanism by which pH is decreasing TM stiffness, we varied TM fixed charge by flooding the TM with excess mobile counterions. By increasing the bath concentration of KCl surrounding the TM from 174 mM to 1M, we increased the charge shielding by free ions around the fixed charges in the TM. By multiplying the concentration of free ions around the TM by roughly a factor of five, we have roughly decreased the TM's effective fixed charge concentration by the same factor [24]. Despite this drastic decrease in the concentration of fixed charge in the TM, we found only a slight decrease in decay constant and no change in TM wave speed as shown in figure 2-9 ($Median \pm \frac{IQR}{2}$ from 10 - 20 kHz for the four TM samples

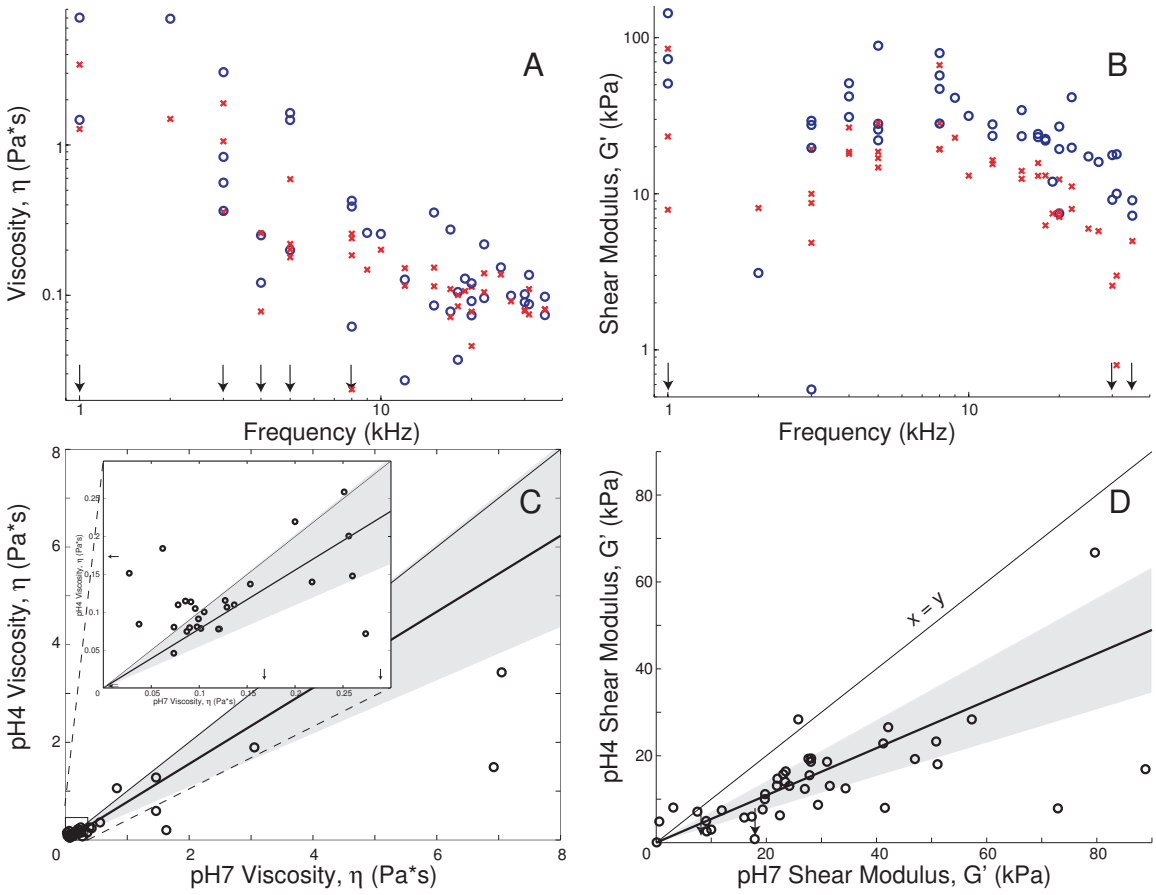

Figure 2-8: TM material properties from shear impedance measurements at physiologic and acidic pH.
A, B: Shear viscosity and shear storage modulus computed from Z_{TM} as described in equation 2.3 and plotted here as a function of frequency. C, D: Material parameters from A and B collapsed across frequency. Each point represents one frequency for a single piece of TM at physiologic (x-axis) and acidic (y-axis) pH values. The thick line indicates the median, and the shaded regions show the interquartile range for the two trials ($\frac{\eta_{pH4}}{\eta_{pH7}} = 0.78 \pm 0.23$; $\frac{G'_{pH4}}{G'_{pH7}} = 0.54 \pm 0.16$ ($MED \pm \frac{IQR}{2}$)). Axis limits were chosen to clearly show the bulk of the data, and any excluded data points are indicated by arrows. The inset shown in E shows the region where the bulk of the shear viscosity data points lie. This inset does not obscure any data points from the figure on which it is superimposed.

measured: $\sigma_{AE} = 147 \pm 63\mu$m and $\sigma_{1MKCl} = 114 \pm 66\mu$m $v_{AE} = 6.7 \pm 1.9$ m/s $v_{1MKCl} = 6.7 \pm 1.7$ m/s). A factor of five change in charge seems to have a smaller effect on TM decay constant – and by extension stiffness – than lowered pH. These findings suggest that charge plays a significantly smaller role in the TM's stiffness change due to pH than a potential conformational change in protein structure. In fact, if the only effect of lowered pH were a two-fold decrease in fixed charge, we would predict little to no change in TM dynamic properties from this effect alone.

2.2.6 Fixed charge measurements of mutant TMs with decreased stiffness

To further clarify the mechanism underlying the role of pH on decreased TM stiffness, we looked at the difference in charge between normal and TectB$^{-/-}$ mutant mouse TMs. Lowering the pH around the TM from 7 to 4 has a similar effect on TM waves as Ghaffari et al. saw in TectB$^{-/-}$ mutant mice, namely a decrease in TM stiffness by roughly a factor of two in the basal regions of the cochlea [30]. We performed charge measurements on TMs extracted from TectB$^{-/-}$ mutants and compared them to normal mice. We found no significant difference in the fixed charge concentration between these mice as shown in figure 2-10 (TectB$^{-/-}$: $c_f = -5.78 \pm 0.35$ mmol/L, n = 4; Wild-type: $c_f = -5.82 \pm 0.61$ mmol/L, n = 4). Since TectB$^{-/-}$ mutants and normal mice have no difference in their fixed charge concentrations, the mechanism underlying decreased stiffness in TectB$^{-/-}$ TMs compared to those from normal mice is likely to be a conformational change in the overall TM structure due to the knocking out of the β-tectorin protein.

2.3 Discussion

Our measurements indicate that TM wave properties in samples from human cadavers are comparable to those from freshly dissected specimens. We found that although fixed charge density is sensitive to the effects of death after two days, this change

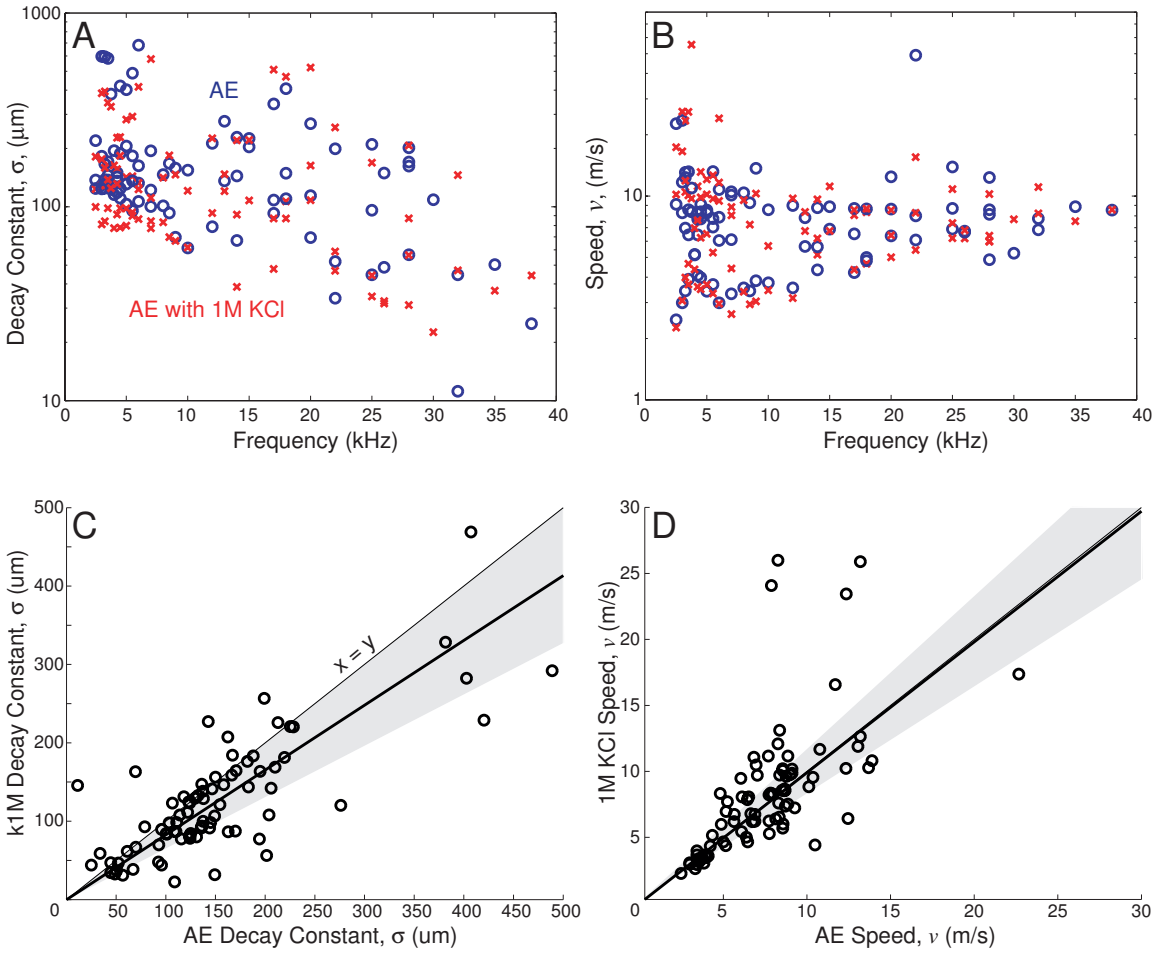

Figure 2-9: TM wave parameters measured at physiologic and elevated KCl concentrations.
A,B: Wave parameters as a function of frequency (n = 4 TM samples). Wave decay constants, σ, and wave speeds, v, are shown with the TM surrounded by AE (o) and AE with 1M KCl (x). The physiologic concentration of KCl in AE is 174 mM. C, D: Wave parameters from the top row collapsed across frequency. Each point represents one frequency for a single piece of TM at physiologic (x-axis) and higher KCl (y-axis) values. Median and inter-quartile ranges are indicated by thick lines and shaded regions, respectively, and should be compared to the thin, unity line ($\frac{\sigma_{1MKCl}}{\sigma_{AE}} = 0.83 \pm 0.17$; $\frac{v_{1MKCl}}{v_{AE}} = 0.99 \pm 0.17$ $(MED \pm \frac{IQR}{2})$).

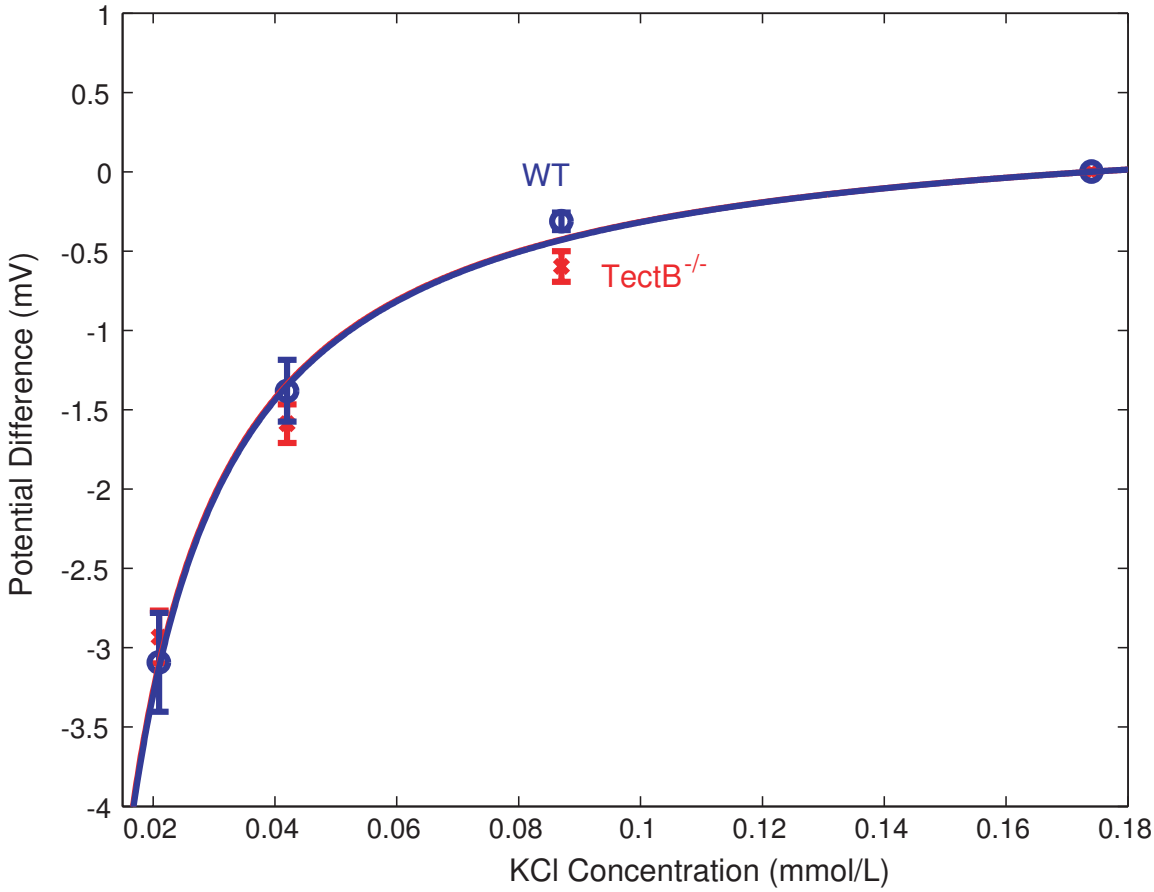

Figure 2-10: Fixed charge measurement of TectB$^{-/-}$ mutant versus wild-type TM samples

The potential difference measured across the TM is plotted against the concentration of KCl in the chamber underneath the TM. Fixed charge values are obtained by fitting a Donnan relationship from equation 2.2. Mean and IQR fixed charge values obtained from these data are as follows: TectB$^{-/-}$ $c_f = -5.78 \pm 0.35$ mmol/L (n = 4); Wild-type $c_f = -5.82 \pm 0.61$ mmol/L (n = 3).

did not significantly impact wave properties. These findings led us to more carefully study the effect of charge on TM waves using pH and charge shielding. We found that reducing bath pH alters TM material properties in a similar way as was observed in TMs from TectB$^{-/-}$ mice. We previously showed that the TectB$^{-/-}$ mutation causes sharper tuning at mid to high frequencies by predominantly altering the shear storage modulus of the TM. The reduction in wave spatial extent by 40% (figure 2-6) at acidic pH is consistent with TectB$^{-/-}$ results and is surprisingly driven by changes in shear storage modulus but not charge. The changes in TM decay constant cannot be explained by a change in TM shear viscosity or damping in the subtectorial space. Rather, the measurements at different bath pH values and ionic concentrations provide new insight into the role of TM charge in controlling stiffness and cochlear spread of excitation.

2.3.1 Molecular mechanisms controlling TM stiffness

Previously, we found that decreasing the pH of AE surrounding the TM from 7 to 3.5 roughly halves the magnitude TM fixed charge (-7.1 mmol/L at pH 7 and +3.0 mmol/L at pH 3.5) [31]. This roughly two-fold drop in the magnitude of fixed charge density could be responsible for a significant decrease in the magnitude of a cartilaginous tissue's shear stiffness [45]. However, another mechanism could be responsible for the decrease in stiffness due to pH. Excess hydrogen ions due to lowered pH could bind to particular sites of macromolecules in the TM, causing conformational changes that result in decreased TM stiffness [24]. It is also possible that the reduced stiffness observed is due to a combination of both conformational and fixed charge effects of pH on the TM.

Our measurements of TM wave properties with greatly increased KCl concentrations surrounding the TM suggest that drastic changes in fixed charge alone do not cause wave properties to change significantly. These findings suggest that despite pH's role in decreasing TM fixed charge, pH decreases TM stiffness by a molecular mechanism that is different from charge. The most likely mechanism is a conformational change in some of the TM protein constituents. To explore this possibility, we

can look at the effect of pH on each individual constituent of the TM. Other than water, the TM is largely composed of collagen and a series of glycoproteins. Previous studies have found partial denaturation of collagen aggregates at pH 4 [76] which could lead to decreased stiffness compared to its normal state. Due to the nature of the ultrastructural studies looking at the role of pH on collagen, it is difficult to determine if this effect due to pH is reversible. However, given that collagen aggregates are largely acellular, one can imagine the effect to mostly reverse once the excess hydrogen ions are removed and pH is returned to normal.

In addition to collagen, the TM contains three glycoproteins that are only found in the inner ear and nowhere else in the mammalian body: α-tectorin, β-tectorin, and otogelin. From polypeptide sequences of the tectorins, it has been revealed that these proteins both have a common zona pellucida (ZP) domain [52] that may be critical to their function. While α-tectorin has two other major constituents – a cystine rich domain and a nidogen/entactin domain, the only constituent of β-tectorin is a single ZP domain. Given the crystal structure of ZP domains [62] and the fact that the vast majority of β-tectorin protein is a ZP domain [32], we can infer how the structure of β-tectorin may contribute to TM mechanical properties. Analysis of ZP domain structure has revealed that components within the domain are oriented so that the protein's overall charge is neutral with opposite charges on its two ends (the ZP-N and ZP-C subdomains) [40]. The overall neutral charge of ZP domains explains why TMs from TectB$^{-/-}$ mice had identical charge to their wild type counterparts. This result also reveals that the bulk of the TM's charge likely comes from other constituents such as the cystine rich and nidogen/entactin domains of α-tectorin. In contrast to the results reported here, point mutations in α-tectorin have revealed a reduction in fixed charge [58], affirming this possibility. Ultimately, these measurements reveal that charge is likely not the dominant factor in controlling TM stiffness since both mutations in α-tectorin [58] and β-tectorin [30] have changes in TM stiffness despite having different fixed charge characteristics.

Our measurements of TM waves and TM shear impedance both involve shearing of the TM. We believe that TM fixed charge density does not play a role in changing

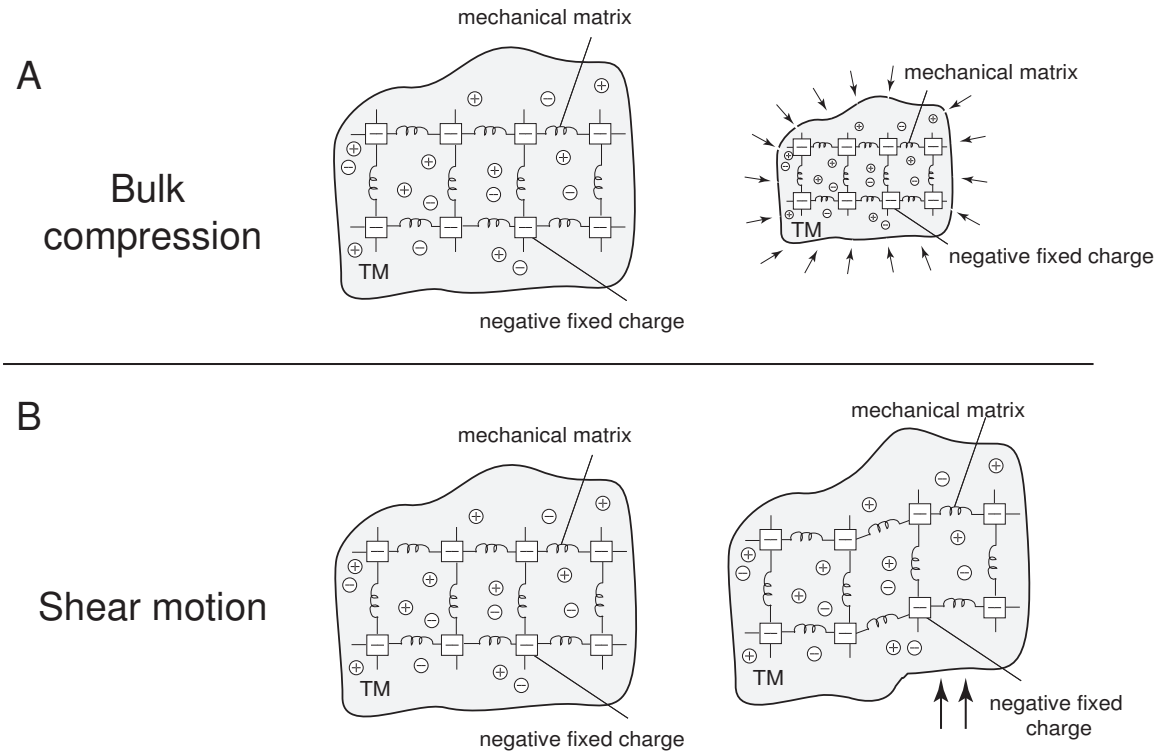

Figure 2-11: The effect of charge on compressive versus shear motions
A: In the case of bulk compression, negative fixed charges get closer together thus changing the material properties of the tissue. B: In the case of shear motion as in TM waves, negative fixed charges remain roughly equally spaced causing little change in TM material properties.

the measurements in this study because of the direction of TM stimulation. If we were to compress the TM through its bulk as shown in figure 2-11, the charges would get closer, resulting in a higher fixed charge density playing a significant role in resisting TM compression. However, in the case of shear motions as shown in figure 2-11, the charges remain roughly equally spaced resulting in little change in the force they feel. The importance of TM fixed charges should also not be neglected due to the findings shown here. TM electrokinetics has been suggested to potentially create a positive feedback mechanism on hair bundle motions in the cochlea [31].

2.3.2 Shear probe versus wave measurements of TM properties

The TM has been previously shown to undergo shear forces in the cochlea [98]. Since shear is the important direction of stimulation for the TM, that is the mode of stimulation used in our wave and shear probe measurements. During our shear probe measurements, the probe is shearing the TM through its bulk; however, in our wave measurements, the TM is being sheared radially with the wave propagating longitudinally. In order to compare these two orthogonal measurements, we considered previous structural studies of the TM's properties suggest that its longitudinal properties are similar to the properties through its bulk [41, 32]. We also used our shear probe estimates of material parameters with changing pH to infer the change in wave properties due to pH as mentioned above. Finally, to confirm that TM stiffness in the longitudinal direction was dropping due to pH as measured by our probe through the TM bulk, we fit our wave data to a finite-element viscoelastic model of TM wave propagation [29]. The fits of this model to our wave data confirm that the decreased wave decay constant with little change in wave speed that we observed due to lowered pH can be achieved by decreased stiffness with little change in shear viscosity.

2.3.3 Implications for models of the TM

To determine if predictions from cochlear models agree with our findings, we compared our measurements of the effect of TM stiffness on spread of excitation to two cochlear models: one by Neely which treats the TM as a traditional resonance structure [65] and one by Meaud and Grosh which includes TM longitudinal coupling [61]. In Neely's model, the BM and TM are treated as coupled, tuned resonators where outer hair cells provide a positive feedback path between the TM and BM. When decreasing the TM stiffness by a factor of two, the Neely model predicts a significant decrease in sensitivity. The model shows this response to decreasing stiffness at locations along the entire length of the cochlea. In Neely's model, the cochlea is treated as a series of coupled resonators which must be tuned to properly interact and create maximum

sensitivity. By reducing TM stiffness, we have cut in half this coupling along the entire length of the cochlea, resulting in a dramatic change in sensitivity. Conversely, in the model by Meaud and Grosh which considers longitudinal coupling of cochlear structures by the TM, they found that decreasing TM stiffness by roughly a factor of two has a very different effect on cochlear properties. In this case, decreasing TM stiffness results in a slight decrease in cochlear bandwidth with little change in sensitivity. Our measurements suggest that decreasing TM stiffness controls spread of excitation in the cochlea via TM waves. These findings agree with those from TectB$^{-/-}$ mutant mice. Based on direct measures of cochlear tuning in these mice, we see that models that neglect the TM's longitudinal coupling properties do not explain TM-based changes in tuning.

2.3.4 Implications for cochlear tuning

Our measurements of TM wave parameters with physiologic and lowered pH suggest that stiffness is controlling the extent of TM waves and having little effect on their speed. We used a measurement of TM material parameters with microfabricated shearing probes and found that stiffness was the predominant parameter that we were controlling with pH. A viscoelastic model of TM wave parameters predicts that decreased stiffness should result in a decreased wave decay constant with little effect on speed, leading to similar effects on tuning as was found in the TectB$^{-/-}$ mutant model.

In the Tectb$^{-/-}$ mutant mouse, segments taken from the base of the cochlea where sharpened tuning was observed had stiffness decreases of roughly a factor of two, similar to the changes observed here due to lowered pH. The exact nature of this mechanism in TectB$^{-/-}$ mutants remains to be determined, but its effect is different along the length of the cochlea. In the basal cochlear regions where sharpened tuning was observed in these mice, the TMs had decreased stiffness with little change in shear viscosity; whereas, in the apical cochlear regions where highly elevated thresholds were observed, the TMs had decreased stiffness and significantly decreased shear viscosity [77, 30].

Similar to the basilar membrane (BM) wave [91, 74, 11], the TM wave has been suggested to have a significant effect on tuning in the cochlea [30]. In particular, as the TM spatial extent decreases, fewer hair cells are stimulated along the cochlea, resulting in more sharply tuned auditory nerve responses. Our findings of changes in TM wave parameters with lowered pH suggest that stiffness in the TM provides a mechanism for altering decay and by extension, tuning, in the cochlea.

2.4 Conclusions

The motivation for this study was the fact that fixed charge density decreases when TM samples are aged 48 hours. We wanted to perform a series of experiments to determine if this decrease in fixed charge density will affect the TM wave measurements from human cadaveric bones.

In this study, we show that pH modulates TM stiffness and the spread of excitation of TM waves. Although pH modulates TM charge, it is possible that another mechanism is responsible for the change in TM stiffness due to pH. Therefore, we modified charge in another way by increasing the charge shielding around the TM using KCl. We show that this causes no significant effect on TM wave properties. We also show that TMs from TectB$^{-/-}$ mutant mice do not show significant changes in fixed charge density, further suggesting that charge is not the important mechanism controlling TM stiffness and cochlear spread of excitation.

Charge is usually associated with stiffness in connective tissues such as cartilage [45] and has been implicated in TM hydration [24], electrokinetics [31], and material properties [23]. These results exclude the possibility that charge plays a role in the TM's shear stiffness. This result is surprising but understandable given that the relevant direction of motion is shear not compression.

Although TM fixed charge density decreased by roughly 30% in aged mouse samples, we conclude that this change in fixed charge density should not affect TM wave properties significantly. In the next chapter, we outline modeling investigations of how TM material properties should affect wave properties. In the following chapter

(chapter 4), we will further investigate the effect of time on wave properties by directly comparing TM wave decay constants and speeds between fresh and aged samples.

Chapter 3

TM dynamic modeling allows predictions of material properties' effect on TM wave parameters

Historically, models of cochlear function have represented the TM as a stiff lever with a compliant hinge, a resonant mass-spring system, or as an inertial body [16, 14, 6, 66, 67, 3, 97, 56]. However, these models exclude important global phenomena, such as longitudinal coupling (spread of excitation) [96, 2, 61]. It is now clear that the TM's physical properties vary with longitudinal position [30, 29, 27, 26, 36, 73, 59, 38, 37], and that longitudinal coupling manifested in the form of traveling waves contributes to hearing mechanisms [29, 30, 80, 72, 39, 61, 5, 55, 47]. These waves extend over large cochlear distances and stimulate multiple rows of hair cells [29]. Sharpness of tuning in the cochlea has been associated with viscous parameters related to the tectorial membrane such as subtectorial damping [3]. However, in the TectB mutant mouse, the only mutant model to date where sharpness of tuning increased due to the mutation [77], TM stiffness decreased with little change in shear viscosity [30]. This suggests that the underlying material properties that govern TM waves may be critical in determining the sensitivity and frequency selectivity of hearing.

In this chapter, we explore two models of TM waves to determine how TM material properties should affect TM wave properties.

3.1 Viscoelastic Model of TM Waves

To determine TM wave parameters from material properties, we used a viscoelastic model [33, 29]. This model predicts wave decay constant, σ, and wave speed, v, from shear storage modulus, G', and shear viscosity, η, as follows:

$$\sigma = \sqrt{\frac{2(G'^2 + \omega^2\eta^2)}{\rho\omega^2(\sqrt{G'^2 + \omega^2\eta^2} - G')}} \qquad v = \sqrt{\frac{2(G'^2 + \omega^2\eta^2)}{\rho(\sqrt{G'^2 + \omega^2\eta^2} + G')}} \tag{3.1}$$

where ρ is the density (taken to be the density of water), and ω is the angular frequency ($\omega = 2\pi f$).

We looked at contour plots of decay constant, σ, and speed, v, against the material parameters of shear storage modulus, G', and shear viscosity, η at 1 kHz and 20 kHz (figure 3-1). At low frequencies, we see that speed depends almost entirely on stiffness with little change caused by changing shear viscosity (figure 3-1 B). However, at high frequencies, which are more relevant to rodent hearing, we see something very different. In the range of material parameters that we measured with our shear impedance probes as highlighted in figure 3-1 C, we see that changes in shear storage modulus, G', have a significant effect on the wave decay constant, σ. Conversely, below 40 kPa, changes in shear storage modulus will roughly follow a constant-speed contour line, resulting in only a slight decrease in wave speed at higher frequencies (figure 3-1 D). This model suggests that at acoustic frequencies relevant to rodent hearing, TM speed is more highly dependent on shear viscosity, η.

The contour plots in figure 3-1 are relevant when we measure TM material properties and wish to determine the wave parameters that should result, as we did with our shear impedance measurements. However, in other cases such as when comparing TM wave properties across species, we take wave measurements and wish to determine the material properties from these values. In that case, it is useful to have the inverse plots of those shown in figure 3-1 where instead of plotting contours of decay constant and speed against shear modulus and viscosity, we look at contour lines of shear modulus and viscosity that should result from given wave speeds and

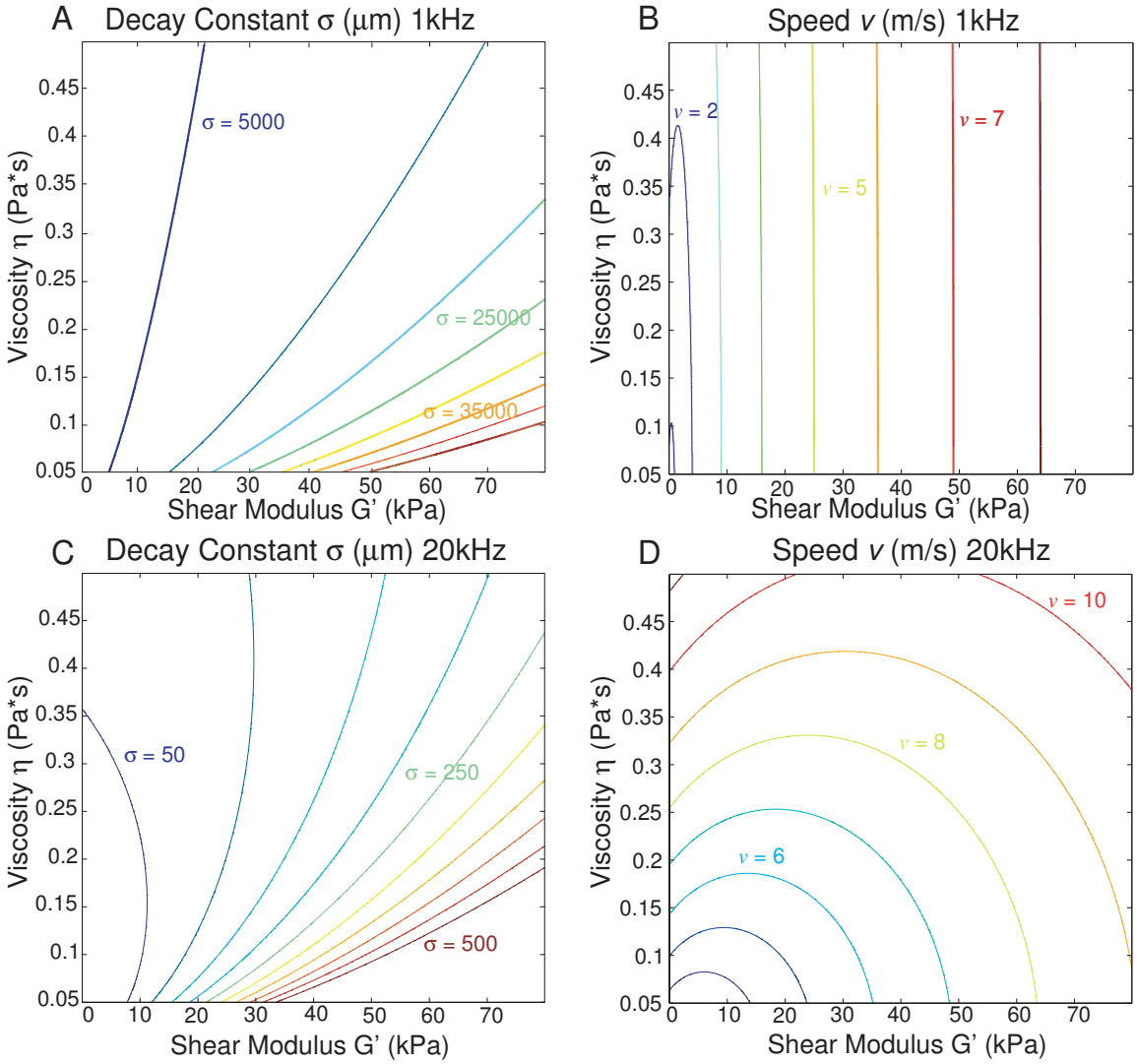

Figure 3-1: Viscoelastic model of TM wave parameters.
A, C: Contour plots of decay constant, σ, against shear viscosity, η, and shear storage modulus, G', at 1 kHz (A) and 20 kHz (C). B, D: Contour plots of speed, v, against shear viscosity, η, and shear storage modulus, G', at 1 kHz (B) and 20 kHz (D). Colored numbers on figures correspond to decay constant in μm or speed in m/s.

decay constants. These contour plots are shown in figure 3-2. These contour lines are effectively inverses of those shown in figure 3-1. We see that as we go from 1 to 20 kHz, the major dependence of shear viscosity rotates from TM wave decay constant to wave speed.

3.1.1 Viscoelastic model correctly predicts effects of changing stiffness and viscosity on TM waves

As outlined in chapter 2, we found that modulating stiffness controlled TM wave decay constant, not speed. This was quite surprising given traditional models of the TM's role in the cochlea. However, upon careful inspection of a viscoelastic model of TM waves that allows the tissue to distribute its action along the length of the cochlea instead of being restricted to a particular cross-section, our measurements of the effect of modulating stiffness fit. We wanted to further test the viscoelastic model by modulating TM viscosity using poly-ethylene glycol (PEG). These measurements were performed by Jon Sellon in our group [78]. In these measurements, Jon found that increasing viscosity affects both TM wave speed and decay constant. Again, we found these results very surprising given that viscosity is the main determinant of TM wave speed, not stiffness as would be assumed in a traditional cochlear model [3].

If we combine the shear impedance material property estimates while modulating stiffness using pH (chapter 2) and modulating viscosity using PEG ([78]), we get a complete picture of the effect of material properties on TM waves as shown in figure 3-3. In particular, following the pH bubbles in figure 3-3, we see that modulating TM stiffness (pH 7 G' 20 kPa; pH 4 G' 9 kPa) should roughly halve the spread of excitation of TM waves but have little effect on TM wave speed, as was shown by direct wave measurements while varying pH in chapter 2. Conversely, following the PEG bubbles in figure 3-3, we see that modulating TM viscosity (AE η 0.15 Pa$*$s; AE + PEG η 0.7 Pa$*$s) should roughly double TM wave speed while also halving spread of excitation. Jon confirmed these predictions with direct wave measurements

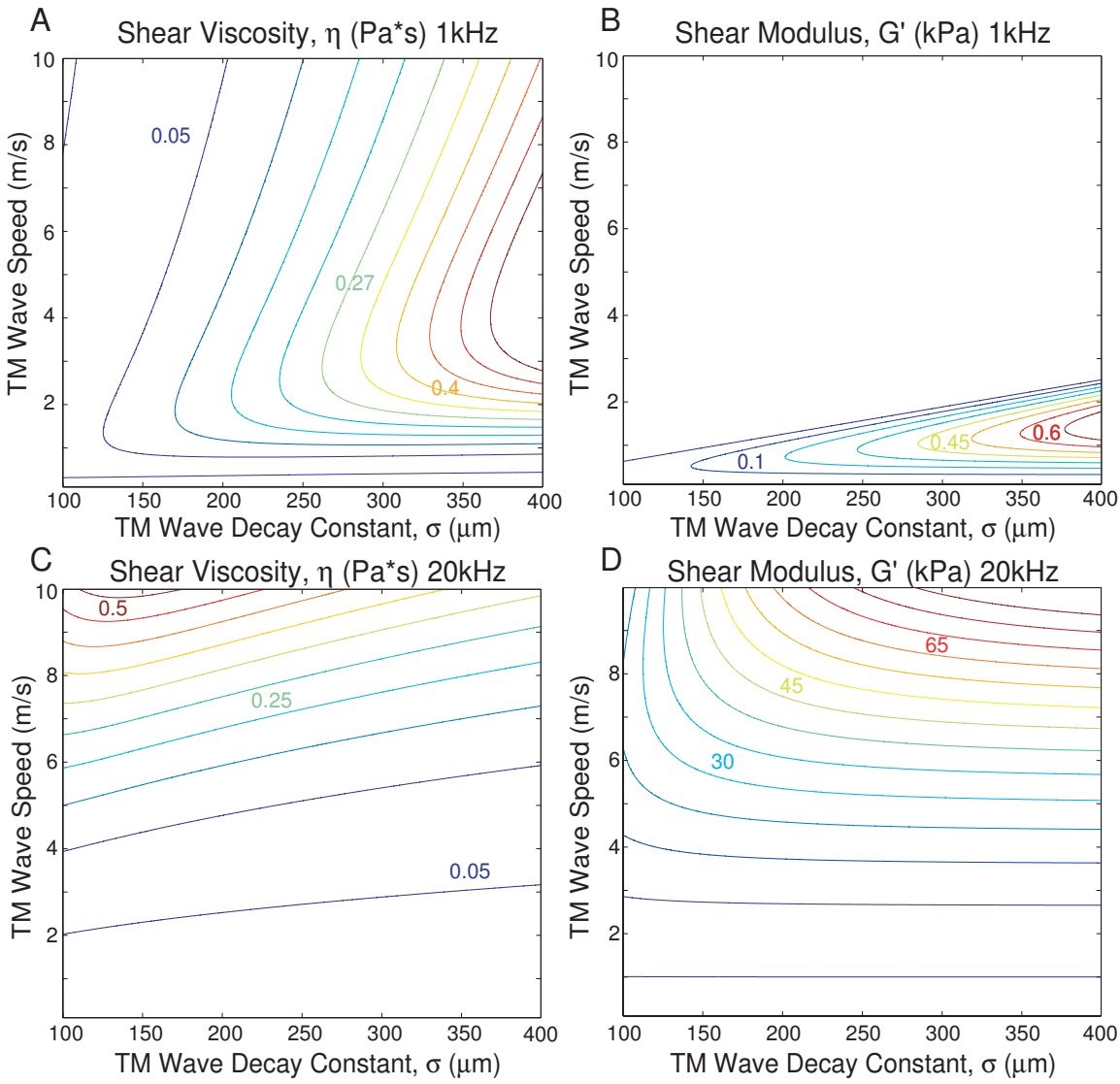

Figure 3-2: Viscoelastic model of TM wave parameters.
A, C: Contour plots of shear viscosity, η, against decay constant, σ, and speed, v, at 1 kHz (A) and 20 kHz (C). B, D: Contour plots of shear modulus, G', decay constant, σ, and speed, v, at 1 kHz (B) and 20 kHz (D). Colored numbers on figures correspond to shear modulus in kPa or shear viscosity in Pa$*$s.

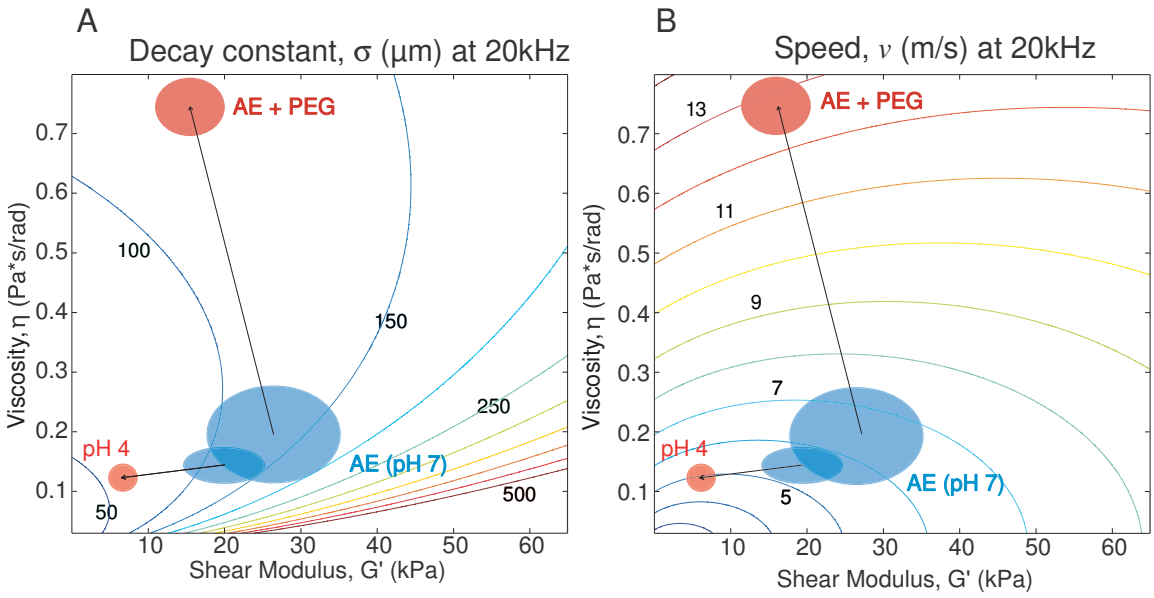

Figure 3-3: Viscoelastic model of TM wave parameters including shear impedance material estimates.
A: Contour plot of decay constant, σ, against shear viscosity, η, and shear storage modulus, G', at 20 kHz. B: Contour plots of speed, v, against shear viscosity, η, and shear storage modulus, G', at 20 kHz. Superimposed on the contour plots, we have included our material property estimates using shear impedance probes while varying pH to modulate stiffness (chapter 2) and varying PEG concentration to modulate viscosity [78]. Colored numbers on figures correspond to decay constant in μm or speed in m/s.

while varying PEG concentration [78].

The dominant effects of stiffness – on spread of excitation – and viscosity – on speed – are both very surprising. Usually, one associates loss mechanisms such as viscosity with spread of excitation and energy storage elements such as stiffness with speed. However, here we see that the dependence of TM wave properties of these material properties is reversed. Although counterintuitive, these measurements follow if we look at the TM as a distributed structure instead of a resonance element [29, 61].

3.2 Poroelastic Model of TM Waves

The TM is a highly hydrated gel made up of 97% water. Therefore, it is feasible that the water could be moving differently from the TM matrix during wave stimulation.

We believe that a viscoelastic model of TM waves is a good approximation since our wave experiments involve pure shear motion. If the TM were being compressed, we would expect fluid to be displaced relative to the matrix to allow for a decrease in volume. In our shear measurements, we expect the relative motion of fluid to solid to be minimal. However, to determine if there might be any relative solid to fluid motion, we created a finite element poroelastic model of TM waves. In this model, the fluid, M_f, and solid, M_M, masses are treated separately (figure 3-4). Adjacent solid masses are coupled by a spring, k_m, and adjacent fluid masses are coupled by a damper, b_f, which relates to the fluid viscosity. The chains of solid and fluid masses are coupled via a damper, b_{sf}, which represents the resistance to the relative motion of the solid and fluid in the TM.

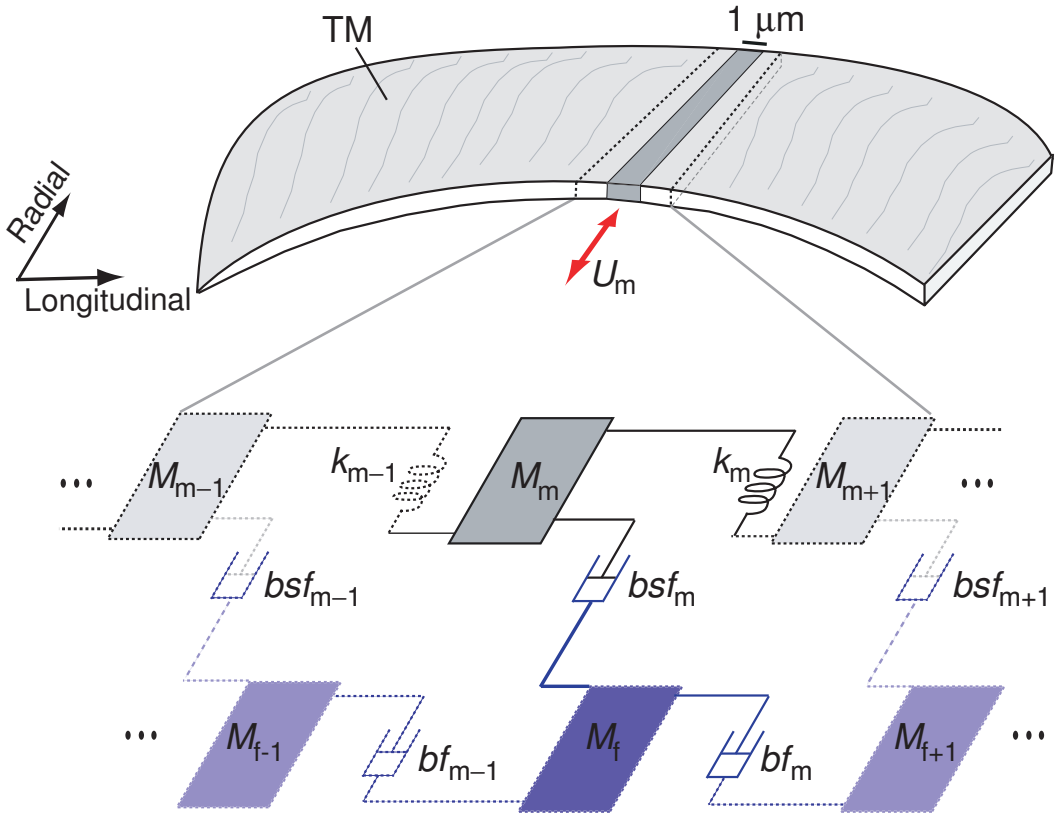

Figure 3-4: Distributed impedance poroelastic model of TM wave parameters. The TM is separated into small slices, each of which is represented by a solid and fluid mass segment. The solid elements are connected by springs. Adjacent fluid elements are connected by dampers, and the solid and fluid elements are coupled by a damper element. Adapted from Ghaffari et al., 2007.

To verify this model, we set the solid to fluid viscosity, b_{sf}, to be zero and simulated the responses. This condition is identical to the viscoelastic case described above. Plotting contour plots from this poroelastic model turned into a viscoelastic model with the contour plots from the viscoelastic equation shown in figure 3-1, we found the curves to lie almost perfectly on top of one another with minimal differences between the two. We therefore concluded from this simple case test that our model simulation was correct.

In figure 3-5, we are showing the results of this model when we vary fluid viscosity and shear modulus, represented in figure 3-4 by the spring k_m. The other poroelastic model parameters for this simulation were set as follows: density of fluid equal to density of water, ρ_f; density of solid, $\rho_s = 1.3 * \rho_f$, $\frac{fractionfluid}{fractionsolid} = 97\%$, $b_{sf} = 0.2$ Pa$*$s. We see that these contour plots look somewhat similar to the plots in figure 3-1. That is, at 1 kHz, wave speed has little to no dependence on the viscosity term; whereas, at 20 kHz, these contour lines curve so that now viscosity largely determines speed. We also see a similar dependence of decay constant on both the viscosity term and the stiffness term at low and high frequencies as we did in the viscoelastic case.

In addition to simulating these parameters, we looked at the effect of varying the solid to fluid viscosity term, b_{sf}, on decay constant and speed, and we tested the effect of varying the ratio of solid to fluid mass on wave parameters. Interestingly, the results of these simulations showed contour lines of decay constant and speed that had no dependence on either b_{sf} or the ratio of solid to fluid mass. Namely, the contour lines were perfectly parallel to the axes for these two parameters, indicating that changes in these parameters do not affect wave decay constants or speeds. This finding suggests that the poroelasticity of the TM is not important for wave propagation. As we originally expected, a viscoelastic model seems to include all of the important parameters for understanding how TM material properties determine wave dynamics.

3.3 Conclusions

Our findings outlined in chapter 2 that stiffness controls the spread of excitation of TM waves were quite counterintuitive. Here we show that they agree with predictions from a simple viscoelastic model of TM wave propagation. We also found that this model correctly predicts the changes in TM wave properties due to increased viscosity. These predictions are opposite those made by classical cochlear models that do not include longitudinal coupling in the TM.

Since the TM is so highly hydrated, we investigate whether a poroelastic model allowing relative solid and fluid motion would yield different results from a viscoelastic case. We found no significant differences between the predictions of the poroelastic case and concluded that the viscoelastic approximation is suitable for TM waves. Since the TM wave involves pure shear motion, it is not surprising that the fluid does not have significantly different motion from the solid matrix of the TM.

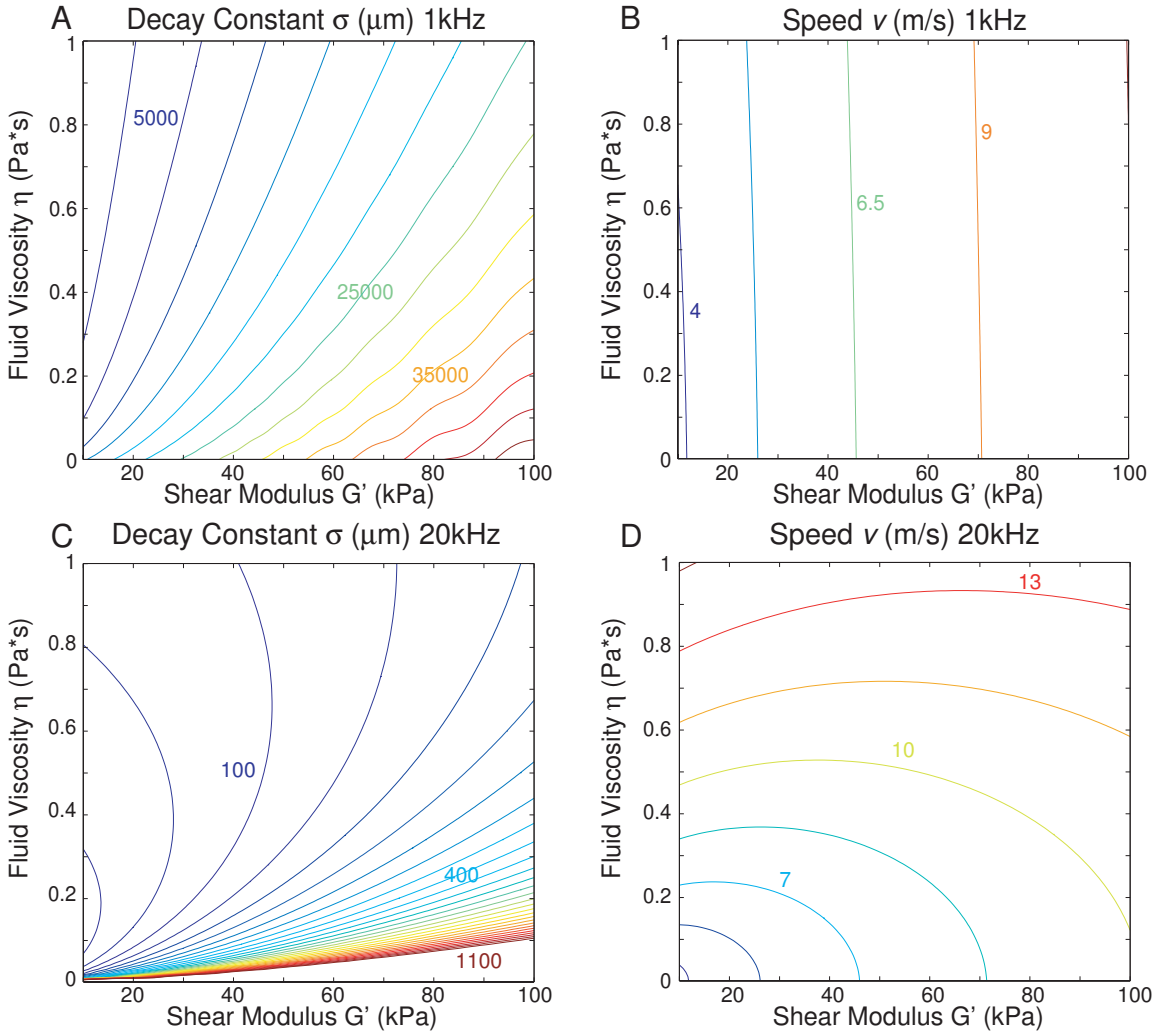

Figure 3-5: Poroelastic model of TM wave parameters.
A, C: Contour plots of decay constant, σ, against fluid viscosity and shear storage modulus, G', at 1 kHz (A) and 20 kHz (C). B, D: Contour plots of speed, v, against fluid viscosity and shear storage modulus, G', at 1 kHz (B) and 20 kHz (D). Colored numbers on figures correspond to decay constant in μm or speed in m/s.

Chapter 4

Cochlear Tuning: Of Mice and Men . . . and Guinea Pigs

Hearing plays a critical role in the development of human speech and intelligence. It is widely known that without hearing, normal speech will not develop. Around the world, newborn babies are now routinely screened at birth for hearing loss because of the significant impact this disability can have on a person's development and early education [94].

Detailed measurements have suggested much better discriminating capabilities in human neural responses and speech discrimination tasks compared to other mammals [7, 85]. These high level differences are not surprising given our sophisticated brains compared to those of other mammals. However, measurements by Shera et al. have suggested that the difference in human hearing also lies in peripheral hearing mechanics [81, 48]. This is far more surprising given that the structure of the organ of Corti is remarkably well conserved across all mammals. The differences between a rodent and human cochlea are only apparent to a trained eye after careful study of the detailed anatomy [63, 21]. As a demonstration here we show three cross-sections of the organ of Corti from a human, guinea pig and mouse in figure 4-1. We have purposely removed all scale bars, and we challenge the reader to guess which organ belongs to which of these three species (the answer can be found in the caption of the figure). From these similarities, one might conclude that the differences in human

hearing should be due to neural processing performed beyond the organ of Corti in the brain. However, the comparative analysis done by Shera and others used measures of cochlear tuning, suggesting that a difference must lie within the peripheral hearing organ.

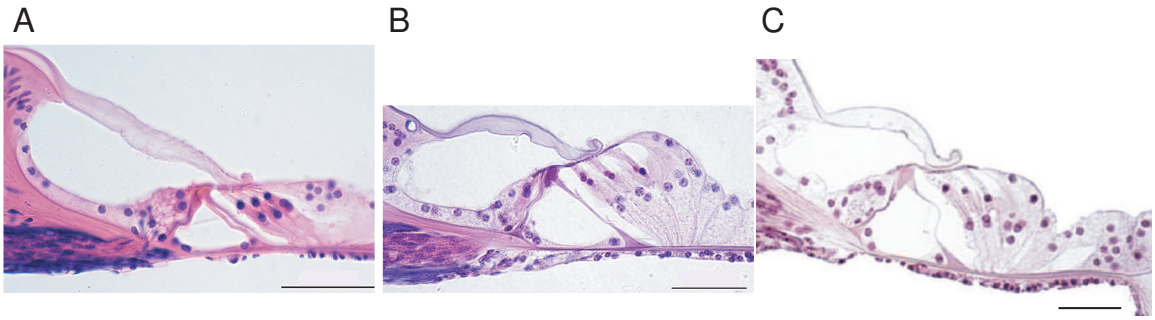

Figure 4-1: Microscopy of organ of Corti sections in human, guinea pig and mouse The reader is challenged to determine which image belongs to which mammal. A: Mouse (image courtesy of Nakajima and O'Malley from the Massachusetts Eye and Ear Otopathology laboratory collection Scale bar = 50 μm). B: Guinea pig (image courtesy of Nakajima and O'Malley from the Massachusetts Eye and Ear Otopathology laboratory collection Scale bar = 50 μm). C: Human (image from Hossler [43] Scale bar = 50 μm)

Gel-like structures such as the tectorial membrane (TM) overlying cochlear hair bundles are associated with almost all hair cell organs, from the simplest lateral line in fish to the mammalian inner ear [57]. In order for gel structures to have withstood millions of years of evolutionary pressure in such a variety of sense organs, they must have played a critical role in the function of these structures.

In this work, we explore the possibility that TM properties could underlie the predicted differences in human cochlear tuning. This structure was recently shown to support longitudinally propagating waves [29]. In a mutant mouse model, TM wave properties were shown to relate to cochlear tuning, linking a passive measurement in an excised cochlear tissue to an active hearing property [30]. Thus the TM wave gives us a window into human cochlear function. In this study, we perform a new measurement of TM waves in humans and compare our findings to TM wave measurements in guinea pigs and mice to determine if the TM plays a role in the predicted tuning differences in humans.

Previously, TM material parameters have been measured along the length of the cochlea and in different regions of the TM in samples taken from gerbils, guinea pigs, and mice [2, 83, 37, 73, 73]; however, the majority of the techniques used have measured these parameters at frequencies of 10 Hz or less. These low frequencies are not relevant to hearing in the rodent species from which TMs were extracted. Microfabricated shear probes have been used to measure mouse TM material properties up to acoustic frequencies of 10 kHz [36]; however, repeating the fine contact required between the microfabricated probe and TM sample across different samples is difficult, making this technique difficult to use across multiple species. Waves have been used to measure TM material properties in samples taken from mice up to acoustic frequencies [29, 30, 47]. In this work we use waves to compare TM material properties across multiple species in frequency ranges relevant to their hearing. Since we are the first to use a single measurement technique across species, we are in a unique position to outline the differences in material properties of TM samples from different mammals.

4.1 Materials and Methods

4.1.1 Extraction of human TM samples

Human temporal bones were obtained from anonymous adult donors after permission was granted to obtain specimens for research at Massachusetts General Hospital. Temporal bones were removed within 24 hours post mortem and were refrigerated in 0.9% normal saline for several hours before being transferred to a bath of artificial endolymph (AE) containing 174 mM KCl, 5 mM Hepes, 3 mM dextrose, 2 mM NaCl, and 0.02 mM $CaCl_2$. The bath was titrated to pH 7.2 using small quantities of KOH or HCl as necessary. Drilling was performed in the Eaton Peabody laboratory at the Massachusetts Eye and Ear Infirmary (MEEI) using universal precautions. After opening the facial recess, the round window and stapes were exposed, and the incudostapedial joint was severed to allow removal of the tympanic membrane and middle

ear cavity without disrupting the inner ear. A surgical drill (Stryker Corp., Portage, MI) with a large stainless steel drill bit was used for the majority of the drilling and a diamond-coated bit for the final thinning of the bone around the organ of Corti. Drilling took approximately three hours and was done in air at room temperature with the bone kept as moist as possible with AE from a dropper.

Once the outline of the cochlear spiral was sufficiently thinned, the bones were transported in AE to MIT where the remaining bone around the cochlear spiral was removed using a scalpel blade (no. 11) and curved surgical scissors under a dissection microscope (Wild Hexagon, Stockholm, Sweden). In one case, the entire bony capsule surrounding the organ of Corti came off. An image of this case is given in figure 4-2 A. Once the bone around the cochlea was opened, the cochlea was kept in AE. Stria vascularis was removed using fine forceps, and a needle (26 ga) was used to scrape out the organ of Corti from along the cochlear spiral. The TM was gently removed from the surface of the organ of Corti using a sterilized eyelash. TM segments were photographed to identify their origin along the cochlea then were cut into 1-2 mm segments using a needle. TM segments were transferred to a clean AE bath using a glass-tipped pipette then were used for wave measurements as described below.

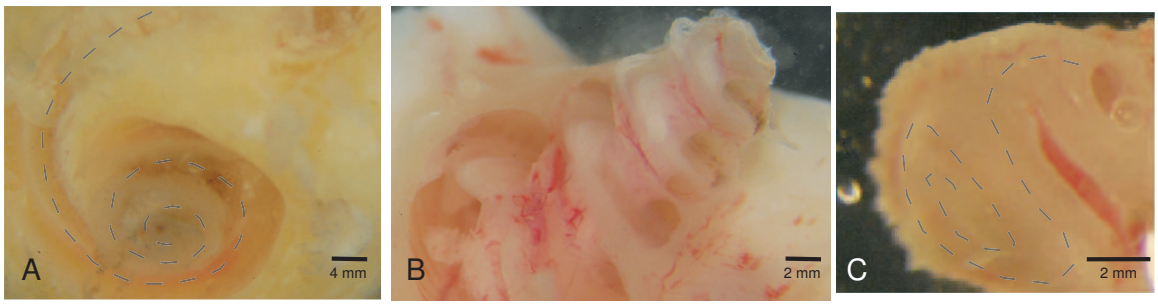

Figure 4-2: Images of isolated cochleae in human (A), guinea pig (B), and mouse (C)

Fifteen temporal bones were used in this study. The first twelve bones were previously fixed or frozen and were used for practicing drilling and TM removal. The remaining three fresh temporal bones were prepared as soon as possible, and all TM wave measurements were performed between 40 to 50 hours post mortem. The data presented here are from 21 TM segments obtained from these three fresh specimens.

4.1.2 Extraction of mouse and guinea pig TM samples

Mice and guinea pigs were euthanized by carbon dioxide asphyxiation or an overdose of urethane, respectively, followed by decapitation. All rodent TMs were extracted as much as possible in a manner similar to the way human TM samples were extracted. To this end, heads were refrigerated overnight after which temporal bones were extracted and bullae were opened and placed in 0.9% saline. After several hours, cochleae were dissected and placed in an artificial endolymph bath as described above. The cochleae were refrigerated in AE until approximately 36 hours after the animal's time of death, at which point the cochleae were dissected using a scalpel blade (no. 11) and TM samples were extracted using a sterilized eyelash. TM wave measurements were performed approximately 48 hours post mortem in both mice and GPs.

4.1.3 Measurement of TM wave properties

TM waves were generated and measured using an optical measurement system and wave chamber as described by Ghaffari et al. [29]. Briefly, isolated TM segments were suspended between two supports using Cell Tak bioadhesive as shown in figure 4-3 (Collaborative Research, Bedford, MA). One of the supports was glued down and thus remained stationary while the other was attached to a piezo-electric actuator (Thorlabs Inc., Newton, NJ). The TM was stimulated in the radial cochlear direction, and motions along its surface were measured at audio frequencies (human: 0.1-20 kHz, GP: 0.1-40kHz, mouse: 1-40kHz). Motion amplitude and phase were measured using a stroboscopic computer vision technique that allows images to be captured at eight phases of motion per cycle [15]. Radial TM displacement and phase were determined from a one-dimensional FFT taken at evenly spaced points of roughly 10 μm along the TM. Spatial decay constant, σ, was defined as the distance in μm along the TM over which the wave magnitude decays by a factor of e. The σ values for each TM were determined by fitting an exponential to the overall magnitude of the response along the TM. Speed, v, was determined by fitting a straight line to the phase as a function of distance along the TM and multiplying the inverse slope by angular

frequency.

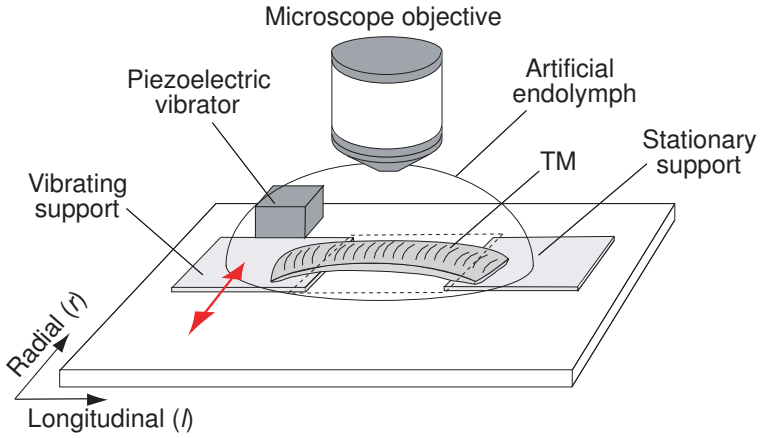

Figure 4-3: TM wave measurement apparatus
Drawing of TM suspended between two supports. A piezo-electric crystal was used to stimulate the vibrating support in the direction shown by the double-headed arrow to launch a longitudinally propagating wave along the surface of the TM. Figure reproduced from Ghaffari et al., 2007 [29].

4.1.4 Measuring TM radial shear impedance

TM shear impedance was measured using microfabricated probes as described previously [36]. Briefly, TM samples were immersed in AE and adhered to a glass slide using Cell Tak. The square tip of a microfabricated probe was then lowered onto the surface of the TM using a micromanipulator (Rucker and Kolls Inc., Milpitas, CA). The base of the probe was stimulated in two orthogonal directions (x and y as shown in figure 4-4) using a piezo-electric actuator from 50 - 800 Hz. Displacements of the base, X_b, and tip, X_p, of the probe were measured. The impedance of the TM in each direction was determined by the following equation:

$$Z_{TM}(\omega) = k_{mp}\frac{D_b(\omega) - D_p(\omega)}{j\omega D_p(\omega)} \tag{4.1}$$

where D_b and D_p represent the displacement of the base and tip, respectively, in either the x or y directions, and k_{mp} is the stiffness of the probe in the in the x (57 mN/m) or y (266 mN/m) direction.

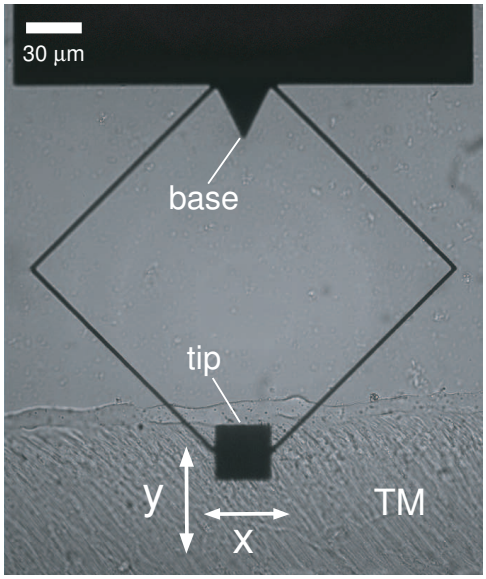

Figure 4-4: TM shear impedance measurement system
Microfabricated probes were lowered onto the surface of human TM samples tacked to a glass slide. The bases of the probes were stimulated in two orthogonal directions (x and y) using a piezo-electric actuator as described in Gu et al. [36].

4.2 Results

4.2.1 Interspecies TM morphology

TM samples obtained from humans were expectedly similar in structure and shape to those obtained from rodents. In figure 4-5, we show representative TM samples from the basal and apical regions of the three species measured. Taking the distance from the marginal band of the TM to the limbal edge, henceforth referred to as W_{TM}, we see roughly a factor of two difference between W_{TM} values in samples from mice and humans taken from analogous regions of the cochlea (tables 4.1 and 4.2). This distance marks the width of the side of the organ of Corti on top of the hair bundles, suggesting that despite the factor of 100 difference in body size of these mammals, the width of the organ of Corti, and by extension, the diameter of hair cells, do not differ as greatly. Previous studies have shown a factor of two difference in the width of the basilar membrane (BM) in guinea pigs versus humans [63]. We compared our data of TM width to previous measurements of BM width in these three species [22, 9]. We

found that in all three species, the TM and BM have comparable widths in the base, but in the apex the BM is almost twice as wide as the TM. Although the overall TM length varies from approximately 7 mm in mice to 35 mm in humans, the width and longitudinal spacing of individual collagen fibers in TMs from these animals do not differ significantly (tables 4.1 and 4.2). Previous measurements of BM width have shown a factor of two to three difference between the width in the base and apex in guinea pigs and humans [22]. The difference between TM width in tables 4.1 and 4.2 is not as great. This may be partly due to the fact that we rarely obtained samples from the extreme base of the cochlea where widths would be narrowest. It also may be that the measurements of BM width were performed on fixed tissue and therefore might not be exactly true to the real anatomy. Nevertheless, it is possible that BM width shows a bigger change from the basal regions of the cochlea to the apical regions than TM width does.

The next parameter that we measured in the tables below is the width of fibers, Δ_{fibers}. In order to measure this parameter, we measured the distance between six fibers near the marginal band of each TM then divided our measurement by 5. We found this parameter to be close to 2 μm in all cases with little to no difference in the spacing between basal TM samples. However, there does seem to be a significant difference in the human apical samples where fiber width is larger than in guinea pigs or mice. Previously, the spacing of fibers has been associated with shear modulus of the TM [83]. Therefore, from the fiber widths alone, we would predict comparable shear moduli for human, guinea pig and mouse basal TM samples but slightly decrease shear modulus for human apical TM samples compared to guinea pigs and mice.

A systematic difference that we observed in TM samples obtained from humans compared to those from rodents is the orientation of collagen fibrils in the TM. In human TM samples, the angle the collagen fibrils make relative to a tangent drawn to the marginal band, ϕ_{fibers}, is smaller than in mice and guinea pigs. This can be seen in figure 4-5 and is quantified in tables 4.1 and 4.2. This was observed in all human TM samples and is consistent with previous observations of human TM morphology [91]. We could imagine that the angle of TM fibers might affect TM shear modulus, but

since the fibers are generally equally spaced, we don't expect this to have a big effect. We also explored what effect the angle of collagen fibers might have on TM motions but did not find systematic differences in the angle of TM wave motion relative to the fiber angle.

Table 4.1: Apical TM widths, fiber widths and fiber angle across human, guinea pig, and mouse samples. All values are represented as median ± half interquartile range. W_{TM}: width of the TM from the marginal band to the limbal edge. $\frac{W_{TM}}{W_{BM}}$: width of TM as a fraction of width of the basilar membrane. Δ_{fibers}: spacing of collagen fibers in the TM. ϕ_{fibers}: angle of collagen fibers relative to the marginal band.

Species	W_{TM} (μm)	$\frac{W_{TM}}{W_{BM}}$ (%)	Δ_{fibers} (μm)	ϕ_{fibers} (degrees)
Human (n = 8)	178 ± 5	44 ± 1 [22]	2.4 ± 0.3	47 ± 7
Guinea pig (n = 9)	145 ± 9	58 ± 4 [22]	1.8 ± 0.1	67 ± 4
Mouse (n = 9)	112 ± 11	64 ± 16 [9]	1.6 ± 0.2	73 ± 6

Table 4.2: Basal TM widths, fiber widths and fiber angle across human, guinea pig, and mouse samples. All values are represented as median ± half interquartile range. W_{TM}: width of the TM from the marginal band to the limbal edge. $\frac{W_{TM}}{W_{BM}}$: width of TM as a fraction of width of the basilar membrane. Δ_{fibers}: spacing of collagen fibers in the TM. ϕ_{fibers}: angle of collagen fibers relative to the marginal band.

Species	W_{TM} (μm)	$\frac{W_{TM}}{W_{BM}}$ (%)	Δ_{fibers} (μm)	ϕ_{fibers} (degrees)
Human (n = 13)	115 ± 11	96 ± 9 [22]	1.9 ± 0.2	55 ± 6
Guinea pig (n = 9)	125 ± 18	125 ± 18 [22]	1.8 ± 0.1	75 ± 2
Mouse (n = 9)	46 ± 10	70 ± 24 [9]	1.4 ± 0.04	73 ± 4

The next set of tables given below show parameters related to Hensen's stripe including its, W_{HS}, and the distance of a perpendicular line drawn from the marginal band to the closest edge of Hensen's stripe, D_{MBtoHS}. For each these, we divide the parameter by the TM width to determine the approximate fraction that they cover. For the distance between the marginal band and Hensen's stripe, we found

that Hensen's stripe was generally positioned roughly in the center of the TM, getting a little closer to the marginal band in apical TM samples compared to basal samples.

A consistent difference in TM morphology across the species studied was the structure of Hensen's stripe. We observed that the width of Hensen's stripe, W_{HS}, was a significantly larger fraction of the overall TM width, W_{TM}, in human samples compared to those from guinea pigs or mice (tables 4.3 and 4.4). This fractional width was also significantly higher in guinea pigs than in mice. When viewing TM samples under high magnification as shown in figure 4-5, we changed the focal plane to determine the minimum width of Hensen's stripe and found this parameter to be significantly higher in humans than in the two rodents studied here. The percentage of TM width covered by Hensen's stripe is 10 - 15% in humans; whereas, in guinea pigs it is 8 - 10 %, and in mice this parameter is between 1-2%. Despite previous observations of unfixed human cochlear tissue [91] and isolated fixed human TM samples [42], to our knowledge, this is the first comparison of Hensen's stripe morphology between humans and other mammals in unfixed TM samples. Hensen's stripe was only visible in two out of nine samples at our magnification level in the mouse apex. In addition, in approximately half of the human basal and apical TM samples, Hensen's stripe was not visible. In a few cases, it was present in half of the TM sample and torn off in the other half. We observed on occasion that Hensen's stripe visibly came off from the TM sample during extraction from the cochlea.

Table 4.3: Apical Hensen's stripe width, W_{HS}, and distance between the marginal band and Hensen's stripe, D_{MBtoHS}, across human, guinea pig, and mouse samples. All values are represented as median ± half interquartile range

Species	W_{HS} (μm)	$\frac{W_{HS}}{W_{TM}}$ (%)	D_{MBtoHS} (μm)	$\frac{D_{MBtoHS}}{W_{TM}}$ (%)
Human (n = 8)	19 ± 2	10 ± 1	82 ± 7	46 ± 3
Guinea pig (n = 9)	12 ± 2	8.0 ± 0.7	63 ± 4	43 ± 2
Mouse (n = 9)	1.1 ± 0.01	0.9 ± 0.1	28 ± 1	31 ± 0.1

Table 4.4: Basal Hensen's stripe width, W_{HS}, and distance between the marginal band and Hensen's stripe, D_{MBtoHS}, across human, guinea pig, and mouse samples. All values are represented as median ± half interquartile range

Species	W_{HS} (μm)	$\frac{W_{HS}}{W_{TM}}$ (%)	D_{MBtoHS} (μm)	$\frac{D_{MBtoHS}}{W_{TM}}$ (%)
Human (n = 13)	20 ± 1	17 ± 1	65 ± 2	57 ± 2
Guinea pig (n = 9)	12 ± 4	9 ± 3	54 ± 9	44 ± 3
Mouse (n = 9)	0.8 ± 0.3	1.6 ± 0.4	22 ± 2	47 ± 3

4.2.2 The effect of time after death on TM wave properties

TM measurements in human samples were made as soon as possible after death; as described above, the measurements on fresh temporal bones were performed on pieces within 48 hours post mortem. The TM is an acellular gel that has been shown to undergo very slow rates of regeneration in the mammal [95]. In a mutant mouse model where the tectorial membrane does not bind to the organ of Corti, researchers found the TM to be fully intact with little change in structure in adults, meaning that the TMs were floating inside the cochlea from the time of birth without undergoing significant deterioration [50]. These findings suggest that the TM is a resilient gel. Nevertheless, we address the potential problem of any change in mechanical properties of the TM that could affect our measurements after death. To more clearly quantify the extent of the changes we could expect due to time after death, we performed a study in mice to measure the changes in TM wave properties when specimens were treated in a similar fashion to the human temporal bones that we obtained. By comparing the TM wave properties of samples dissected immediately after death versus 48 hours post mortem, we can quantify the extent of changes we expect in our human TM waves compared to more freshly collected samples.

In figure 4-6, we show mouse TM wave properties (decay constant, σ, and speed, v) in a number of basal and apical pieces that were from fresh and purposely aged samples. We found that mouse TM wave properties in purposely aged samples were not measurably different from those taken from freshly dissected cochleae. In every

case, we find that the median estimates for the two conditions in the frequency regions of interest for these samples overlap with the 90% confidence intervals, leading us to conclude that there would be no significant change in human TM wave properties in TM samples measured 48 hours post mortem.

To clarify the differences in decay constants and speeds due to time after death, we plotted the median lines and 95% confidence intervals alone shown in figure 4-7.

Our data in figure 4-6 seems to contradict our findings in chapter 2 that waiting 48 hours post-mortem changes TM fixed charge density. However, as we showed in chapter 2, we have found that TM fixed charge does not affect TM wave parameters. Therefore, although we see an approximately 30% decrease in TM fixed charge density when leaving mouse TM's for 48 hours before performing our measurements, from our measurements in chapter 2, we fully expect this change in charge density to have little to no effect on TM wave parameters.

4.2.3 TM wave parameters are similar across species

We compiled TM wave properties from three species in figure 4-8. We separated samples into basal and apical segments, depending from which half of the cochlea they were taken. As expected from Ghaffari et al. [29], we find that in mice, apical segments have larger decay constants and smaller speeds compared to basal segments. Here we show that these differences also hold for TM segments taken from guinea pigs and humans.

Given that the TM samples from these three species are largely similar in structure and morphology (figure 4-5), it is not surprising that their wave properties do not differ significantly. Looking at the median of the wave parameters across the three species, we see that the differences across mammals is small compared to the variability in the measurements from different pieces of TM for each mammal.

To clarify the differences in TM wave properties across species, we plotted the median lines and 95% confidence intervals alone shown in figure 4-9.

4.2.4 Statistical analysis of difference in TM wave parameters across species

To quantify the statistical significance of the differences seen across species, we performed analysis of variance (ANOVA) on the data shown in figure 4-8. In tables 4.5 and 4.6, we show the results of these statistical analyses. In all cases the error median square among the three species is smaller than or close to the error median square within measurements from each individual species. This shows that the differences in wave parameters are not significant across the three species measured. The only exception to this is a difference in the basal median square error within species of decay constants compared to the median square error among species, but using an f-test for this, we find that the difference is not big enough to be considered significant. The detailed ANOVA tables used for this analysis are included in the appendix.

Table 4.5: ANOVA parameters for TM wave decay constant, σ. MS = median square error

Basal σ MS among species (μm^2)	Basal σ MS within species (μm^2)
9702	2074
Apical σ MS among species (μm^2)	Apical σ MS within species (μm^2)
53	6406

Table 4.6: ANOVA parameters for TM wave speed, v. SS = sum of squares. MS = median square error

Basal v MS among species (m/s)^2	Basal v MS within species (m/s)^2
4.9	18
Apical v MS among species (m/s)^2	Apical v MS within species (m/s)^2
2.0	1.8

4.2.5 TM dynamic material properties

To determine TM material properties for humans, guinea pigs, and mice from our wave measurements in figure 4-8, we used a distributed impedance model implementation of the TM [29]. We fit the measured TM displacements along the surface of the gel with estimated displacements for a series of viscoelastic elements. This model represents the TM as a series of distributed masses coupled by springs and dashpots. By determining the best fits for the springs and dashpots to our measurements, we estimated the TM's shear modulus and shear viscosity at each frequency from our wave data. The resulting shear modulus, G', and shear viscosity, η, values are given in figure 4-10 as a function of frequency for the three species.

To clarify the differences in material properties across species, we plotted the median lines and 95% confidence intervals alone shown in figure 4-11.

4.2.6 Human shear impedance measurement

To explore the fact that the collagen fibers in human TM samples were at a much sharper angle relative to the marginal band compared to those from mice, we used shear impedance probes to measure human TM impedance in two directions. In the first case, we placed the probe perpendicular to the marginal band as we have done for mouse TM samples in the past [36]. We measured impedances in two orthogonal directions (x and y as shown in figure 4-12) in this orientation. For the mouse, previous studies have shown impedances in the direction of radial fibers to be twice as big as impedances in the direction perpendicular to that [2, 36, 26]. For the human samples, after performing measurements in this orientation, we rotated the probe so that its motions would be parallel and perpendicular to the collagen fibers as shown in figure 4-12. We remeasured the TM impedance in two orthogonal directions in this case as well.

We found that when the probe was oriented parallel to the collagen fibers, the y-direction shear impedances were roughly 1.5 - 2 times greater than the x-direction shear impedances, similar to what has previously been seen in the mouse. However,

when the probe was oriented perpendicular to the marginal band as it typically would be for mouse measurements, we found that the y-direction impedance was close to half the x-direction impedance (figure 4-12). These results show that the orientation of the human collagen fibers affects the direction of TM's anisotropy.

4.2.7 TM wave parameters in cochlear units show systematic differences across species which correlate with cochlear tuning

Although we don't see significant differences in TM waves or material properties across mammalian samples, we've so far only considered wave parameters in standard units (σ in μm and v in m/s). Since the cochlea maps location to frequency, the unit of measure that we must use to help us understand cochlear tuning curves should relate to the frequency map of the cochlea. In order to make this transformation, we can look at representative cochlear maps for the three species under study. Cochlear maps relate cochlear location, x, to center frequency, CF, logarithmically. The standard Greenwood relation is represented as follows [35]:

$$CF = A(10^{ax} - k) \tag{4.2}$$

The parameter k is typically small and only significant at the very apex of the cochlea; therefore it will be neglected here. If we transform the frequency place map to a base two exponent, we get the following:

$$CF = B(2^{x/D}) \tag{4.3}$$

where D is now the distance over which frequency in the cochlea changes by an octave. In the three mammals under consideration here, the most convenient

units to use for CF and x are kHz and mm, respectively. We show representative cochlear spirals for humans, guinea pigs, and mice including the typical frequency limits, overall cochlear length, and the parameter D in figure 4-13.

When we normalize our TM wave data from figure 4-8 by the distance over which frequency changes by a factor of two, D, for each species, we get the normalized TM wave parameters shown in figure 4-14. Now we are looking at wave parameters in units that are relevant to the cochlea, namely decay constant in octaves instead of μm, and speed in octaves/s instead of m/s. We see that performing this normalization has increased the median difference in the wave parameters observed across the three species. In particular, we see that median normalized decay constants, $\frac{\sigma}{D}$, in humans are smaller than those measured in guinea pigs or mice in both basal and apical samples. We also see that the median normalized TM wave speeds, $\frac{v}{D}$, in humans are smaller than those measured in guinea pigs and mice.

To clarify the differences in normalized TM wave properties across species, we plotted the median lines and 95% confidence intervals alone shown in figure 4-15.

4.2.8 Statistical analysis of difference in normalized TM wave parameters across species

To quantify the statistical significance of the differences seen across species, for normalized TM wave parameters, we performed ANOVA analysis on the data shown in figure 4-13. In tables 4.7 and 4.8, we show the results of these statistical analyses. The F-values given in the tables below indicate that the normalization of our TM wave data to parameters that are relevant to the cochlea results in a significant difference in the decay constants ($p<0.025$) and speeds ($p<0.05$) measured across humans, guinea pigs, and mice. The detailed ANOVA tables used for this analysis are included in the appendix.

Table 4.7: ANOVA parameters for TM wave decay constant, σ. MS = median square error. $F_s = \frac{MS_{among}}{MS_{within}}$

Basal σ MS among species $(\text{octaves})^2$	Basal σ MS within species $(\text{octaves})^2$	Basal σF_s
0.0082	0.00032	25.6
Apical σ MS among species $(\text{octaves})^2$	Apical σ MS within species $(\text{octaves})^2$	Apical σF_s
0.026	0.0012	22.2

Table 4.8: ANOVA parameters for TM wave speed, v. MS = median square error. $F_s = \frac{MS_{among}}{MS_{within}}$

Basal v MS among species $(\text{octaves/s})^2$	Basal v MS within species $(\text{octaves/s})^2$	Basal F_s
42582089	1616481	26.3
Apical v MS among species $(\text{octave/s})^2$	Apical v MS within species $(\text{octave/s})^2$	Apical F_s
3392114	303495	11.2

4.3 Discussion

In this work we study the dynamic mechanical properties of unfixed human TM samples for the first time. We compare human TM properties to those from two other mammalian species and show that they do not differ significantly when measured in standard units (σ in μm and v in m/s). However, when these measures of wave properties are normalized to the length associated with the frequency map of the mammalian cochlea, we see that the normalized TM properties differ in a way that suggests sharper cochlear tuning in humans compared to guinea pigs and mice.

4.3.1 The TM offers a unique look at cochlear mechanics

Despite the wide variety of measurements of cochlear micromechanics in a variety of mammalian models, these mechanical measurements are impossible to do in humans. Even in animal models, the measurements are often not possible along the entire length of the cochlea in situ. Since we can remove TM samples from along the entire length of the cochlea, we are given a unique opportunity to compare the mechanical

properties of this important structure throughout its length.

The cochlea's mechanical properties are irreversibly altered upon death [69], making it impossible to directly measure its mechanical properties in humans. However, from TectB mutant mice, we know that measurements of extracted TM wave properties relate to relevant cochlear parameters in vivo. Therefore, extracting TM samples from humans and measuring their wave properties gives us a unique window into human cochlear micromechanics.

4.3.2 TM material parameter estimates across species

In this work, we present the first interspecies comparison of TM material properties using a single technique. We show that human TM material properties are similar to those from other mammalian species when compared at similar frequencies. We are in a unique position to make this statement since we are the first to measure unfixed human TM properties, and our wave measurement technique allows us to measure properties at acoustic frequencies. As predicted by several previous studies [57, 73, 29, 47], we found here that TM samples from basal regions of the cochlea are stiffer than those taken from the apical regions. These stiffness differences between the base and apex follow intuitively from the fact that apical TM samples are wider than basal samples. A similar size difference results in stiffness gradients responsible for basilar membrane tonotopicity [18, 19].

Previously, TM material parameters have been measured in samples taken from guinea pigs [83, 37, 73]; however, the techniques used measured these parameters at frequencies of 10 Hz or less. These low frequencies are not relevant to hearing in this mammal. TM material properties have been measured with greater success at acoustic frequencies in mice, using magnetic beads [2], microfabricated shear probes [36], and waves [29, 30, 47]. Using the most versatile of these techniques (waves) we show that the differences between TM material properties across these three very different species is small. Given the many similarities in TM morphology outlined above, it is not surprising to see that TM material properties are similar. Furthermore, given that the TM wave properties across species are not significantly different, and our

material properties are derived directly from these wave measurements, we expected TM material properties not to be significantly different across species.

4.3.3 Similarity of TM wave properties across species

Ghaffari et al. showed that TM wave properties relate strongly with hearing parameters [29, 30]. Here, we have performed the first interspecies comparison of TM wave parameters. We show a number of similarities in the TM wave properties of humans and guinea pigs when compared to mice. In particular, we find that TM decay constants, σ, are larger in TM samples from the apical half of the cochlea than in samples taken from the basal half of the cochlea (figure 4-8). This variation in spread of excitation along the cochlea relates to the fact that tuning measured at the auditory nerve fibers in a variety of mammalian species has always been sharper in fibers from the basal, high-frequency region of the cochlea compared to the apical, low-frequency region [20, 53, 89]. We also see that, as was seen by Ghaffari et al. in the mouse, TM wave speeds in guinea pigs and humans are measurably smaller in samples taken from the apical half of the cochlea compared to samples from the basal half. This difference relates to the decreased basilar membrane speeds measured in apical regions of the cochlea compared to basal regions [74]. The fact that TM wave properties relate to important cochlear properties in such a wide spectrum of mammals speaks to their universality as a hearing mechanism.

Not only did TM wave parameters have similar properties in the three species studied when comparing basal and apical properties, but we also found that the quantities were comparable. Decay constants, σ, measured in μm, and speeds, v, measured in m/s were not measurably different between TM samples from mice, guinea pigs, and humans (figure 4-8). This agrees with the prediction made by Shera et al. that the spatial extent of excitation in humans, cats, guinea pigs, and chinchillas does not differ significantly despite their predicted differences in tuning [82]. Shera et al. made this prediction using otoacoustic emission data, but here we support this prediction directly using TM waves.

4.3.4 TM wave spatial extents suggest TM plays a role in determining cochlear sharpness of tuning

Since the TM couples adjacent hair cells in the cochlea, its spread of excitation relates to cochlear tuning [30]. In particular, a smaller spread of excitation of TM waves should result in fewer hair cells being coupled due to an input sound, and a sharper tuning curve response from the auditory nerve. Here we see that when we consider units that are relevant to the mammalian cochlea, the spread of excitation of TM waves, $\frac{\sigma}{D}$, becomes smaller as we go from mice to guinea pigs to humans. Another way of looking at this is to relate TM spread of excitation in μm to frequency bandwidth using the cochlear map of each species as shown in figure 4-16. We see that the human has the steepest cochlear map of the three species studied, so a given distance will couple the smallest number of different frequencies resulting in the most sharply tuned frequency response.

By extension, if we had an animal whose cochlear map was such that D was larger than it is in humans, we would predict that its tectorial membrane would have a similar decay constant, σ, to rodents and humans when measured in μm but that this animal would have sharper cochlear tuning due to a smaller value of the dimensionless quantity $\frac{\sigma}{D}$. This phenomenon was measured by von Békésy in the basilar membrane of elephants [91]. Although his measurements were taken in a cadaveric bone, even in this condition, he found the elephant cochlea to have sharper tuning by roughly a factor of two than humans. The cochlear map parameter D in elephants is double what it is in humans [34], further suggesting that it is an important determinant of sharpness of tuning.

We are in a position to use our normalized TM decay constant data (figure 4-8) to predict sharpness of tuning in these three species. We find roughly a factor of two increase in normalized TM wave decay constants between human and guinea pig samples. This falls on the lower end of the range of predicted tuning differences between these two species using otoacoustic emissions [81]. From our mouse data, we see a factor of 1.5 larger spread of excitation when compared to guinea pig samples

from the base and over a factor of two in samples from the apical regions. Comparing our data for mice and humans, we would predict human cochlear tuning to be sharper by a factor of three in basal regions and a factor of four in apical regions. Comparing cochlear delays from otoacoustic emissions in mouse [4] and human [81], and using Shera et al.'s theory about the relationship between cochlear delay and sharpness of tuning, we would predict a factor of two to five increase in Q_{10dB} in humans compared to mice.

We can also compare our TM wave spread of excitation data to sharpness of tuning measurements obtained from auditory nerve threshold tuning curves in mice and guinea pigs. Q_{10dB} values taken from auditory nerve fiber recordings in mice [89] and guinea pigs [20] predict sharper tuning in guinea pigs compared to mice below 10 kHz, but a reversal of this trend above at higher frequencies. Interestingly, we see this reversal in TM decay constants between mice and guinea pigs in figure 4-15. When comparing otoacoustic emissions data in mice from Banakis and Siegel [4] to the measurements of Shera et al. for guinea pig [81], using median values we would predict that guinea pig tuning is roughly two times sharper in the apex than mouse tuning. However, this relationship reverses in the base where the emissions delay data would predict sharper tuning in the mouse than in the guinea pig. Our measurements of TM wave spread of excitation suggest that guinea pigs should have sharper cochlear tuning than mice at low frequencies but similar or less sharpness of tuning at high frequencies (figure 4-15).

Interestingly, data from Shera and others in a variety of species predict a greater difference in sharpness of tuning when looking at low frequency regions compared to higher frequency regions [81, 48]. As outlined above, our normalized TM wave decay constants support this predicted difference when we compare mouse and human TM data and when we compare guinea pig and human TM measurements.

4.3.5 TM wave speeds suggest TM plays a role in determining cochlear sensitivity

In order for TM waves to interfere constructively with BM waves in the cochlea, the two waves should have similar wavelengths [44, 29, 30]. Since wavelength, λ, is directly proportional to speed ($v = f\lambda$), it follows that the TM and BM wave should have similar speeds in order to interfere constructively and stimulate hair bundles maximally. In order to determine BM wave speed in the three species studied here, we found BM frequency response measurements from the literature. Guinea pig and mouse BM measurements have been performed in vivo in sensitive cochleae; however, it is not possible to perform these measurements in a live human. From animal studies, we know that the BM phase versus frequency does not change significantly after death [68, 75, 70]. Since BM speed can be determined from the phase of BM responses versus frequency as described below, we can get a good estimate of human BM speed in vivo using post-mortem measurements of BM phase.

In figure 4-17, we have plotted BM phase versus frequency using data from others that measured these parameters in the basal (A) and apical (B) turns of humans, guinea pigs, and mice. The responses for the human samples [87, 91] and the mouse apical sample [S.L. Page unpublished] were measured post-mortem, but the measurements in guinea pigs [68, 12] and mouse base [77] were performed in live animals. The curves are given in cycles versus frequency. For each species, the x-axis was transformed to cochlear distance (in mm) to determine the length of one wavelength, (λ). This was taken as the distance over which phase changed by one cycle. The wavelength was then multiplied by frequency to get speed ($c = f * \lambda$). The values of frequency, wavelength, and BM speed in m/s for the three species are given in table 4.9 for basal regions of the cochlea and table 4.10 for apical regions. From the values obtained, we see that the BM speeds measured in m/s determined for these three species are not measurably different. We see that this rough equality of speeds across species roughly holds for the measured TM wave speeds of segments taken from the base and apex as well (figure 4-8). However, we must keep in mind that our TM wave

speeds are comparable when viewed at similar frequencies; whereas, measurements of BM speed are not available at the same frequencies for these three species. We must keep in mind the big difference in frequencies between the mouse, guinea pig, and human measurements when interpreting the BM speed data of figure 4-17.

We can also compare the values of wavelength, λ, in tables 4.9 and 4.10 for the BM to those in figure 4-18 for the TM. From figure 4-18 panels A and B, we see that not only are λ values quite similar across species when compared at different frequencies, but we also see that the values are comparable to those estimated for the BM below. Namely, at frequencies around 1 kHz, we see wavelengths of 2 - 3 μm, and at higher frequencies approaching 40 kHz, we see that these wavelengths have decreased to roughly 100 μm.

Table 4.9: Basilar membrane speed estimates at the best frequency for the basal turn of a human, guinea pig, and mouse

Species	Frequency (kHz)	Wavelength, λ (mm)	Speed (m/s)	Normalized Speed (octaves/s)	Reference
Human	2.5	2.9	7.3	1460	[87]
Guinea pig	18	0.43	7.8	2955	[68]
Mouse	53	0.14	7.3	5840	[77]

Table 4.10: Basilar membrane speed estimates at the best frequency for the apical turn of a human, guinea pig, and mouse

Species	Frequency (Hz)	Wavelength, λ (mm)	Speed (m/s)	Normalized Speed (octaves/s)	Reference
Human	300	2.7	0.81	162	[91]
Guinea pig	400	1.95	0.8	303	[12]
Mouse	7000	0.11	0.77	616	S.L. Page unpublished

If we normalize the BM speeds in tables 4.9 and 4.10 by the cochlear distance, D, for each species (D_{human} = 5 mm/octave, $D_{guineapig}$ = 2.64 mm/octave, and D_{mouse} = 1.25 mm/octave), we can determine normalized BM speeds in units of octaves/s instead of m/s. These values have been computed in table 4.9 and show a significant difference across species. Namely, the normalized BM speed in humans is significantly

smaller than in guinea pigs and mice. We can see that this agrees with our TM wave measurements in figure 4-14.

It has long been known that BM speeds are significantly higher in the high-frequency, basal region of the cochlea than in the low-frequency, apical region across mammals [74]. Comparing tables 4.9 and 4.10, we see that BM speed estimates in the apical regions of the cochlea for human, guinea pigs and mouse are significantly smaller than those in the basal region. Previously, Ghaffari showed that TM waves in apical segments had lower speeds than waves in basal TM segments [29]. Here we see that this holds true for TMs from guinea pigs and humans as well, suggesting that the TM in all mammalian cochleae is optimized to interact constructively with the BM.

The fact that our TM wave speeds when measured in m/s are similar across species, and we can see that BM wave speeds do not vary significantly across these species, suggests that TM and BM waves could have similar wavelengths across different mammals. This property could allow the two waves to interact constructively, providing greater cochlear sensitivity than could be achieved with only a BM. Here we see that this feature holds true for a wide variety of mammalian species, suggesting that, with the possible exception of bats, it is true in all mammals.

4.4 Conclusions

We compared human TM samples to those from the other two mammals and found some systematic differences in their morphology. Namely, human TM samples have a sharper angle of collagen fibers and a thicker Hensen's stripe compared to guinea pigs and mice. Otherwise, TM samples from humans are comparable to those from guinea pigs and mice.

Human TM measurements were performed a few days after the each donor passed away. To determine what effect this amount of time could have on TM properties, we aged mouse bones and compared the resulting properties to those from freshly dissected samples. We found that TM wave properties in aged samples were not

significantly different from those in fresh preparations.

Our measurements of TM wave decay constant in μm and wave speed in m/s do not show significant differences between samples from humans, guinea pigs, and mice. However, we show that by scaling TM wave properties by the cochlear map so that we compare them in units that are relevant to the cochlea, human TM wave decay constants are significantly smaller than those in mice and guinea pigs. We conclude that this smaller spread of excitation in TM waves contributes to the sharper frequency selectivity in humans. Although the organs of Corti are indistinguishable in these three species when viewed in radial cross-section, when considering the longitudinal coupling of the TM over the cochlear spiral in each animal, we conclude that there are significant differences in sharpness of tuning.

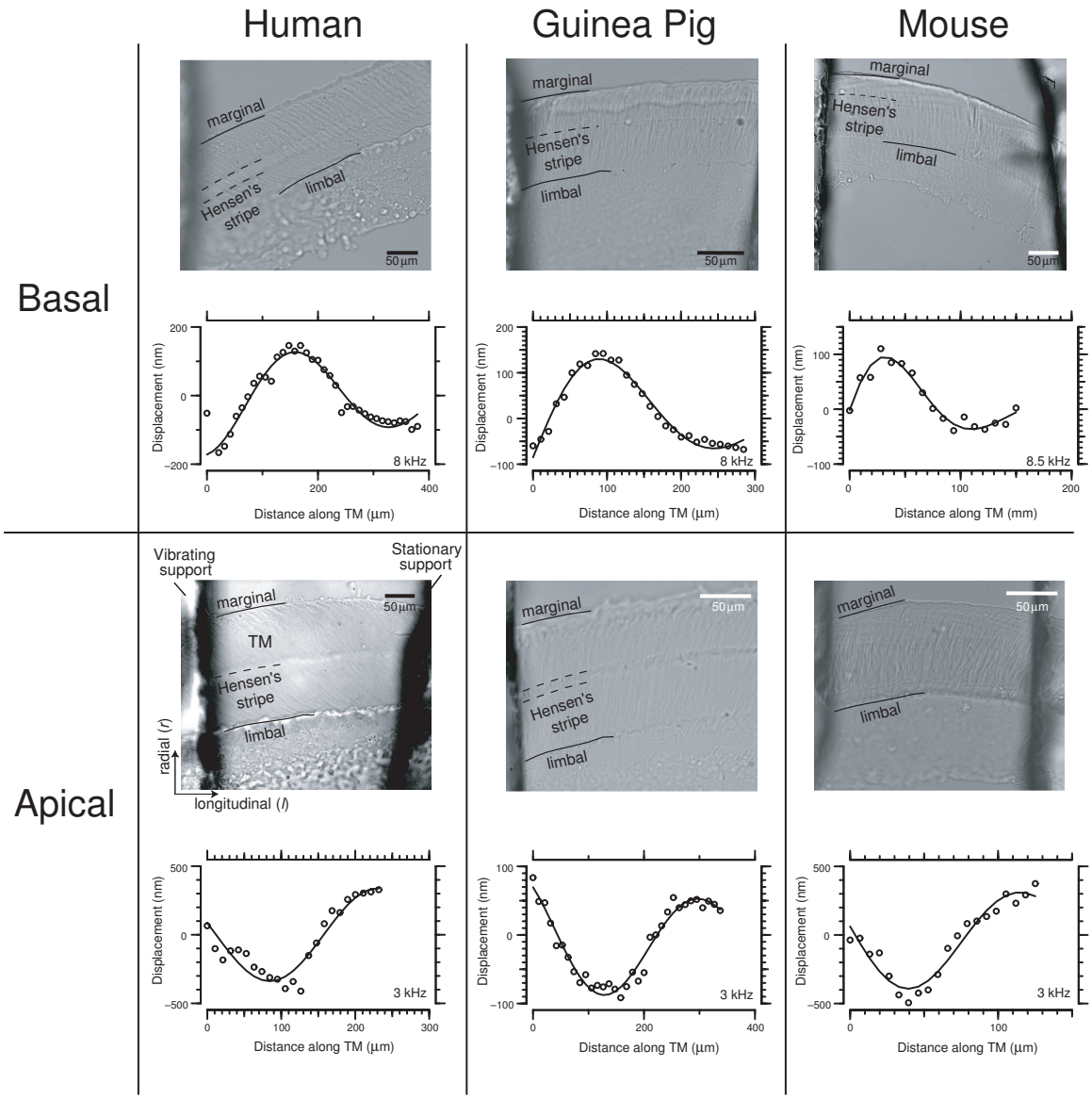

Figure 4-5: Images of TM samples taken from three species.
Top row: samples taken from basal cochlear regions for each animal. Bottom row: samples from apical regions. Each sample is suspended in the wave chamber apparatus with the vibrating support on the left and the stationary support on the right. Below each image is an example of wave motion in a relevant frequency range for the given species.

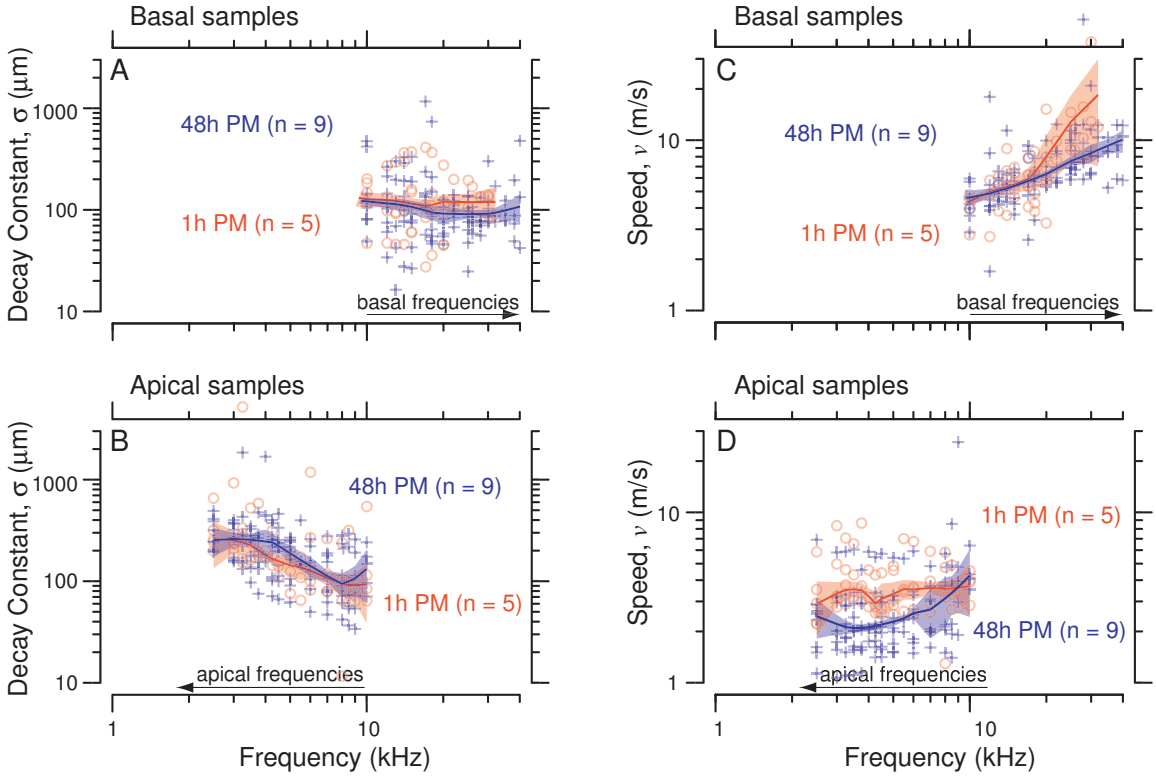

Figure 4-6: The effect of time after death on mouse TM wave properties. A, B: TM wave decay constant, σ, in basal (A) and apical (B) TM segments. C, D: TM wave speed, v, in basal (C) and apical (D) samples. Fresh samples (o) are overlayed with samples purposely aged for 48 hours (+) ($f_{apical} < 10$ kHz, $f_{Basal} > 10$ kHz). Thick lines were obtained from loess smoothing. Shaded regions indicate 95% confidence intervals estimated using resampling.

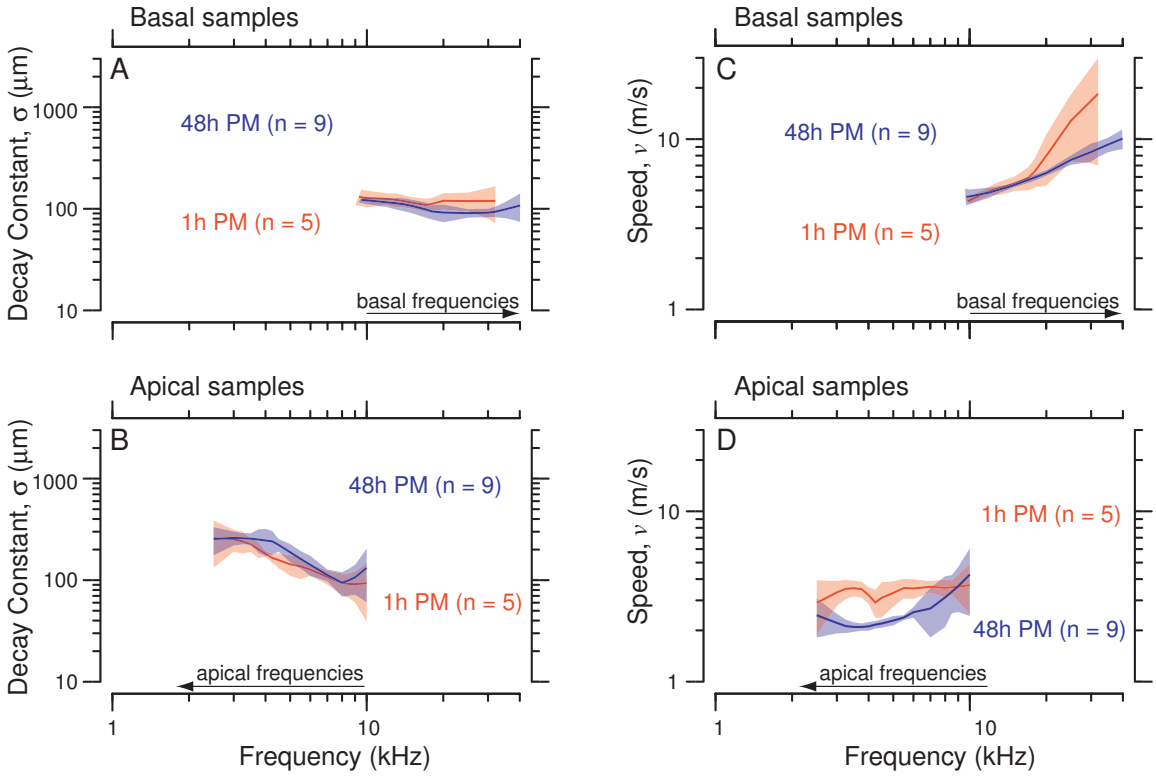

Figure 4-7: Median and 95% confidence intervals looking at the effect of time after death on TM waves.
A, B: TM wave decay constant, σ, in basal (A) and apical (B) TM segments. C, D: TM wave speed, v, in basal (C) and apical (D) samples. Lines were obtained using loess smoothing method from the data in figure 4-6. 95% confidence intervals estimated using resampling.

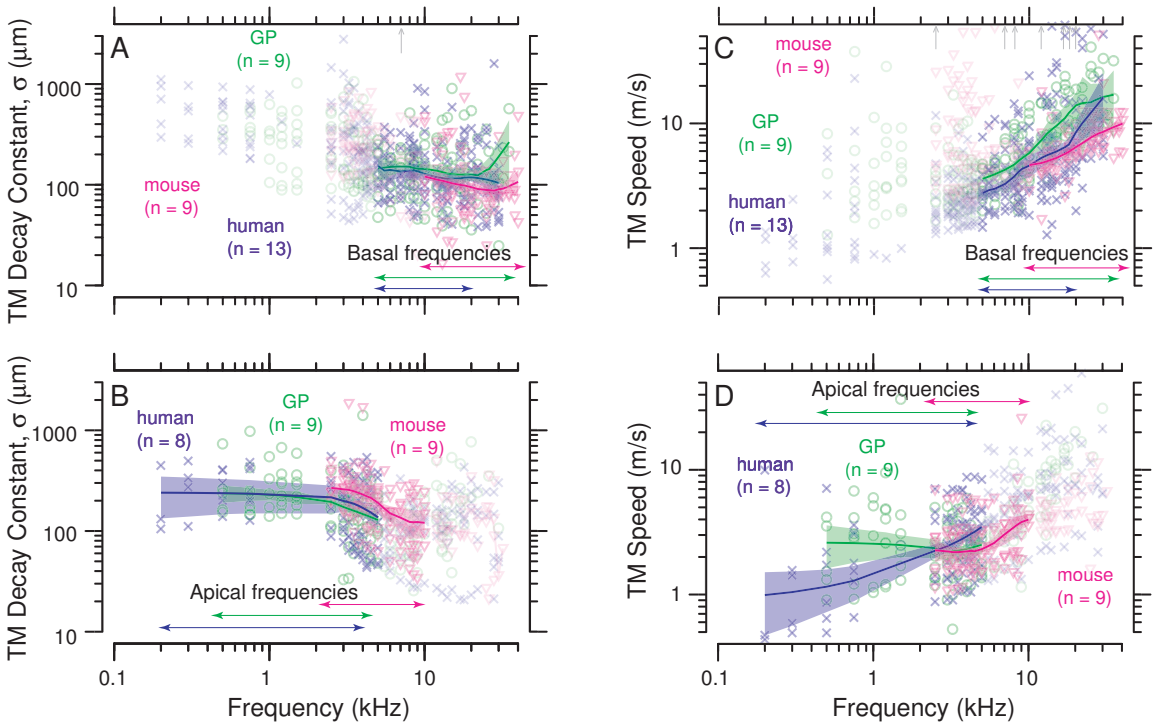

Figure 4-8: TM wave properties in samples taken from three species
A, B: TM wave decay constant, σ in μm, against frequency for human (x), guinea pig (o), and mouse (Δ) basal (A) and apical (B) samples. C, D: TM wave speed, v in m/s, in basal (C) and apical (D) samples. The number of TM samples measured for each region of each species is given in brackets next to the species name. All data points are shown, and for each species, a dark line was obtained from loess smoothing. Shaded regions indicate 95% confidence intervals estimated using resampling. The relevant frequency range of hearing is approximately indicated by horizontal arrows in each panel of the figure. To account for the difference in the frequency range of hearing, the following frequencies, $f_{A|B}$, were used to mark the apical to basal transition for each species: human $f_{A|B} = 5$ kHz, guinea pig $f_{A|B} = 5$ kHz, mouse $f_{A|B} = 10$ kHz.

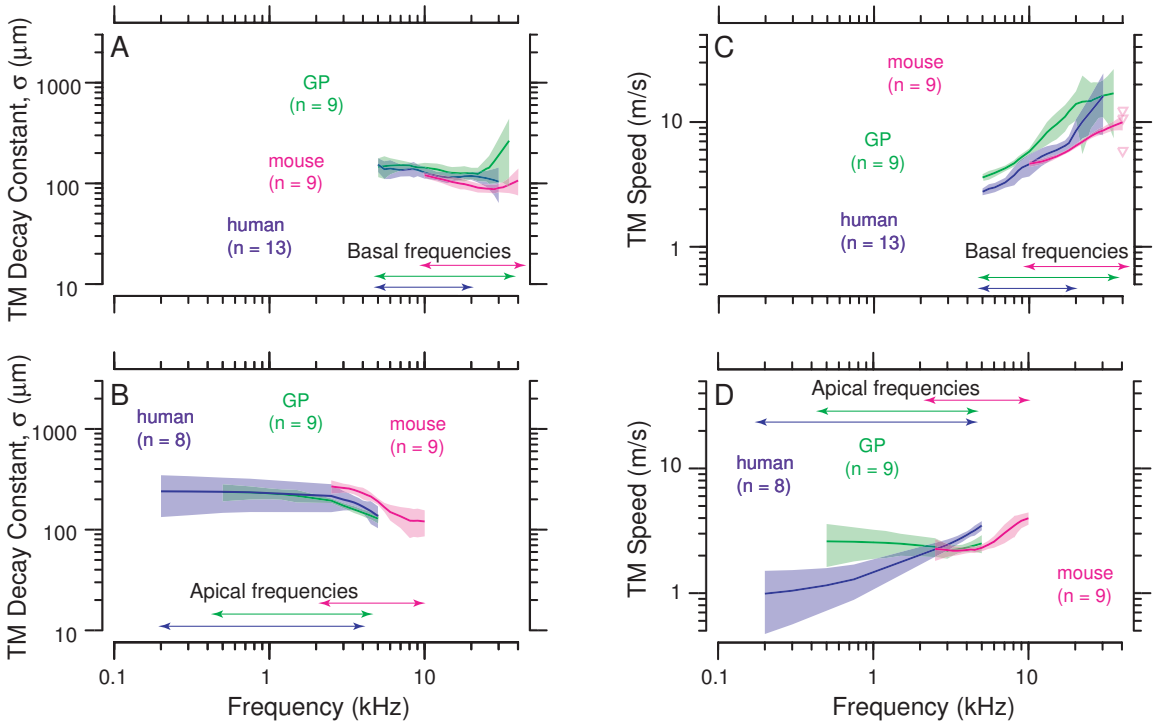

Figure 4-9: Median and 95% confidence intervals of interspecies TM wave properties A, B: TM decay constant, σ, in basal (A) and apical (B) TM segments. C, D: TM wave speed, v, in basal (C) and apical (D) samples. Lines were obtained using loess smoothing method from the data in figure 4-8. 95% confidence intervals estimated using resampling.

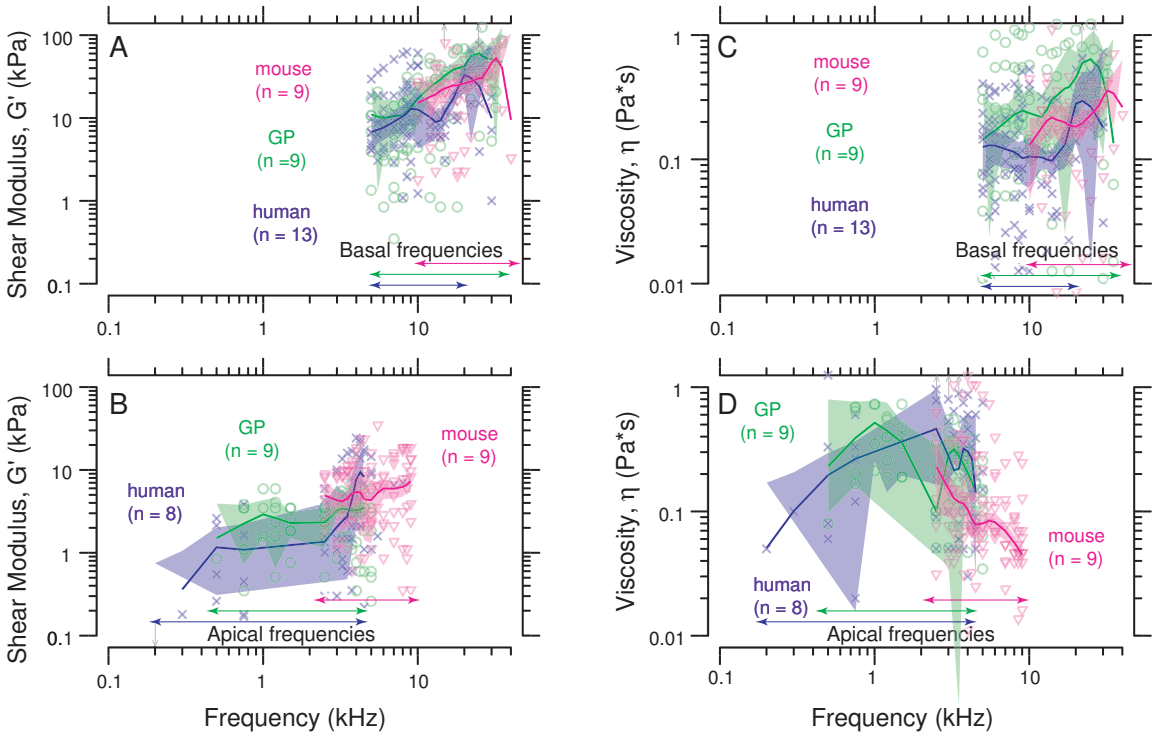

Figure 4-10: TM material properties in samples taken from three species
A, B: TM shear modulus, G' in kPa, against frequency for human (x), guinea pig (o), and mouse (Δ) basal (A) and apical (B) samples. C, D: TM viscosity, η in Pa*s, in basal (C) and apical (D) samples. The number of TM samples measured for each region of each species is given in brackets next to the species name. All data points are shown, and for each species, a dark line was obtained from loess smoothing using $\alpha = 0.35$ as a smoothing parameter. Shaded regions indicate 95% confidence intervals estimated using resampling. The relevant frequency range of hearing is approximately indicated by horizontal arrows in each panel of the figure. To account for the difference in the frequency range of hearing, the following frequencies, $f_{A|B}$, were used to mark the apical to basal transition for each species: human $f_{A|B} = 5$ kHz, guinea pig $f_{A|B} = 5$ kHz, mouse $f_{A|B} = 10$ kHz.

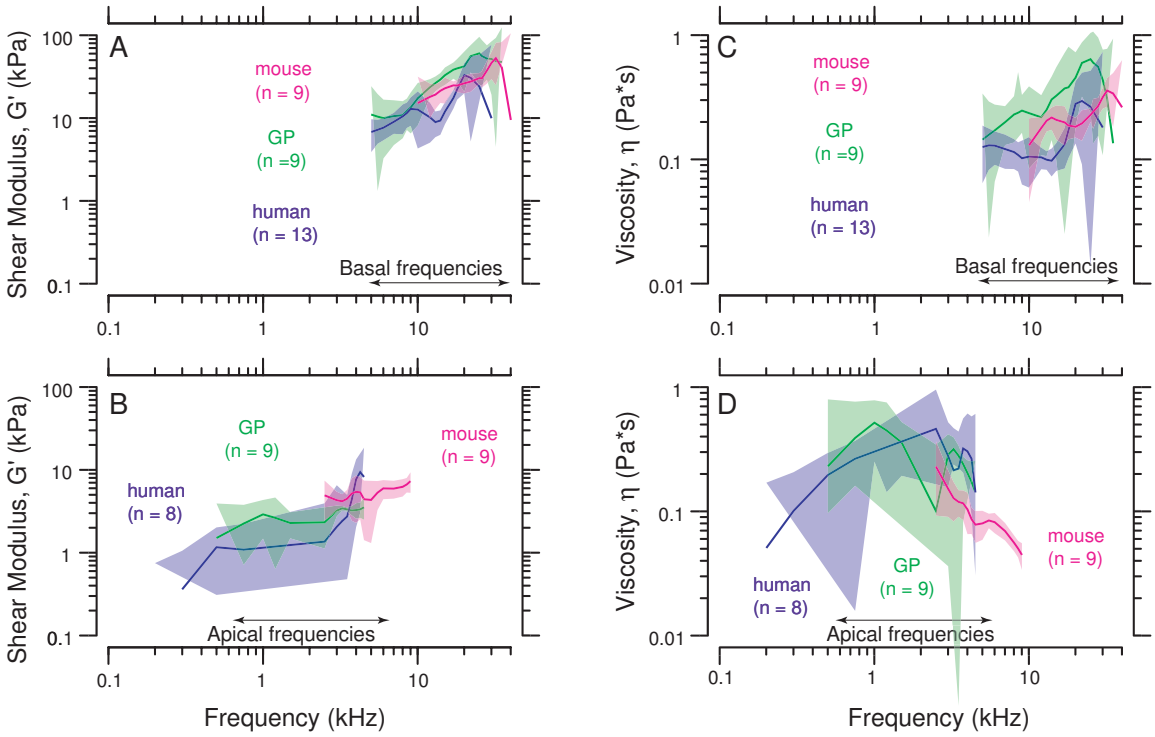

Figure 4-11: Median and 95% confidence intervals of interspecies material properties A, B: TM shear modulus, G', in basal (A) and apical (B) TM segments. C, D: TM shear viscosity, η, in basal (C) and apical (D) samples. Lines were obtained using loess smoothing from the data in figure 4-10. 95% confidence intervals estimated using resampling.

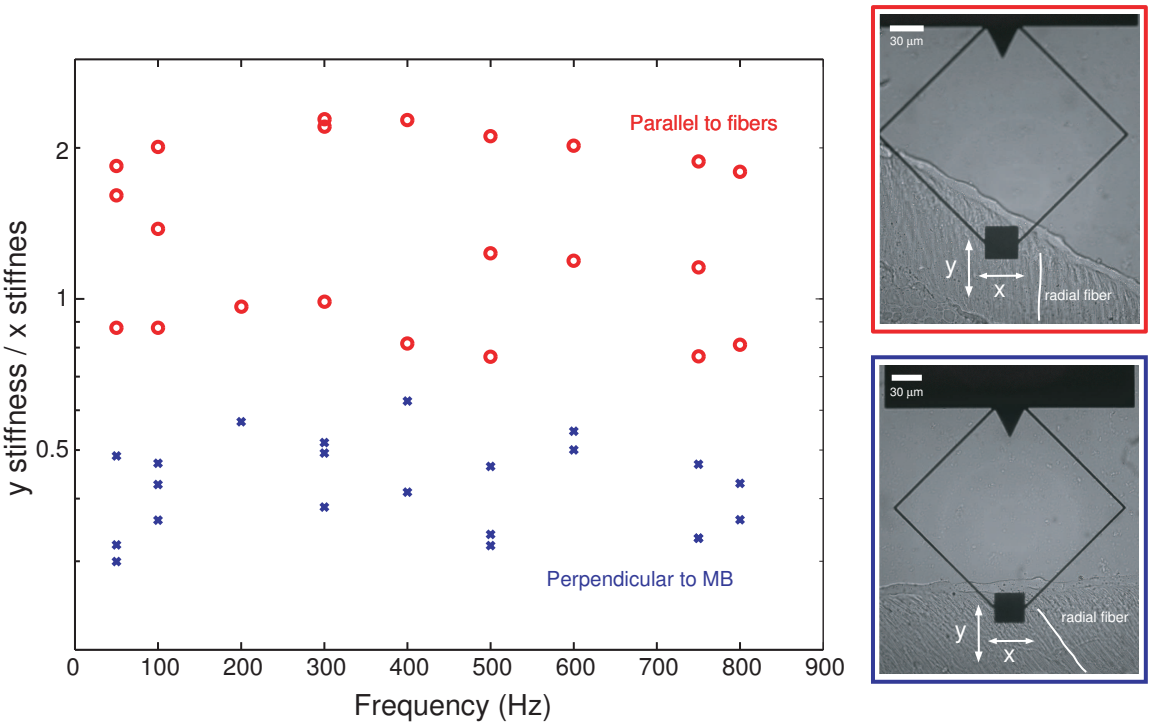

Figure 4-12: Human shear impedance measurements
We show the ratio of impedances in the y stimulus direction to the x stimulus direction with the shear probe oriented perpendicular to the marginal band (red x symbols) and parallel to the collagen fibers (blue o symbols) (n = 3). On the right we show images of the shear probe in the two orientations on human TM samples where we have highlighted the orientation of the radial fibers.

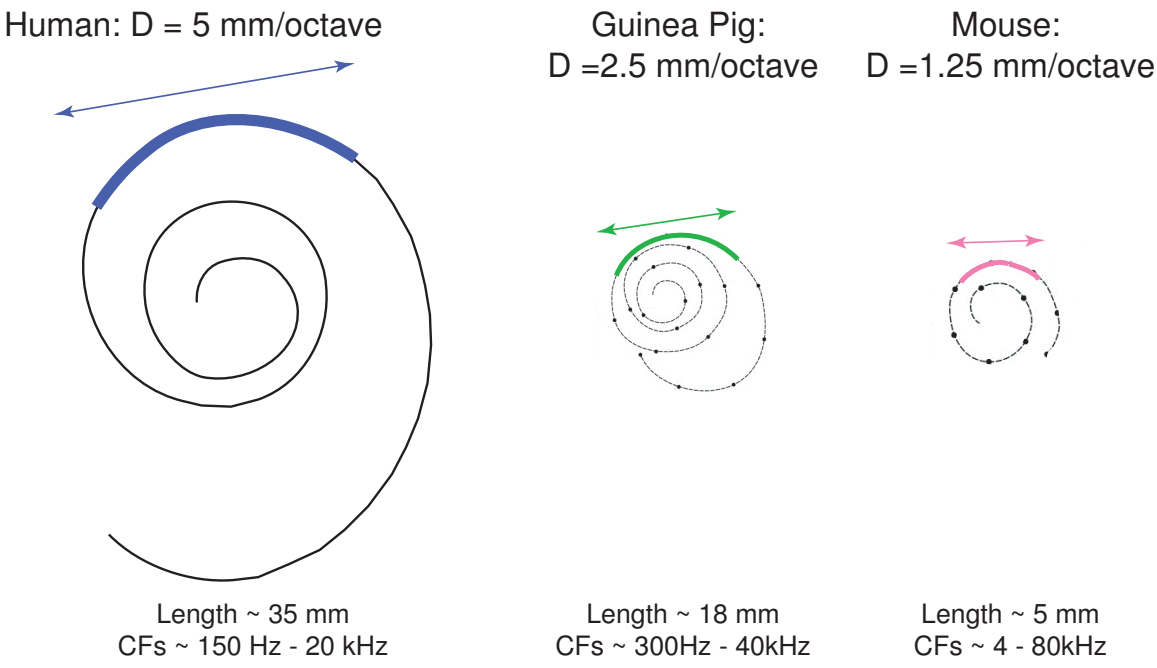

Figure 4-13: Cochlear spirals of human, guinea pig, and mouse.
On each cochlear spiral, we have highlighted the distance over which frequency changes by an octave or D. Below each spiral, we indicate the typical cochlear length and frequency range of hearing for each mammal. Rodent cochlear spirals adapted from Viberg and Canlon [90], and human spiral adapted from Stakhovskaya et al. [86].

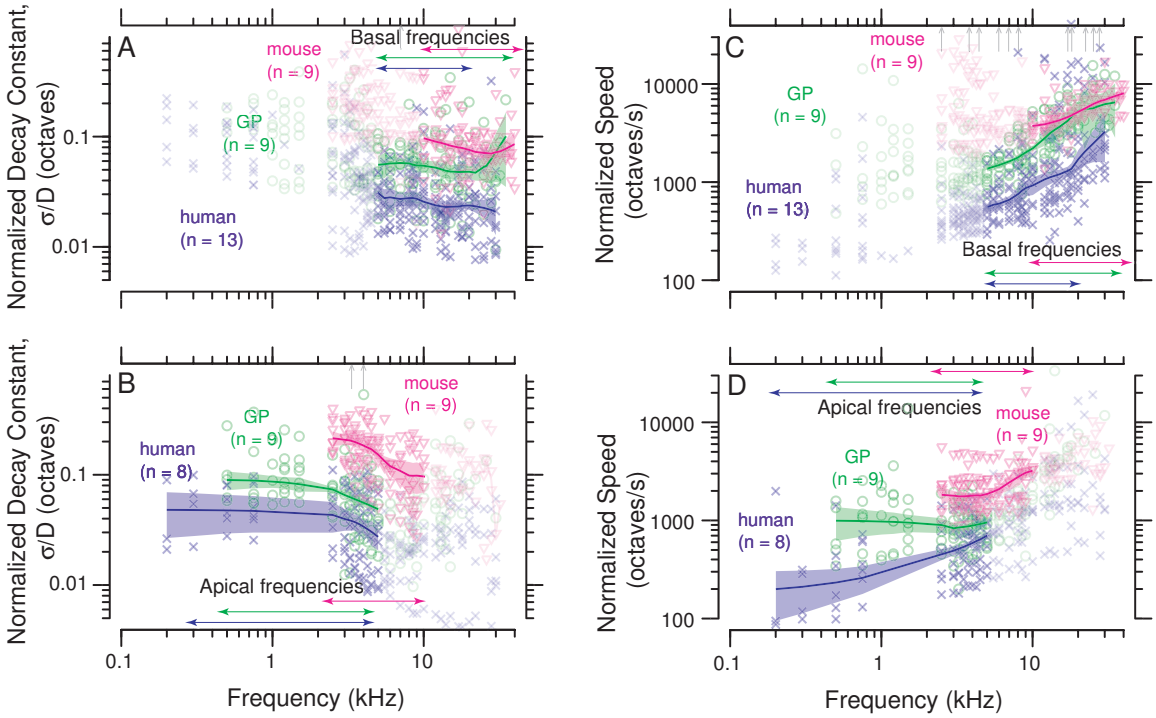

Figure 4-14: Normalized TM wave properties in samples from three species. A, B: TM wave decay constants from figure 4-8 normalized by cochlear map, $\frac{\sigma}{D}$ in octaves, against frequency for human (x), guinea pig (o), and mouse (Δ) basal (A) and apical (B) samples. C, D: TM wave speeds from figure 4-8 normalized by cochlear map, $\frac{v}{D}$ in octaves/s, in basal (C) and apical (D) samples. The number of TM samples measured for each region of each species is given in brackets next to the species name. All data points are shown, and for each species, a dark line was obtained from loess smoothing using $\alpha = 0.35$ as the smoothing parameter. Shaded regions indicate 95% confidence intervals estimated using resampling. The relevant frequency range of hearing is approximately indicated by horizontal arrows in each panel of the figure. However, to account for the difference in the frequency range of hearing, the following frequencies, $f_{A|B}$, were used to mark the apical to basal transition for each species: human $f_{A|B} = 5$ kHz, guinea pig $f_{A|B} = 5$ kHz, mouse $f_{A|B} = 10$ kHz.

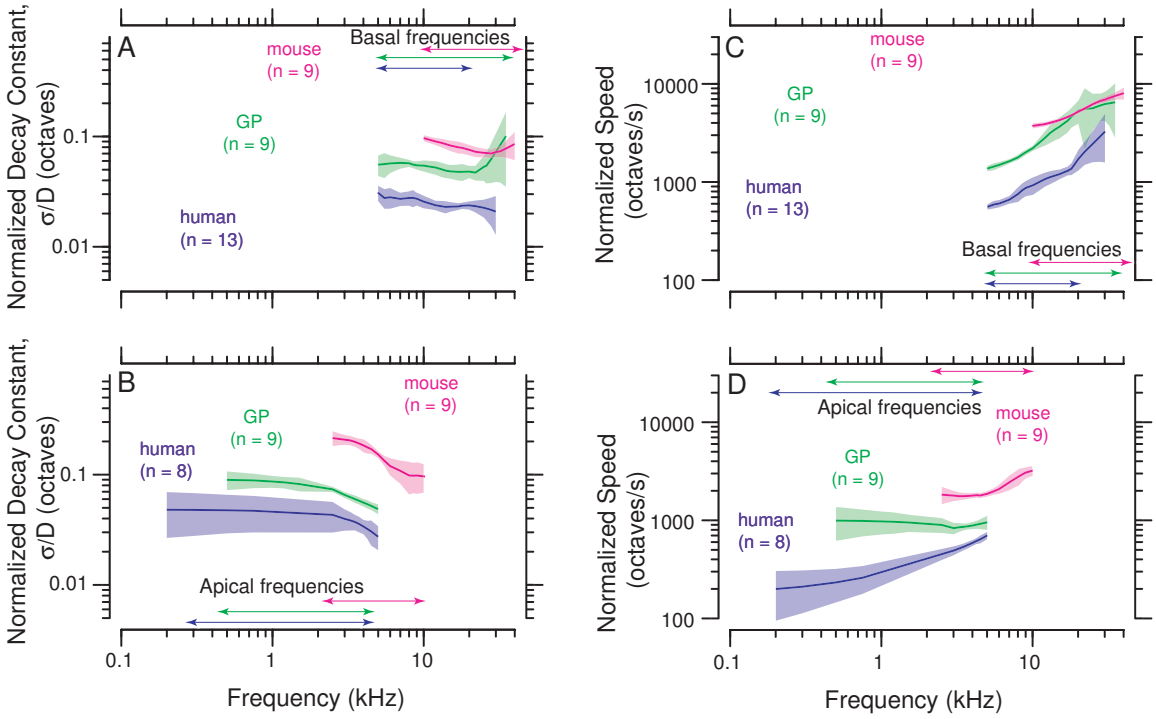

Figure 4-15: Median and 95% confidence intervals of interspecies normalized wave properties

A, B: Normalized TM decay constant, $\frac{\sigma}{D}$, in basal (A) and apical (B) TM segments. C, D: Normalized TM wave speed, $\frac{v}{D}$, in basal (C) and apical (D) samples. Lines were obtained using loess smoothing from the data in figure 4-14. 95% confidence intervals estimated using resampling.

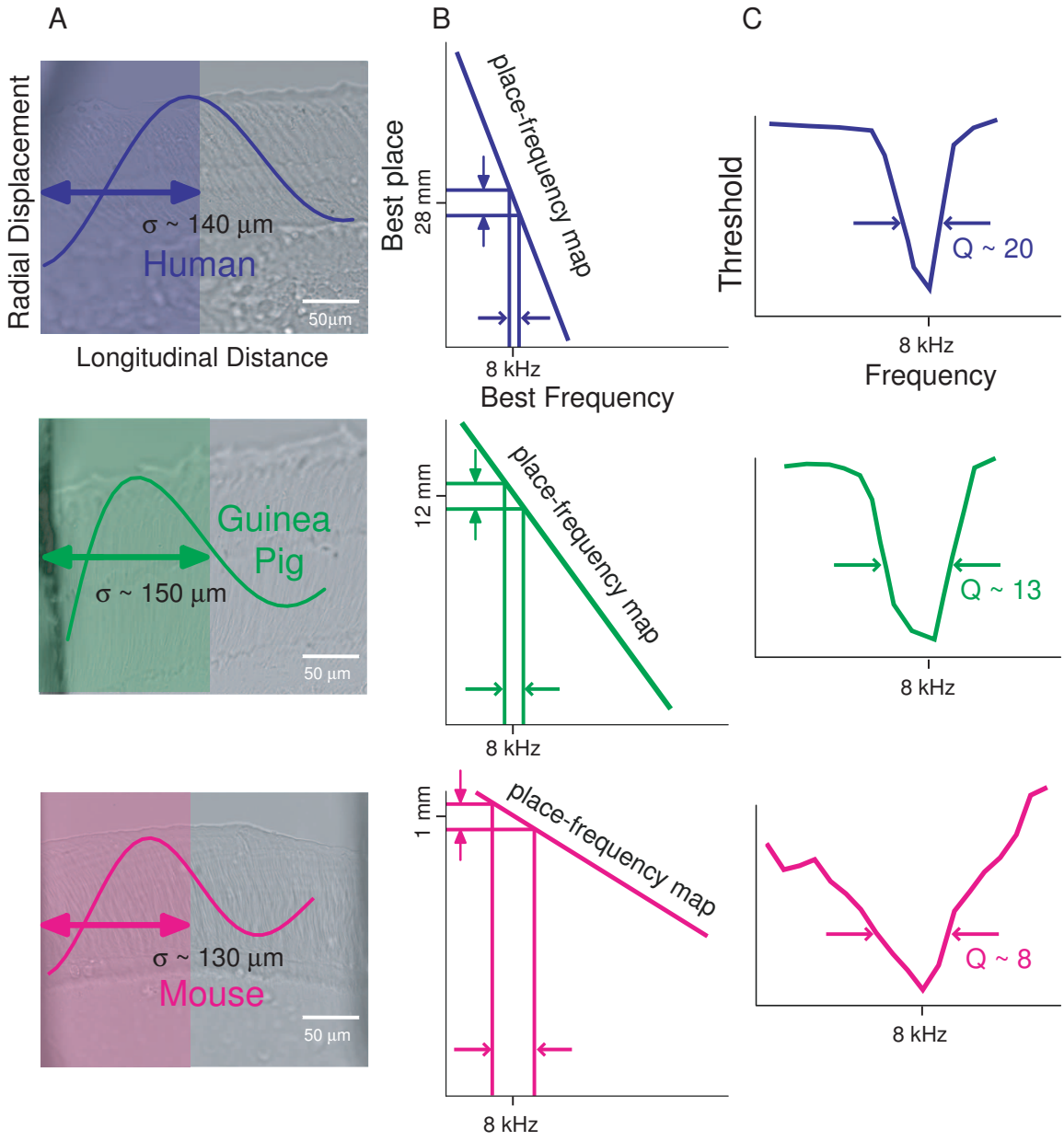

Figure 4-16: TM wave properties relate to frequency tuning via the cochlear map A: TM samples from human, guinea pig and mouse with fits to wave snapshots given on the surface of each sample. The decay constant for each wave is highlighted in each picture. B: Frequency placemaps for the three species showing the relationship between spread of the TM wave and frequency spread. Best place measurements for each species indicate the distance from the apex of the cochlea. C: Cartoons of predicted tuning curves for each species based on TM wave spread of excitation. Q values are for 8kHz based on auditory nerve fiber measurements for mice [89] and guinea pigs [20] and otoacoustic emissions based estimates for humans [82]

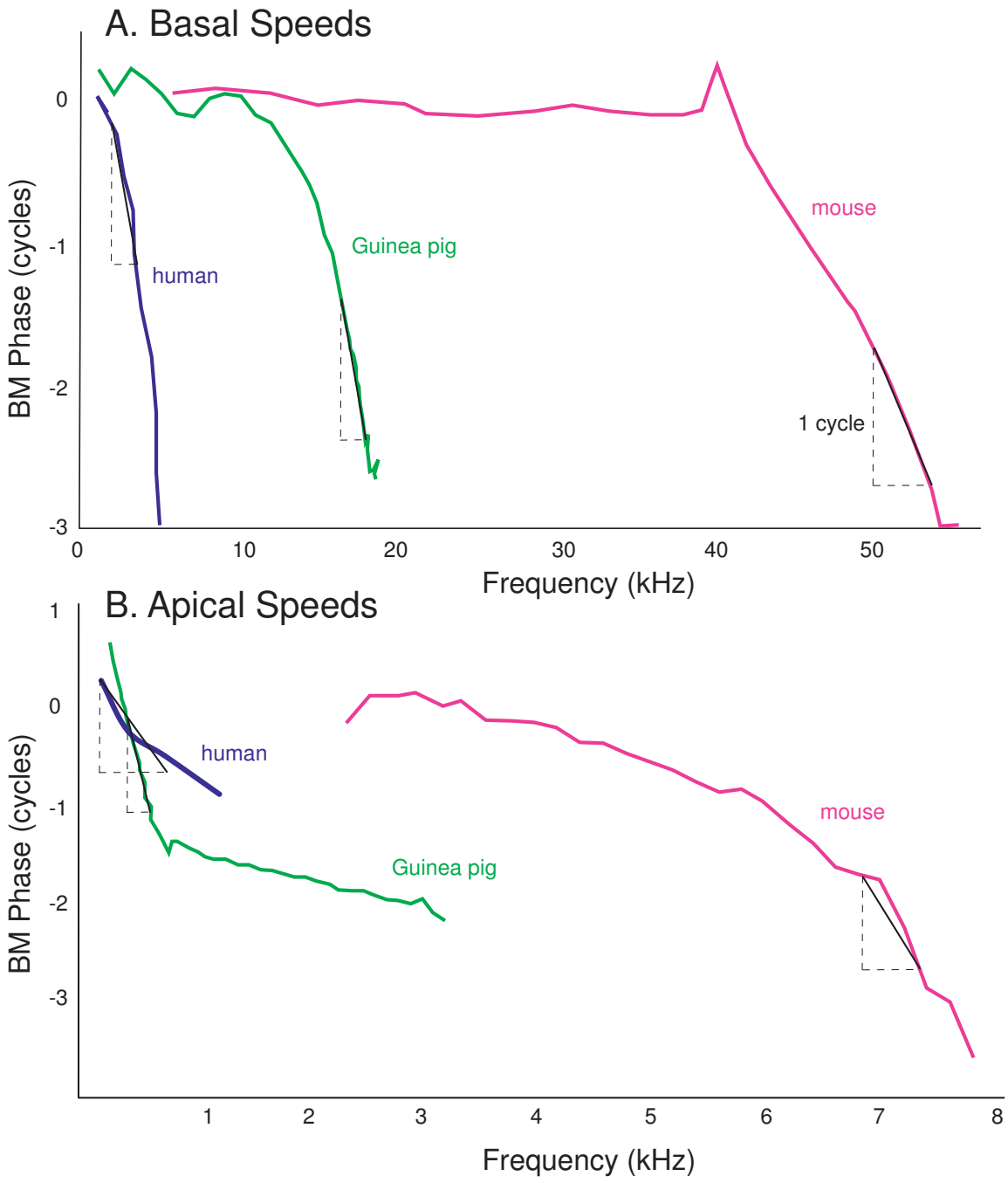

Figure 4-17: Basilar membrane speed estimates for human, guinea pig and mouse A: BM phase versus frequency in the base of a human [87], guinea pig [68], and mouse [77]. B: BM phase versus frequency curves in the apex of a human [91], guinea pig [12], and mouse [S.L.Page unpublished]. The approximate tangent to the phase versus frequency curve at the best frequency for each animal is shown with the vertical dashed lines indicating one cycle of phase change and the horizontal lines indicating the change in frequency used to compute wavelength, λ, using the cochlear map for each animal.

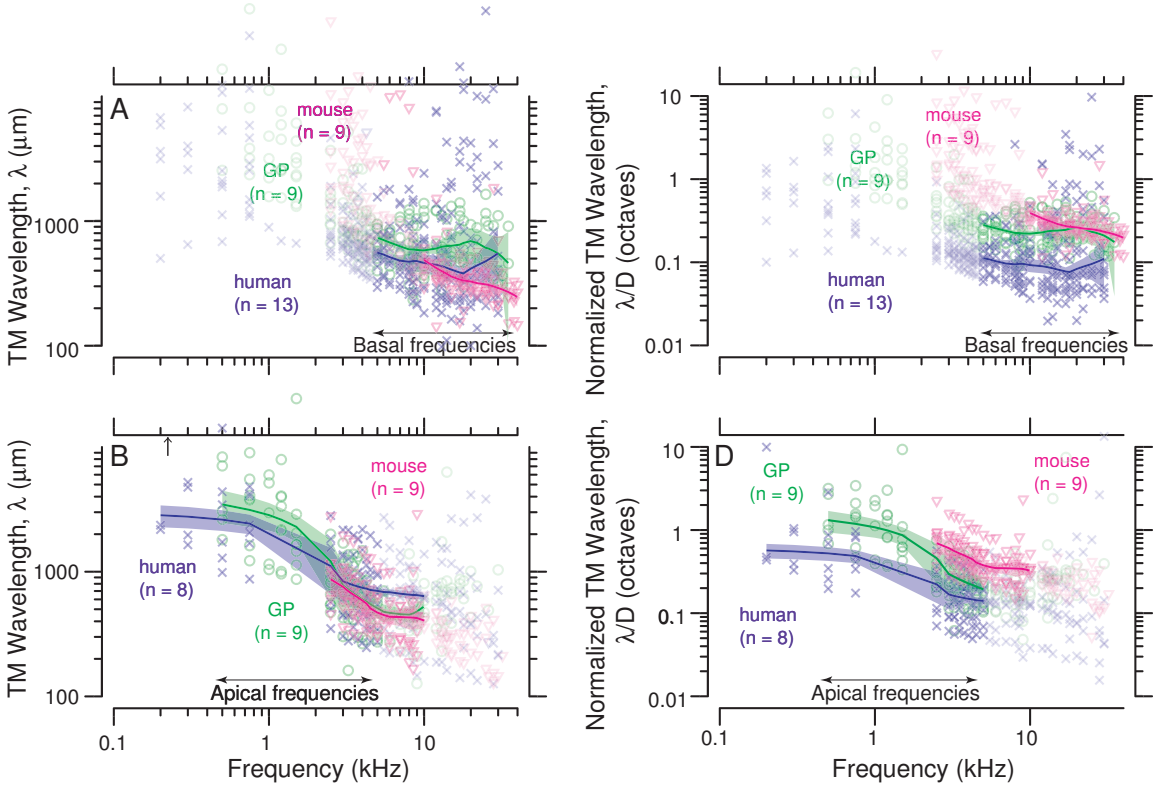

Figure 4-18: TM wavelength in samples taken from three species
A, B: TM wavelength, λ, in μm, against frequency for human (x), guinea pig (o), and mouse (Δ) basal (A) and apical (B) samples. C, D: TM wavelength normalized by cochlear distance, $\frac{\lambda}{D}$, octaves, in basal (C) and apical (D) samples. The number of TM samples measured for each region of each species is given in brackets next to the species name. All data points are shown, and for each species, a dark line was obtained from loess smoothing using $\alpha = 0.35$ as the smoothing parameter. Shaded regions indicate 95% confidence intervals estimated using resampling.. The relevant frequency range of hearing is approximately indicated by horizontal arrows in each panel of the figure. However, to account for the difference in the frequency range of hearing, the following frequencies, $f_{A|B}$, were used to mark the apical to basal transition for each species: human $f_{A|B} = 5$ kHz, guinea pig $f_{A|B} = 5$ kHz, mouse $f_{A|B} = 10$ kHz.

Chapter 5

Conclusion

The goal of this thesis was to measure human TM wave properties to see if these would account for sharper tuning in the human cochlea compared to two other mammals: guinea pigs and mice.

We compared TM morphology in samples from humans, guinea pigs and mice and found some systematic differences in human samples, namely a difference in the angle of collagen fibers and a thicker Hensen's stripe compared to TMs from guinea pigs and mice. Otherwise, TM samples from humans are quite comparable to those from other mammalian species in morphology.

Before comparing TM dynamic properties across species, we determined if measuring TM wave properties in samples several days after death would cause changes. Using mice as a model, we found differences in fixed charge density when aging bones for about two days before taking measurements. To see how charge affects TM wave properties, we systematically studied this by modulating TM fixed charge using pH and charge shielding. Although pH had a significant effect on TM wave properties, we found that increasing charge shielding did not. Therefore, we conclude that the mechanism by which pH changes TM wave properties is different from charge and that charge does not play a role in TM wave properties. This may be expected since TM waves involve purely shear displacements without any bulk compression of the tissue. Although TM fixed charge density decreased by roughly 30% in aged mouse samples, this change in fixed charge density should not affect TM wave properties

significantly. We confirmed this finding by directly measuring TM waves in freshly dissected versus aged mouse samples. We found that the best fit curves through the data overlapped significantly for these two cases.

Comparing human TM wave properties to those from guinea pigs and mice, we found no significant difference in wave decay constant in μm and wave speed in m/s. However, we show that by scaling TM wave properties by the cochlear map so that we compare them in units that are relevant to the cochlea, human TM wave decay constants are significantly smaller than those in mice and guinea pigs. We conclude that this smaller spread of excitation in TM waves contributes to the sharper frequency selectivity in humans. Although the organs of Corti are indistinguishable in these three species when viewed in radial cross-section, when considering the longitudinal coupling of the TM over the cochlear spiral in each animal, we conclude that there are significant differences in sharpness of tuning.

Chapter 6

Appendix

6.0.1 ANOVA tables

	Sigma	3			3	
	Human Basal Med Sigma	GP Basal Med Sigma	Mouse Basal Med Sigma	Human Apical Med Sigma	GP Apical Med Sigma	Mouse Apical Med Sigma
	159.53	100.406	95.6728	105.0198	128.7037	245.0706
	86.0417	157.74	46.4725	390.3061	237.2856	173.2026
	100.5978	214.4958	48.2878	137.9237	153.1117	156.8054
	164.1418	146.76	87.8502	217.1875	156.34	168.7858
	124.2192	86.7215	91.1222	68.2624	188.3665	99
	87.4635	168.4826	91.1222	80.0085	196.7789	217.65
	119.0652	78.162	121.1297	293.0929	242.673	66.35
	223.4748	73.2205	76.1	242.4293	70.4346	197.05
	181.3186	159.6705	140		175.58	255
	94.0512					
	105.7048					
	116.5867					
	207.2532					
iqr	63.544	72.949	19.5728	156.328225	43.6672	60.8446
median	119.0652	146.76	91.1222	177.5556	175.58	173.2026
n	13	9	9	8	9	9
sum of squares	29490.44465	21214.3098	7374.95136	92683.49745	23049.884	31611.97419
grand median	105.7048			174.3913		
SS among	19404.13877			105.5364943		
SS within	58079.70584			147345.3561		
SS total	77483.84461			147450.8925		
Msamong	9702.069387			52.76824717		
Mswithin	2074.275209			6406.319828		
Fs	4.677329868					

	Speed	3			3	
	Human Basal Med Speed	GP Basal Med Speed	Mouse Basal Med Speed	Human Apical Med Speed	GP Apical Med Speed	Mouse Apical Med Speed
	20.1571	14.6049	6.7228	1.36	1.9658	2.8466
	5.1235	5.2092	5.2866	3.5456	4.6345	2.5374
	7.6798	9.5549	4.7212	2.4508	3.5424	2.0866
	3.9919	9.3813	9.6052	4.6393	1.2	2.2103
	3.1305	4.2861	7.1229	1.6698	2.4632	1.6728
	2.4459	8.3401	6.0379	1.067	3.4656	1.6116
	2.7745	3.6494	5.81	3.5745	1.7732	1.414
	14.3515	4.9626	6.745	6.2476	2.1606	3.684
	6.768	3.0554	5.95		1.2438	3.91
	5.4642					

	3.0313					
	6.1553					
	4.3408					
iqr	3.6375	5.0952	0.935	2.24835	1.6924	1.1738
sum	85.4143	63.0439	58.0016	2.9982	2.1606	2.2103
median	5.1235	5.2092	6.0379	8	9	9
n	13	9	9	22.36110402	11.775445	6.8693872
sum of squares	344.5146811	142.357996	17.2297481	2.33055		
grand median	5.81			3.956139765		
SS among	9.8427607			41.00593583		
SS within	504.102425			44.9620756		
SS total	513.9451857			1.978069883		
Msamong	4.92138035			1.782866775		
Mswithin	18.00365804					

Normalized ANOVA

	Sigma/D	3			3	
	Human Basal Med Sigma	GP Basal Med Sigma	Mouse Basal Med Sigma	Human Apical Med Sigma	GP Apical Med Sigma	Mouse Apical Med Sigma
	0.0319060	0.0380326	0.0765382	0.0210040	0.0487514	0.1960565
	0.0172083	0.0597500	0.0371780	0.0780612	0.0898809	0.1385621
	0.0201196	0.0812484	0.0386302	0.0275847	0.0579969	0.1254443
	0.0328284	0.0555909	0.0702802	0.0434375	0.0592197	0.1350286
	0.0248438	0.0328491	0.0728978	0.0136525	0.0713509	0.0792000
	0.0174927	0.0638192	0.0728978	0.0160017	0.0745375	0.1741200
	0.0238130	0.0296068	0.0969038	0.0586186	0.0919216	0.0530800
	0.0446950	0.0277350	0.0608800	0.0484859	0.0266798	0.1576400
	0.0362637	0.0604813	0.1120000		0.0665076	0.2040000
	0.0188102					
	0.0211410					
	0.0233173					
	0.0414506					
sum	0.353890	0.2346219	0.46532592	0.3068460	0.4017373	0.59509152
median	0.023813	0.0555909	0.0728978	0.0355111	0.0665076	0.1385621
n	13.000000	9	9	8.0000000	9	9
sum of squares	0.001179618	0.0030438	0.00471997	0.00370734	0.0033072	0.020231663
grand median	0.0380326			0.0689293		
SS among	0.0163434			0.0526255		
SS within	0.0089434			0.0272462		
SS total	0.0252868			0.0798717		
Msamong	0.0081717			0.0263128		
Mswithin	0.0003194			0.0011846		
Fs	25.58393622			22.21202842		

	Speed	3			3	
	Human Basal Med Speed	GP Basal Med Speed	Mouse Basal Med Speed	Human Apical Med Speed	GP Apical Med Speed	Mouse Apical Med Speed
	4031.42	5532.1591	5378.24	272	744.62121	2277.28
	1024.7	1973.1818	4229.28	709.12	1755.4924	2029.92
	1535.96	3619.2803	3776.96	490.16	1341.8182	1669.28
	798.38	3553.5227	7684.16	927.86	454.54545	1768.24
	626.1	1623.5227	5698.32	333.96	933.0303	1338.24
	489.18	3159.1288	4830.32	213.4	1312.7273	1289.28
	554.9	1382.3485	4648	714.9	671.66667	1131.2
	2870.3	1879.7727	5396	1249.52	818.40909	2947.2
	1353.6	1157.3485	4760		471.13636	3128

ANOVA

	1092.84					
	606.26					
	1231.06					
	868.16					
sum	17082.86	14678.144	36245.28	4910.92	6542.2348	7744.72
median	1024.7	1973.1818	4830.32	599.64	818.40909	1768.24
n	13	9	9	8	9	9
sum of squares	13780587.24	20425562	11055334.47	894444.1608	1689543.8	4396407.808
grand median	1973.181818			1032.115152		
SS among	85164178.18			6784228.709		
SS within	45261483.56			6980395.789		
SS total	130425661.7			13764624.5		
Msamong	42582089.09			3392114.355		
Mswithin	1616481.556			303495.4691		
Fs	26.3424528			11.17682041		

Bibliography

[1] C. C. Abnet. *Measuring mechanical properties of the tectorial membrane with a magnetizable bead*. PhD thesis, Massachusetts Institute of Technology, Cambridge, MA, 1998.

[2] C.C. Abnet and D.M. Freeman. Deformations of the isolated mouse tectorial membrane produced by oscillatory forces. *Hear Res*, 144:29–46, 2000.

[3] J. B. Allen. Cochlear micromechanics — a physical model of transduction. *J Acoust Soc Am*, 68:1660–1670, 1980.

[4] R. Banakis and J. Siegel. Spontaneous and tone-evoked otoacoustic emissions in mice. In *Abstracts of the Thirty-first Midwinter Research Meeting*, Phoenix, Arizona, February 2008. Association for Research in Otolaryngology.

[5] C. Bergevin, D. S. Velenovsky, and K. E. Bonine. Tectorial membrane morphological variation: Effects upon stimulus frequency otoacoustic emissions. *Biophys J*, 99:1064–1072, 2010.

[6] M. Billone and S. Raynor. Transmission of radial shear forces to cochlear hair cells. *J Acoust Soc Am*, 54:1143–1156, 1973.

[7] Y. Bitterman, R. Mukamel, R. Malach, I. Fried, and I. Nelken. Ultra-fine frequency tuning revealed in single neurons of human auditory cortex. *Nature*, 451(7175):197–201, 2008.

[8] W. E. Brownell, C. R. Bader, D. Bertrand, and Y. de Ribaupierre. Evoked mechanical responses of isolated cochlear hair cells. *Science*, 227:194–196, 1985.

[9] H. Burda, L. Ballast, and V. Bruns. Cochlea in old world mice and rats (muridae). *Journal of morphology*, 198(3):269–285, 1988.

[10] R. W. Chan. Measurements of vocal fold tissue viscoelasticity: approaching the male phonatory frequency range. *J Acoust Soc Am*, 115:3161–3170, 2004.

[11] NP Cooper and WS Rhode. Basilar membrane mechanics in the hook region of cat and guinea-pig cochleae: sharp tuning and nonlinearity in the absence of baseline position shifts. *Hear Res*, 63:163–190, 1992.

[12] NP Cooper and WS Rhode. Nonlinear mechanics at the apex of the guinea-pig cochlea. *Hear Res*, 82:225–243, 1995.

[13] P. Dallos. Overview: Cochlear neurobiology. In P. Dallos, A. N. Popper, and R. R. Fay, editors, *The Cochlea*, volume 8 of *Springer Handbook of Auditory Research*. Springer-Verlag, New York, 1996.

[14] P. Dallos, M. C. Billone, J. D. Durrant, C. Wang, and S. Raynor. Cochlear inner and outer hair cells: functional differences. *Science*, 177:356–358, 1972.

[15] C. Q. Davis and D. M. Freeman. Using a light microscope to measure motions with nanometer accuracy. *Optical Engineering*, 37:1299–1304, 1998.

[16] H. Davis. Biophysics and physiology of the inner ear. *Physiol Rev*, 37:1–49, 1957.

[17] H. Davis. A mechano-electrical theory of cochlear action. *Ann Otol Rhino Laryngol*, 67:789–801, 1958.

[18] Günter Ehret. Stiffness gradient along the basilar membrane as a basis for spatial frequency analysis within the cochlea. *The Journal of the Acoustical Society of America*, 64:1723, 1978.

[19] G. Emadi, C.-P. Richter, and P. Dallos. Stiffness of the gerbil basilar membrane: radial and longitudinal variations. *J Neurophysiol*, 91:474–488, 2004.

[20] EF Evans. The frequency response and other properties of single fibres in the guinea-pig cochlear nerve. *The Journal of physiology*, 226(1):263–287, 1972.

[21] H. Felix. Anatomical differences in the peripheral auditory system of mammals and man. In D. Felix and E. Oestreicher, editors, *rational Pharmacotherapy of the Inner Ear*. Karger, 2002.

[22] C. Fernández. Dimensions of the cochlea (guinea pig). *The Journal of the Acoustical Society of America*, 24:519, 1952.

[23] D.M. Freeman, C.C. Abnet, W. Hemmert, B.S. Tsai, and T.F. Weiss. Dynamic material properties of the tectorial membrane: a summary. *Hear Res*, 180:1–10, 2003.

[24] D.M. Freeman, K. Masaki, A.R. McAllister, J.L. Wei, and T.F. Weiss. Static material properties of the tectorial membrane: a summary. *Hear Res*, 180:11–27, 2003.

[25] N. Gavara and R. Chadwick. Measurement of anisotropic mechanical properties of cochlear tectorial membrane. In *Abstracts of the Thirty-First Midwinter Research Meeting*, Phoenix, AZ, February 2008. Association for Research in Otolaryngology.

[26] N. Gavara and R.S. Chadwick. Collagen-based mechanical anisotropy of the tectorial membrane: implications for inter-row coupling of outer hair cell bundles. *PLoS One*, 4, 2009.

[27] N. Gavara and R.S. Chadwick. Noncontact microrheology at acoustic frequencies using frequencymodulated atomic force microscopy. *Nat. Methods*, 7:650–654, 2010.

[28] R. Ghaffari. *The functional role of the mammalian tectorial membrane in the cochlear mechanics*. PhD thesis, Massachusetts Institute of Technology, Cambridge, MA, 2008.

[29] R. Ghaffari, A. J. Aranyosi, and D. M. Freeman. Longitudinally propagating traveling waves of the mammalian tectorial membrane. *Proc Nat Acad Sci USA*, 104:16510–16515, 2007.

[30] R. Ghaffari, A. J. Aranyosi, G. P. Richardson, and D. M. Freeman. Tectorial membrane traveling waves underlie abnormal hearing in tectb mutants. *Nature Communications*, 1, 2010.

[31] R. Ghaffari, S. L. Page, S. Farrahi, J. B. Sellon, and D. M. Freeman. Electrokinetic properties of the mammalian tectorial membrane (in press). *Proc Nat Acad Sci USA*, 110:4279–84, 2013.

[32] R. J. Goodyear and G. P. Richardson. Extracellular matrices associated with the apical surfaces of sensory epithelia in the inner ear: Molecular and structural diversity. *J. Neurobiol*, 53:212–227, 2002.

[33] J. F. Greenleaf, M. Fatemi, and M. Insana. Selected methods for imaging elastic properties of biological tissues. *Ann Rev Biomed Eng*, 91:57–78, 2003.

[34] D. D. Greenwood. Critical bandwidth and the frequency coordinates of the basilar membrane. *J Acoust Soc Am*, 33:1344–1356, 1961.

[35] D. D. Greenwood. A cochlear frequency-position function for several species - 29 years later. *J Acoust Soc Am*, 87:2592–2605, 1990.

[36] J. W. Gu, W. Hemmert, D. M. Freeman, and A. J. Aranyosi. Frequency-dependent shear impedance of the tectorial membrane. *Biophys J*, 95:2529–38, 2008.

[37] R. Gueta, D. Barlam, R. Z. Shneck, and I. Rousso. Measurement of the mechanical properties of isolated tectorial membrane using atomic force microscopy. *Proc Natl Acad Sci USA*, 103:14790–14795, 2006.

[38] R. Gueta, D. Barlam, R. Z. Shneck, and I. Rousso. Sound-evoked deflections of outer hair cell stereocilia arise from tectorial membrane anisotropy. *Biophys J*, 94:4570–4576, 2008.

[39] J. J. Guinan and N. Cooper. Medial olivocochlear efferent inhibition of basilar-membrane responses to clicks: Evidence for two modes of cochlear mechanical excitation. *J Acoust Soc Am*, 124:1080–1092, 2008.

[40] L. Han, M. Monné, H. Okumura, T. Schwend, A. L. Cherry, D. Flot, T. Matsuda, and L. Jovine. Insights into egg coat assembly and egg-sperm interaction from the x-ray structure of full-length zp3. *Cell*, 143:404–415, 2010.

[41] J. A. Hasko and G. P. Richardson. The ultrastructural organization and properties of the mouse tectorial membrane matrix. *Hear Res*, 35:21–38, 1988.

[42] T. Hoshino. Contact between the tectorial membrane and the cochlear sensory hairs in the human and the monkey. *Archives of oto-rhino-laryngology*, 217:53–60, 1977.

[43] F. Hossler. Human organ of corti. `http://www.allposters.com/-sp/Organ-of-Corti-in-the-Human-Cochlea-Posters_i6014169_.htm`. Accessed: 2013-05-20.

[44] A. E. Hubbard. A traveling-wave amplifier model of the cochlea. *Science*, 259:68–71, 1993.

[45] M. Jin and A. J. Grodzinsky. Effect of electrostatic interactions between glycosaminoglycans on the shear stiffness of cartilage: A molecular model and experiments. *Macromolecules*, 34:8330–9, 2001.

[46] B. M. Johnstone, J. R. Johnstone, and I. D. Pugsley. Membrane resistance in endolymphatic walls of the first turn of the guinea-pig cochlea. *The Journal of the Acoustical Society of America*, 40:1398, 1966.

[47] G. P. Jones, V. A. Lukashkina, I. J. Russell, S. J. Elliott, and A. N. Lukashkin. Frequency-dependent properties of the tectorial membrane facilitate energy transmission and amplification in the cochlea. *Biophys J*, 104:1357–66, 2013.

[48] P.X. Joris, C. Bergevin, R. Kalluri, M. McLaughlin, P. Michelet, M. van der Heijden, and C.A. Shera. Frequency selectivity in old-world monkeys corroborates sharp cochlear tuning in humans. *PNAS*, 108:17516–20, 2011.

[49] M. Kössl and I. J. Russell. Basilar membrane resonance in the cochlea of the mustached bat. *Proc Natl Acad Sci USA*, 92:276–279, 1995.

[50] P. K. Legan, V. A. Lukashkina, R. J. Goodyear, A. N. Lukashkin, K. Verhoeven, G. V. Camp, I. J. Russell, and G. P. Richardson. A deafness mutation isolates a second role for the tectorial membrane in hearing. *Nature Neuroscience*, 8:1035–1042, 2005.

[51] P.K. Legan, V.A. Lukashkina, R.J. Goodyear, M. Kössl, I.J. Russell, and G.P. Richardson. A targeted deletion in α-tectorin reveals that the tectorial membrane is required for the gain and timing of cochlear feedback. *Neuron*, 28:273–285, 2000.

[52] P.K. Legan, A. Rau, J.N. Keen, and G.P. Richardson. The mouse tectorins. modular matrix proteins of the inner ear homologous to components of the sperm-egg adhesion system. *J Biol Chem*, 272:8791–801, 1997.

[53] M Charles Liberman. Auditory-nerve response from cats raised in a low-noise chamber. *The Journal of the Acoustical Society of America*, 63:442, 1978.

[54] D. J. Lim. Cochlear anatomy related to cochlear micromechanics. a review. *J Acoust Soc Am*, 67:1686–1695, 1980.

[55] A. N. Lukashkin, G.P. Richardson, and I. J. Russell. Multiple roles for the tectorial membrane in the active cochlea. *Hear. Res.*, 266:26–35, 2010.

[56] F Mammano and R Nobili. Biophysics of the cochlea: linear approximation. *J Acoust Soc Am*, 93:3320–3332, 1993.

[57] G. A. Manley. Cochlear mechanisms from a phylogenetic viewpoint. *Proc Nat Acad Sci USA*, 97:11736–11743, 2000.

[58] K. Masaki, R. Ghaffari, J. W. Gu, G. P. Richardson, D. M. Freeman, and A. J. Aranyosi. Tectorial membrane material properties in tecta$^{Y1870C/+}$ heterozygous mice. *Biophysical Journal*, 99:3274–3281, 2010.

[59] K. Masaki, T. F. Weiss, and D. M. Freeman. Poroelastic bulk properties of the tectorial membrane measured with osmotic stress. *Biophys. J.*, 91:2356–2370, 2006.

[60] W.T. McGuirt, S.D. Prasad, A.J. Griffith, H.P. Kunst, G.E. Green, K.B. Shpargel, C. Runge, C. Huybrechts, R.F. Mueller, E. Lynch, M.C. King, H.G. Brunner, C.W. Cremers, M. Takanosu, S.W. Li, M. Arita, R. Mayne, D.J. Prockop, G. Van Camp, and R.J. Smith. Mutations in COL11A2 cause non-syndromic hearing loss (DFNA13). *Nat Genet*, 23:413–419, 1999.

[61] J. Meaud and K. Grosh. The effect of tectorial membrane and basilar membrane longitudinal coupling in cochlear mechanics. *J Acoust Soc Am*, 127:1411–1421, 2010.

[62] M. Monné, L. Han, T. Schwend, S. Burendahl, and L. Jovine. Crystal structure of the zp-n domain of zp3 reveals the core fold of animal egg coats. *Nature*, 456:653–657, 2008.

[63] J. B. Nadol. Comparative anatomy of the cochlea and auditory nerve in mammals. *Hearing Research*, 34:253–266, 1988.

[64] SS. Narayan, AN. Temchin, A. Recio, and MA. Ruggero. Frequency tuning of basilar membrane and auditory nerve fibers in the same cochleae. *Science*, 282:1882–4, 1998.

[65] S. T. Neely. A model of cochlear mechanics with outer hair cell motility. *J Acoust Soc Am*, 94:137–146, 1993.

[66] S. T. Neely and D. O. Kim. An active cochlear model showing sharp tuning and high sensitivity. *Hear Res*, 9:123–130, 1983.

[67] S. T. Neely and D. O. Kim. A model for active elements in cochlear biomechanics. *J Acoust Soc Am*, 79:1472–1480, 1986.

[68] A.L. Nuttall and D.F. Dolan. Steady-state sinusoidal velocity responses of the basilar membrane in the guinea-pig. *J Acoust Soc Am*, 99:1556–1565, 1996.

[69] E. L. Le Page and B. M. Johnstone. Nonlinear mechanical behavior of the basilar membrane in the basal turn of the guinea pig cochlea. *Hear Res*, 2:183–189, 1980.

[70] T. Ren. Longitudinal pattern of basilar membrane vibration in the sensitive cochlea. *Proc Nat Acad Sci USA*, 99(4):17101–17106, 2002.

[71] G.P. Richardson, J.B. de Monvel, and C. Petit. How the genetics of deafness illuminates auditory physiology. *Annu. Rev. Physiol.*, 73:1–24, 1987.

[72] G.P. Richardson, A.N. Lukashkin, and I.J. Russell. The tectorial membrane: One slice of a complex cochlear sandwich. *Curr Opin Otolaryngol Head Neck Surg*, 16:458–464, 2008.

[73] C.-P. Richter, G. Emadi, G. Getnick, A. Quesnel, and P. Dallos. Tectorial membrane stiffness gradients. *Biophys J*, 93:2265–2276, 2007.

[74] L. Robles and M. A. Ruggero. Mechanics of the mammalian cochlea. *Physiol Rev*, 81:1305–1352, 2001.

[75] M. A. Ruggero, N. C. Rich, A. Recio, S. S. Narayan, and L. Robles. Basilar-membrane responses to tones at the base of the chinchilla cochlea. *J Acoust Soc Am*, 101:2151–63, 1997.

[76] A. E. Russell. Effect of ph on thermal stability of collagen in the dispersed and aggregated states. *Biochem J*, 139:277–280, 1974.

[77] I. J. Russell, P. K. Legan, V. A. Lukashkina, A. N. Lukashkin, R. J. Goodyear, and G. P. Richardson. Sharpened cochlear tuning in a mouse with a genetically modified tectorial membrane. *Nature Neurosci*, 10:215–223, 2007.

[78] J. B. Sellon. Viscosity and porosity contribute to both speed and decay of tectorial membrane traveling waves. Master's thesis, Massachusetts Institute of Technology, Cambridge, MA, 2013.

[79] D. Shah, D. M. Freeman, and T. F. Weiss. The osmotic response of the isolated, unfixed mouse tectorial membrane to isosmotic solutions: Effect of (Na^+), (K^+), and (Ca^{2+}) concentration. *Hearing Res.*, 87:187–207, 1995.

[80] C.A. Shera and J.J. Guinan. Cochlear traveling-wave amplification, suppression, and beamforming probed using noninvasive calibration of intracochlear distortion sources. *J Acoust Soc Am*, 121:1003–1016, 2007.

[81] C.A. Shera, J.J. Guinan, and A.J. Oxenham. Revised estimates of human cochlear tuning from otoacoustic and behavioral measurements. *PNAS*, 99:3318–3323, 2002.

[82] C.A. Shera, J.J. Guinan Jr, and A.J. Oxenham. Otoacoustic estimation of cochlear tuning: validation in the chinchilla. *Journal of the Association for Research in Otolaryngology*, 11(3):343–365, 2010.

[83] B. Shoelson, E. K. Dimitriadis, H. Cai, B. Kachar, and R. S. Chadwick. Evidence and implications of inhomogeneity in tectorial membrane elasticity. *Biophys J*, 87:2768–2777, 2004.

[84] M.C. Simmler, M. Cohen-Salmon, A. El-Amraoui, L. Guillaud, J.C. Benichou, C. Petit, and J.J. Panthier. Targeted disruption of otog results in deafness and severe imbalance. *Nat Genet*, 24:139–143, 2000.

[85] J. M. Sinnott, M. D. Beecher, D. B. Moody, and W. C. Stebbins. Speech sound discrimination by monkeys and humans. *The Journal of the Acoustical Society of America*, 60:687, 1976.

[86] Olga Stakhovskaya, Divya Sridhar, Ben H Bonham, and Patricia A Leake. Frequency map for the human cochlear spiral ganglion: implications for cochlear implants. *Journal for the Association for Research in Otolaryngology*, 8(2):220–233, 2007.

[87] Stefan Stenfelt, Sunil Puria, Naohito Hato, and Richard L Goode. Basilar membrane and osseous spiral lamina motion in human cadavers with air and bone conduction stimuli. *Hearing research*, 181(1):131–143, 2003.

[88] H. Suzuki, Y.C. Lee, M. Tachibana, K. Hozawa, and H. Wataya et al. Quantitative carbohydrate analyses of the tectorial and otoconial membranes of the guinea pig. *Hear. Res.*, 60:45–52, 2005.

[89] A. M. Taberner and M. C. Liberman. Response properties of single auditory nerve fibers in the mouse. *J Neurophysiol*, 93:557–569, 2005.

[90] A. Viberg and B. Canlon. The guide to plotting a cochleogram. *Hearing Research*, 197:1–10, 2004.

[91] G. von Békésy. *Experiments in Hearing*. McGraw-Hill, New York, 1960.

[92] T.F. Weiss and D.M. Freeman. Equilibrium behavior of an isotropic polyelectrolyte gel model of the tectorial membrane: The role of fixed charges. *Auditory Neurosci*, 3:351–361, 1997.

[93] A. Xia, S. S. Gao, T. Osborn, and A. Bress et al. Deficient forward transduction and enhanced reverse transduction in the alpha tectorin c1509g human hearing loss mutation. *Dis. Model. Mech.*, 3:209–223, 2010.

[94] C. Yushinaga-Itano, A. L. Sedey, D. K. Coulter, and A. L. Mehl. Language of early- and later-identified children with hearing loss. *Pediatrics*, 102(5):1161–1171, 1998.

[95] D.-S. Zhang, V. Piazza, B. J. Perrin, A. K. Rzadzinska, J. C. Poczatek, M. Wang, H. M. Prosser, J. M. Ervasti, D. P. Corey, and C. P. Lechene. Multi-isotope imaging mass spectrometry reveals slow protein turnover in hair-cell stereocilia. *Nature*, 481:520–524, 2012.

[96] J. J. Zwislocki. Tectorial membrane: a possible sharpening effect on the frequency analysis in the cochlea. *Acta Otolaryngol*, 87:267–269, 1979.

[97] J. J. Zwislocki. Five decades of research on cochlear mechanics. *J Acoust Soc Am*, 67:1679–1685, 1980.

[98] J.J. Zwislocki and L.K. Cefaratti. Tectorial membrane. II: Stiffness measurements in vivo. *Hear Res*, 42:211–227, 1989.